Quantifying and Understanding the Linkages between Clouds and the General Circulation of the Atmosphere

Bernard R. Lipat

Submitted in partial fulfillment of the

requirements for the degree of

Doctor of Philosophy

in the Graduate School of Arts and Sciences

COLUMBIA UNIVERSITY

2018

ABSTRACT

Quantifying and Understanding the Linkages between

Clouds and the General Circulation of the Atmosphere

Bernard R. Lipat

Due to the wide range of physical scales involved, clouds cannot be fully resolved in models of the global climate, and so are parameterized. The resultant model deficiencies in simulating important cloud processes within the current climate are strongly implicated in the large uncertainty in model predictions of future climate changes. Previous work has highlighted the uncertainties in predictions of future climate related to thermodynamic cloud changes, understanding of which requires detailed observations of small-scale cloud microphysics. In this thesis, we argue that understanding the linkages between mid-latitude clouds and the general circulation of the atmosphere can advance efforts to constrain their response to climate forcing. We make this argument with three main methods of analysis: 1) observations, 2) state-of-the-art general circulation models, and 3) experiments with an idealized model of the global climate.

First, we perform a comprehensive investigation of the observed inter-annual relationships between clouds, their radiative effects, and key indices of the large-scale atmospheric circulation. Using reanalysis data and satellite retrievals, we find a relationship between the edge of the Hadley circulation (HC) and the high cloud field that is largely robust against season and ocean basin. In contrast, shifts of the mid-latitude eddy-driven jet latitude, which had been the focus of previous work on the coupling between mid-latitude clouds and cir-

culation, only correlate with the high cloud field in the wintertime North Atlantic. In that season and basin, poleward shifts of the circulation are associated with anomalous shortwave cloud radiative warming. During all seasons in the Southern Hemisphere, however, poleward shifts of the circulation are associated with anomalous shortwave cloud radiative cooling.

Second, we examine Coupled Model Intercomparison Project phase 5 (CMIP5) model output to evaluate the models' simulation of the inter-annual co-variability between the Southern Hemisphere HC extent and the shortwave cloud radiative effect. In the control climate runs, during years when the HC edge is anomalously poleward, most models reduce their cloud cover in the lower mid-latitudes (approximately 30°S - 45°S) and allow more sunlight to warm the region, although we find no such shortwave radiative warming in observations. We correlate these biases in the co-variability between the HC extent and shortwave cloud radiative anomalies with model biases in the climatological HC extent. Models whose climatological HCs are unrealistically equatorward compared to the observations exhibit weaker climatological subsidence in the lower mid-latitudes and exhibit larger increases in subsidence there with poleward HC extent shifts than models with more realistic climatological HCs. This behavior, based on control climate variability, has important implications for the model response to forcing. In $4\times CO_2$-forced runs, models with unrealistically equatorward HCs in the control climatology exhibit a stronger shortwave cloud radiative warming response in the lower mid-latitudes and tend to have larger values of equilibrium climate sensitivity than models with more realistic HCs in the control climatology.

The above correlative analyses suggest that uncertainty in the linkages between mid-latitude clouds and the general circulation of the atmosphere contributes to uncertainty in the model response to forcing. Finally, we use simulations of the global climate in an idealized aquaplanet model to show that the biases in the climatological Southern Hemisphere circulation do indeed contribute to much of the model spread in the cloud-circulation coupling. We find that for the same 1° latitude poleward shift, simulations with narrower climatological HCs exhibit stronger mid-latitude shortwave cloud radiative warming anomalies than simulations with wider climatological HCs. The shortwave cloud radiative warming anomalies result predominantly from a subsidence warming of the planetary boundary layer, which decreases low-level cloud fraction and is stronger for narrower HCs because of a tighter mean meridional circulation. A comparison of the spread across aquaplanet simulations with that across CMIP5 models suggests that about half of the model uncertainty in the mid-latitude cloud-circulation coupling stems from this impact of the circulation on the large-scale temperature structure of the boundary layer, and thus can be removed by improving the representation of the climatological circulation in models. Therefore, a more realistic representation of the Hadley circulation in models can improve their representation of the linkage between mid-latitude clouds and the atmospheric circulation in the current climate and increase overall confidence in predictions of future climate.

Contents

List of Tables

List of Figures

Acknowledgements

I would like to express my deep gratitude for my advisors Dr. George Tselioudis and Dr. Lorenzo M. Polvani. I am also sincerely appreciative of the other members of my thesis committee: Dr. Adam Sobel, Dr. Michela Biasutti, and Dr. Michael Tippett.

I would like to acknowledge the important contributions to this work by Dr. Kevin Grise, Dr. Aiko Voigt, and Dr. Dimitra Konsta. This thesis would not have been possible without funding from the NASA Earth and Space Science Fellowship. Finally, I thank my family and friends for their encouragement and support.

Dedicated to

Lucas and Lua

Chapter 1

Introduction

The climate of the Earth has been changing over the recent past and is predicted to continue to change into the future as a result of increasing concentrations of greenhouse gases (IPCC 2013). One might characterize the changes to the climate system that have been observed and/or are expected to be observed as thermodynamic changes or as dynamical changes. The thermodynamic changes can be directly associated with the warming of the global-mean surface air temperature induced by increasing concentrations of greenhouse gases, chiefly carbon dioxide. Such thermodynamic climate changes might include an increase in the global-mean mixing ratio of water vapor and an intensification of the hydrological cycle (Held and Soden 2006). Other climate changes might be more naturally associated with a change in the general circulation of the atmosphere and ocean. These dynamical climate changes might include a change in the geographic patterns of rainfall; for example, a narrowing of the intertropical convergence zone (Byrne and Schneider 2016; Su et al. 2017), an expansion of the subtropical dry zones (Hu and Fu 2007; Seidel et al. 2008; Johanson and Fu 2009), and a poleward shift of the extra-tropical storm tracks (Bender, Ramanathan, and Tselioudis 2012; Barnes and Polvani 2013). The thermodynamic and dynamical climate changes are not necessarily independent of one another, and are both expressions of the response of the climate system to external forcing.

While there is now little doubt that the climate has changed and will continue to change as a result of increased concentrations of carbon dioxide (CO_2), there does still remain some uncertainty in the magnitude of that change (IPCC 2013). This uncertainty derives from

three main sources: internal variability, forcing uncertainty, and model response (Hawkins and Sutton 2009; Deser et al. 2012). Internal variability is the intrinsic noise of the climate system, or the natural background fluctuations of fields such as winds, sea surface temperature, insolation, etc. Forcing uncertainty includes the uncertainty in the pathway of future natural and anthropogenic emissions of forcing agents such as CO_2. Model uncertainty is the spread in the thermodynamic and dynamical climate changes that different climate models predict given the same radiative forcing. This model uncertainty, or response uncertainty, stems largely from model differences in the choices of which climate processes to include, which processes to simulate explicitly, and how to parameterize the rest (Tebaldi and Knutti 2007). Further, it is by reducing this model uncertainty that the confidence in projections of future climate conditions can most readily be increased.

To tease out the response uncertainty from internal variability and forcing uncertainty, one can define a statistically steady-state metric of the climate response to a standard radiative forcing. The climate response metric for thermodynamic changes has traditionally been the equilibrium climate sensitivity. It derives from a forcing-feedback framework of the global-mean energy balance model of the climate (e.g. Roe 2009), which we briefly review. The global-mean surface air temperature T_s responds in time to an external radiative forcing F at the top-of-atmosphere (TOA) with a net TOA radiative flux response R:

$$C\frac{dT_s}{dt} = R + F \tag{1.1}$$

where C is the heat capacity of the climate system. In equilibrium, the TOA radiative forcing balances the net TOA radiative response at TOA: $F = -R$. It is assumed that the net TOA radiative response depends on T_s. Since it is expected that the global-mean surface air temperature response ΔT_s to a standard TOA radiative forcing $F_{2\times CO_2}$ of a doubling of the CO_2 concentration will be small compared to the climatological global-mean surface

air temperature $\bar{T}_s$ of about 300 K, one can linearize the net TOA radiative response about the global-mean surface air temperature:

$$R \approx \left.\frac{\partial R}{\partial T}\right|_{\bar{T}_s} + \sum_i \left(\left.\frac{\partial R}{\partial x_i}\right|_{\bar{T}_s} \frac{\Delta x_i}{\Delta T_s} \right) \Delta T_s \tag{1.2}$$

where $\left.\frac{\partial R}{\partial T}\right|_{\bar{T}_s}$ is the Planck response and the x_i represent the parameters of the many positive and negative climate feedback processes that may amplify or dampen, respectively, the radiative response of the climate system; such as, changes in sea ice, water vapor, clouds, etc. Thus, the equilibrium response of the global-mean surface air temperature to a doubling of the CO_2 concentration can be estimated as

$$\Delta T_s \approx F_{2\times CO_2} \left[\left.\frac{\partial R}{\partial T}\right|_{\bar{T}_s} + \sum_i \left(\left.\frac{\partial R}{\partial x_i}\right|_{\bar{T}_s} \frac{\Delta x_i}{\Delta T_s} \right) \right]^{-1} \tag{1.3}$$

The equilibrium climate sensitivity (ECS) metric of the thermodynamic model responses to increasing concentrations of CO_2 does not necessarily measure the dynamical model responses (Shepherd 2014; Grise and Polvani 2014a; Grise and Polvani 2016). Nevertheless, the confidence in predictions of the future climate state, and how well the current climate system is understood, is often measured by the uncertainty in the model estimates of ECS. In this respect, not much progress has been made in the past 40 years (compare Charney et al. 1979 with IPCC 2013), despite more powerful computers and increasingly sophisticated climate models. While there still does remain some small inter-model spread in the direct radiative forcing associated with a doubling of the CO_2 concentration $F_{2\times CO_2}$, the range of model uncertainty in estimates for ECS has not decreased due largely to poor constraints on the strength of the global-mean feedback parameter $\left.\frac{\partial R}{\partial T}\right|_{\bar{T}_s} + \sum_i \left.\frac{\partial R}{\partial \alpha_i}\right|_{\bar{T}_s} \frac{\Delta \alpha_i}{\Delta T_s}$.

The single largest contributor to the uncertainty in the global-mean climate feedback parameter is the uncertainty associated with net TOA radiative response brought about by

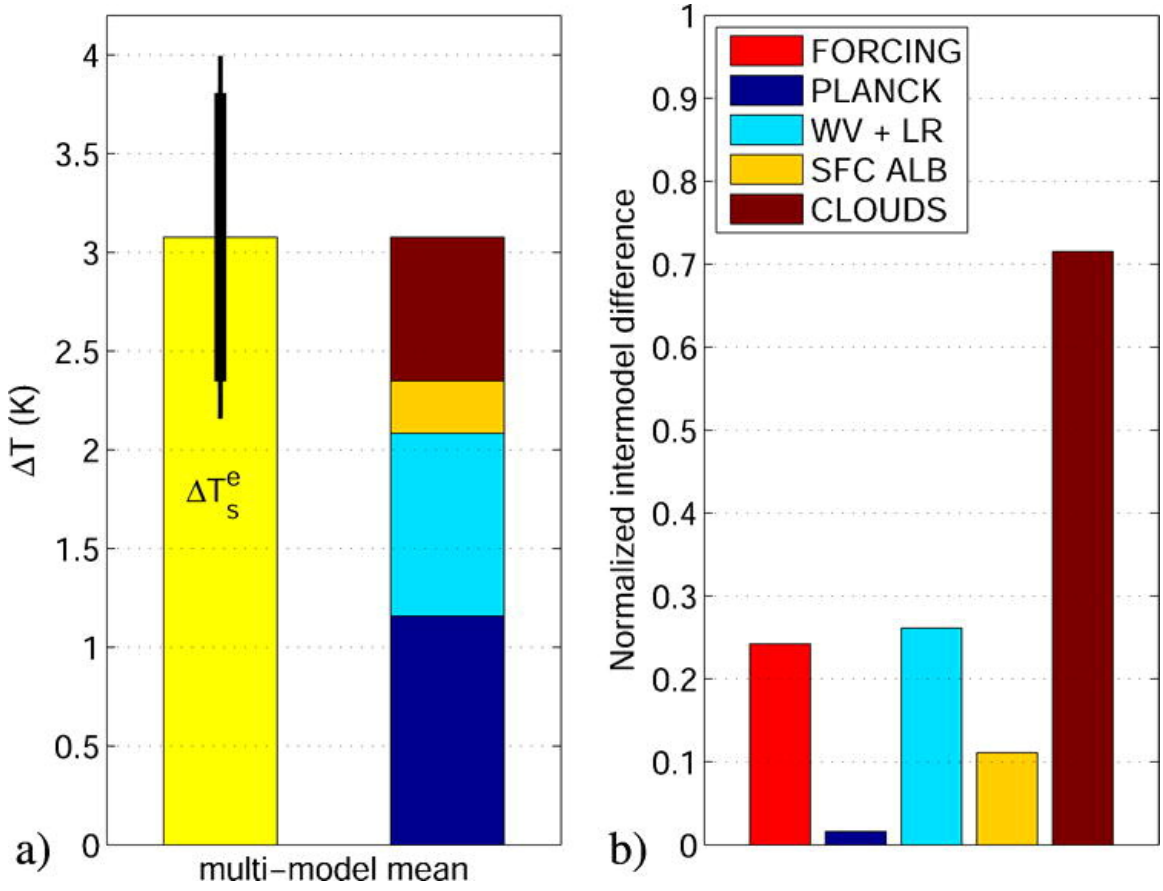

Figure 11: For a CO_2 concentration doubling, the CMIP3/AR4 (a) multi-model mean ±1 standard deviation (thick line) and 5% - 95% interval (thin line) of the equilibrium temperature change (ΔT_s^e), and contributions to this temperature change associated with the Planck response, combined water vapor and lapse-rate (WV+LR) feedback, surface albedo feedback, and cloud feedback. (b)The inter-model standard deviation of the temperature change estimates associated with the radiative forcing, the Planck response, and the various feedbacks normalized by the inter-model standard deviation of the equilibrium temperature change ΔT_s^e reported in (a). Taken from Figure 1 of Dufresne and Bony 2008

future changes in clouds. For example, Figure 11a, taken from Dufresne and Bony 2008, depicts the range of estimates for ECS and shows it to be between about 2 and 4 K (thin black vertical line on left bar). Figure 11a also depicts an estimate of the contributions to the global-mean warming from individual feedback processes (right bar) and shows that the global-mean cloud radiative feedback (brown) onto the CO_2-forced global-mean surface warming contributes a good portion to the overall warming response, about 1 K. Further, Figure 11b, also taken from Dufresne and Bony 2008, displays the contributions to the inter-model spread in the global-mean warming and shows that the uncertainty in how clouds will respond to warming (brown) is by far the largest culprit in terms of the model uncertainty in ECS. Not only is the uncertainty in future cloud changes culpable for the uncertainty in the thermodynamic model response, the uncertainty in cloud changes has also been implicated in the uncertainty of the dynamical model response (Ceppi et al. 2012; Ceppi, Zelinka, and Hartmann 2014; Voigt and Shaw 2015; Ceppi and Hartmann 2016). Constraining the model uncertainty in the global or even the regional (Roe et al. 2015) cloud radiative feedback can lead to more confident predictions of future climate, which is of vital importance. Accordingly, Clouds, Circulation, and Climate Sensitivity is designated by the World Climate Research Program as one of the five Grand Challenges of climate science (Bony et al. 2015).

Part of the reason for the large uncertainty in the future global-mean cloud radiative feedback is that clouds exert strong and competing influences on the climatological energy budget of the Earth. Clouds warm the planet by trapping the longwave radiation emitted by the Earth. This longwave cloud radiative effect arises because the longwave radiation emitted by the climate system scales with temperature according to Stefan-Boltzmann, under the assumption that the Earth emits like a blackbody. There is more longwave radiation emitted in the absence of clouds, when the emission of longwave radiation scales with the warm surface temperature, than there is in the presence of clouds, when the emission of longwave

radiation scales with the cloud tops which are farther aloft and are therefore colder than the surface.

Clouds also cool the Earth by reflecting the shortwave radiation emitted by the sun. This shortwave cloud radiative effect arises because clouds tend to be brighter than the dark ocean surfaces which cover most of the Earth. The brightness of the clouds is measured by the cloud albedo or optical depth, the value of which results from a complex interaction of both macrophysical cloud properties – cloud physical depth, cloud areal coverage, cloud lifetime, etc. – and microphysical cloud properties – cloud droplet size, cloud droplet concentration, cloud thermodynamic phase, etc. It is no surprise, then, that the global-mean shortwave cloud radiative feedback tends to be more uncertain than the global-mean longwave cloud radiative feedback (e.g. Caldwell et al. 2016).

Clouds and their radiative properties are expected to change in response to increasing concentrations of CO_2. Some of the robust cloud changes that have been seen or are expected to be seen tend to be thermodynamic cloud changes. For example, one robust cloud change seems to be the longwave cloud height feedback in the tropics (Wetherald and Manabe 1980; Hartmann and Larson 2002; Zelinka and Hartmann 2011). As tropical isotherms shift upward, and given the assumption that relative humidity is determined uniquely by temperature, the cloud top temperature will remain fixed, so that the cloud tops will rise. Given the fixed cloud top temperature but the warming tropical surface (or emission) temperature, clouds will tend to trap more longwave radiation in the climate system, resulting in a warming or positive longwave cloud radiative feedback.

Another robust cloud change in response to increasing concentrations of CO_2 is the shortwave cloud phase feedback in the high-latitudes (Storelvmo, Tan, and Korolev 2015; McCoy et al. 2016; Ceppi, Hartmann, and Webb 2016). As the freezing isotherm shifts upward and poleward in response to the warming caused by an increase in the concentration of CO_2, clouds which were previously composed largely of ice droplets will "melt"

into liquid clouds; that is, clouds composed of a greater proportion of ice droplets to liquid droplets will become less frequent at the expense of clouds composed of a greater proportion of liquid droplets to ice droplets which will become more frequent. Liquid clouds tend to have a greater optical thickness and albedo for two reasons: 1) there generally exist more cloud condensation nuclei than cloud freezing (ice) nuclei such that, the water content being the same, liquid clouds tend to consist of a greater number of cloud droplets each of smaller size than ice clouds which consist of a smaller number of droplets each of greater size; and 2) given that the droplets of ice clouds are larger than the droplets of liquid clouds, ice clouds tend also to precipitate more readily and hence are shorter-lived (Pruppacher and Klett 1997). Therefore, liquid clouds reflect more shortwave radiation away from the climate system more often, and their greater likelihood of occurrence with increasing concentrations of CO_2 results in a cooling or negative shortwave cloud radiative feedback (Mitchell, Senior, and Ingram 1989; Zelinka, Klein, and Hartmann 2012a; Zelinka, Klein, and Hartmann 2012b; Zelinka et al. 2013).

These two cloud radiative feedbacks are illustrative of much of the previous work on constraining cloud feedbacks. There have been many studies on the tropical cloud radiative feedback (Bony and Dufresne 2005; Su et al. 2014; Myers and Norris 2016; Brient et al. 2016), and justifiably so, since the tropics comprise a large portion of the global surface area. Figure 12 (left bar), taken from Vial, Dufresne, and Bony 2013, decomposes the multi-model mean global-mean warming response to increasing CO_2 concentrations into contributions by region: tropics, mid-latitudes, and poles. The tropics (light orange) are the largest contributor to the global-mean warming response. The mid-latitudes (dark orange), on the other hand, act over less surface area than do the tropics, but contribute comparably to the estimated global-mean warming.

Not only does warming in the mid-latitudes contribute a great deal to the global-mean warming response to increasing CO_2 concentrations, but the model uncertainty in the mag-

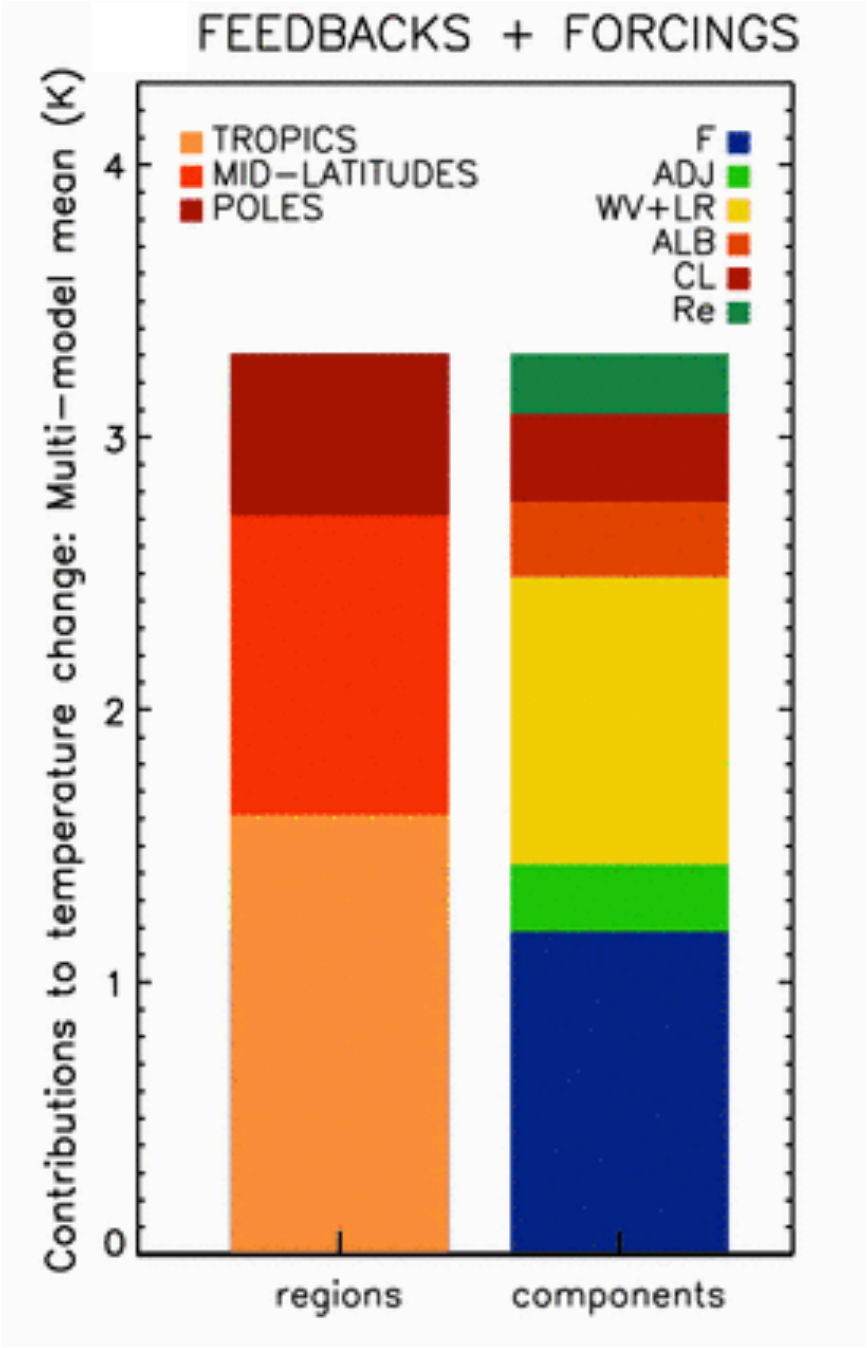

Figure 12: The CMIP5 multi-model mean of the equilibrium climate sensitivity estimate, separated into regional contributions from the tropics (between 30°S and 30°N), the mid-latitudes (between 30° and 60° in each hemisphere) and the poles (between 60° and 90° in each hemisphere) (left) and into its different components, including the Planck response to stratosphere-adjusted forcing (F), the Planck response to the adjustments to CO_2 forcing and land surface warming (ADJ), the combined water vapor and lapse rate (WV+LR), the albedo (ALB), the cloud (CL) feedbacks and the feedback residual term (Re) (right). Taken from Figure 5a of Vial, Dufresne, and Bony 2013.

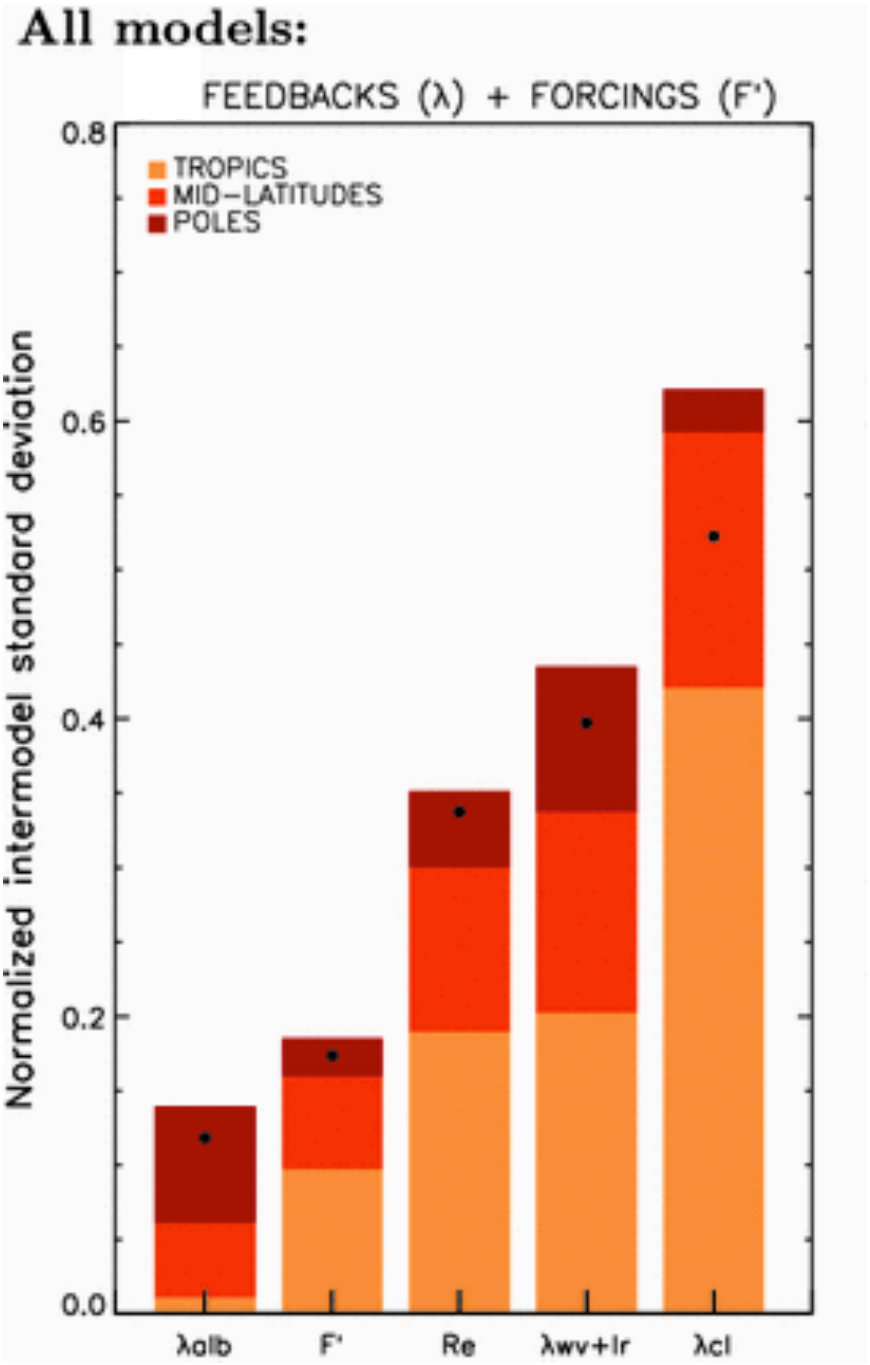

Figure 13: The CMIP5 inter-model standard deviation of equilibrium climate sensitivity estimates associated with the atmosphere-adjusted forcing (F', which includes the Planck response to the stratosphere-adjusted forcing and to the adjustments) and the feedbacks (albedo λ_{alb}, water vapor and lapse rate λ_{wv+lr}, and cloud λ_{cld}) as well as a residual (Re) in each region, normalized by the inter-model standard deviation of ΔT_s^e (no units). Note that for this metric, the contributions from the different regions are not additive, and the normalized inter-model standard deviation of ΔT_s^e over the globe is reported as black dots. Taken from Figure 6a of Vial, Dufresne, and Bony 2013.

nitude of the mid-latitude warming is a large contributor to the model uncertainty in the global-mean warming response. Figure 13 further decomposes the contributors to the model uncertainty in the global-mean warming response by region as well as by climate process (adjusted forcing and feedbacks). Although the global-mean cloud radiative feedback is not the largest contributor to the magnitude of the warming response (dark red in right bar of Figure 12), it is clear from Figure 13 that the cloud radiative feedback in the tropics alone is the single largest culprit in the uncertainty in the magnitude of the warming response. The mid-latitude cloud radiative feedback also contributes substantially to the the model response uncertainty, comparable to the albedo feedback, the tropical water vapor and lapse rate feedback, and the adjusted radiative forcing by CO_2 itself, despite the mid-latitude cloud radiative feedback's being much less studied. Understanding and constraining the mid-latitude cloud radiative feedback seems to be a promising approach toward increasing confidence in predictions of future climate.

The cloud radiative feedback exhibits a strong and robust warming in the regions between the tropics and the high-latitudes (see, e.g., Figure 14, 33, and 34 herein, and Figure 7 of Zelinka, Zhou, and Klein 2016). However, understanding of this strong and robust climate feedback remains unclear. In this thesis, we address the gap in our knowledge of the cloud radiative feedback by focusing on the cloud radiative feedback in the mid-latitudes.

There has recently been some work on quantifying and understanding the mid-latitude cloud radiative feedback. The proposed mechanism for the mid-latitude cloud radiative feedback, as articulated and popularized by the IPCC (Boucher et al. 2013) is that as the storm tracks shift poleward, storm clouds will shift from lower latitudes with stronger insolation to higher latitudes with weaker insolation, resulting in a net warming and hence a positive cloud radiative feedback. This has been referred to as a cloud curtain effect (Tselioudis and Konsta 2017) because the radiative effect is analogous to opening the cloud curtain and letting in more sunlight (Tselioudis and Konsta 2017)

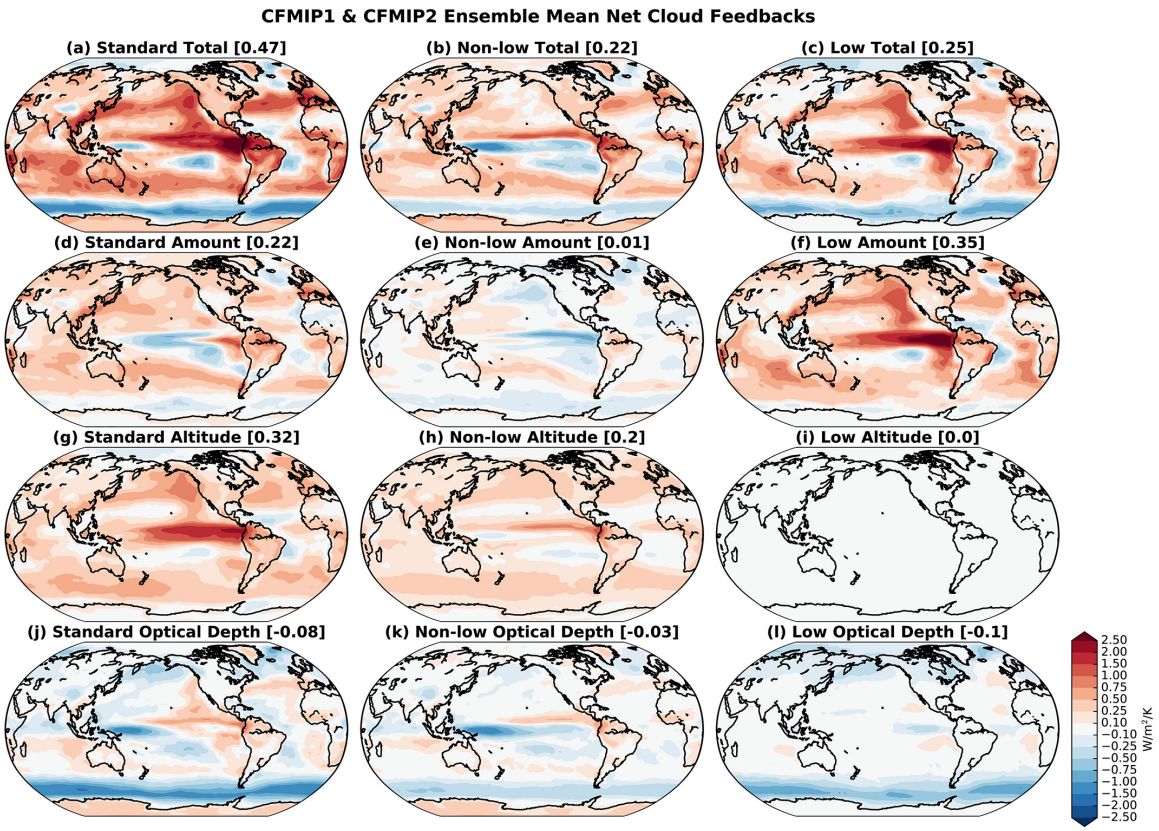

Figure 14: Multi-model mean net cloud feedback and its breakdown into amount, altitude, and optical depth components. Decompositions are computed using (a, d, g, and j) all clouds, (b, e, h, and k) only free tropospheric clouds with cloud top pressure $\leq$680 hPa, and (c, f, i, and l) only low clouds with cloud top pressure $>$680 hPa. Global mean values (in $Wm^{-2}K^{-1}$) are shown in brackets in the title of each panel. Taken from Figure 2 of Zelinka, Zhou, and Klein 2016.

However, the recent literature has also presented evidence that disputes this proposed mechanism. The common justification that has been argued is that the shortwave cloud radiative feedback projected from the shortwave cloud radiative anomalies associated with inter-annual shifts of the mid-latitude eddy-driven jet together with projections of the CO_2-forced poleward shift of the mid-latitude eddy-driven jet is too weak compared to the realized shortwave cloud radiative feedback as predicted from state-of-the-art global climate models (Kay et al. 2014; Ceppi and Hartmann 2015). There is, however, some nuance to this.

Time-series analysis of satellite-derived observational data by Bender, Ramanathan, and Tselioudis 2012 suggest that mid-latitude clouds have shifted poleward over the last 30 years in all ocean basins and seasons, and that this has resulted in a net positive shortwave radiative feedback. Bender, Ramanathan, and Tselioudis 2012 attribute those poleward shifts in the mid-latitudes clouds primarily to poleward shifts in the mid-latitude eddy-driven jet. Eastman and Warren 2013 find similar poleward shifts in the mid-latitude clouds using surface-based cloud observations. Further, Li et al. 2014 show that in the wintertime (December, January, February; DJF) North Atlantic, high clouds shift consistently with the sign of the Northern Annular Mode and North Atlantic Oscillation; that is, high clouds shift poleward with poleward shifts of the circulation. They also find longwave cloud radiative anomalies that are consistent with high cloud shifts: longwave cloud radiative warming on the poleward flank of the storm track where the high clouds have increased, and longwave cloud radiative cooling on the equatorward flank of the storm track where the high clouds have decreased. However, Li et al. 2014 suggest that the shortwave cloud radiative anomalies with meridional shifts in the circulation are negligible in the wintertime North Atlantic.

In a modeling study using the National Center for Atmospheric Research (NCAR) Community Atmospheric Model, version 3 (CAM3; Collins et al. 2006) coupled to a slab ocean, Grise et al. 2013 show that over the summertime (DJF) Southern Hemisphere, high clouds shift consistently with the sign of the Southern Annular Mode; that is, high clouds shift poleward with poleward shifts of the circulation. They also find consistent longwave cloud radiative anomalies. In contrast to Li et al. 2014, Grise et al. 2013 find large positive shortwave cloud radiative anomalies and attribute them to poleward shifts in the mid-latitude eddy-driven jet. Kay et al. 2014, however, using a newer version of the model used by Grise et al. 2013 – the Community Earth System Model with the Community Atmosphere Model version 5 (CESM?CAM5; Hurrell et al. 2013) – and with coupling to fully-dynamic

ocean, suggest that in the summertime Southern Hemisphere, the cloud changes forced by increasing concentrations of CO_2 are not related to shifts of the eddy-driven jet but rather are related to thermodynamic changes. Ceppi and Hartmann 2015 support and extend the work of Kay et al. 2014, showing that the magnitude of the CO_2-forced annual-mean shortwave cloud radiative response in the Southern Hemisphere as well as in the North Atlantic and North Pacific cannot come from eddy-driven jet shifts alone.

Toward a resolution of the disagreeing results, Grise and Polvani 2014b find that the shortwave cloud radiative anomalies associated with the inter-annual variability of the summertime Southern Hemisphere eddy-driven jet are strongly dependent on the model used: models with the correct observed magnitude but incorrect spatial pattern of climatological shortwave reflection by clouds (Type I models) display substantial shortwave cloud radiative anomalies with eddy-driven jet shifts, while models with the correct observed spatial pattern but deficient magnitude of climatological shortwave reflection by clouds (Type II models) do not display any large shortwave cloud radiative anomalies with eddy-driven jet shifts. Grise and Medeiros 2016 suggest that the behavior of the Type I models stems largely from a univariate dependence of shortwave cloud radiative anomalies on subsidence while the shortwave cloud radiative anomalies of Type II models and the observations are dependent on both subsidence as well as the strength of the boundary inversion.

In this thesis, we seek to reconcile the diverse findings of the previous observational and modeling work on the linkages between clouds and circulation in the mid-latitudes. We here propose and explore an alternate mechanism for the both mid-latitude cloud radiative anomalies on inter-annual time-scale and the response to increasing CO_2 concentrations – namely, that the Hadley circulation is a key explanatory factor.

The expansion of the Hadley circulation has been listed as a potential mechanism for cloud radiative feedbacks in Boucher et al. 2013. Norris et al. 2016 mention the expansion of the tropical circulation as a possible explanation for reduced cloudiness in the sub-tropics

and lower mid-latitudes over the last 30 years. Bender, Ramanathan, and Tselioudis 2012, like much of the work, highlight the importance of meridional shifts of the storm track, but discuss that expansion of the Hadley circulation may explain why they find a stronger poleward shift of clouds on the equatorward flank of the storm track compared to that on the poleward flank of the storm track.

Analyses of weather data for the observational era find consistent poleward shifts in the mid-latitude eddy-driven jets or storm tracks mostly in the SH summer and autumn seasons (e.g. Fyfe 2003; Wang, Swail, and Zwiers 2006). The North Atlantic eddy-driven jet does not robustly shift poleward during winter, and the North Pacific eddy-driven jet robustly shifts poleward only during autumn (Barnes and Polvani 2013; Grise and Polvani 2016). Analyses of the tropical circulation, however, find consistent signs of poleward expansion of the Hadley circulation across all regions and seasons (e.g. Seidel et al. 2008; Johanson and Fu 2009; Schwendike et al. 2015; Grise and Polvani 2016), and so the poleward expansion of the Hadley circulation may be a more robust dynamical response to increasing CO_2 concentrations than the poleward shift of the storm tracks.

Grise and Polvani 2014a and Grise and Polvani 2016 find that among three metrics of the magnitude of the dynamical change that results from increasing concentrations of CO_2 – poleward shifts of the eddy-driven jet latitude, poleward shifts of the edge latitude of subtropical dry zone, and poleward shifts of the edge latitude of the Hadley circulation – only the poleward shift in the Hadley circulation edge latitude correlates significantly with the equilibrium climate sensitivity metric of the CO_2-forced thermodynamic change. That is, the Hadley circulation, being a mediator between the thermally-driven tropics and the eddy-driven extra-tropics, might serve as a convenient bridge between atmospheric thermodynamics and dynamics that may help to explain recent past climate changes as well as help to predict future climate changes in cloud radiative properties associated with increasing concentrations of CO_2.

In this thesis, we analyze the linkages between mid-latitude clouds and the large-scale atmospheric circulation using three main approaches: analysis of satellite-retrieval observations and re-analysis data, analysis of a suite of fully-coupled global climate models, and numerical experiments with an idealized model of the global climate. The structure of this thesis follows accordingly.

In Chapter 2, we quantify the linkages between mid-latitude clouds, their radiative effects, and the large-scale atmospheric circulation with a comprehensive correlative analysis of the observations of the recent past. We find that, as hypothesized, the only correlation among indices of clouds, their radiative effects, and the large-scale circulation on inter-annual timescales that is robust against ocean basin and season is the relationship between clouds and the Hadley circulation. In light of this result, we suggest that the recent trends in cloudiness might be better explained by the poleward expansion of the Hadley circulation rather than the poleward shift of the storm track.

Studying how clouds, their radiative effects, and dynamics mutually co-vary on inter-annual time-scales can be an invaluable tool for understanding the nature and mechanisms of their interaction, for producing meaningful metrics for model evaluation, and for constraining the forced response to increasing CO_2 concentrations. In Chapter 3, we quantify the linkages between mid-latitude clouds and the Hadley circulation in global climate models to evaluate whether climate models can simulate the consistent and robust relationships found from the observations in Chapter 2. We find that model representations of the unforced control climate are systematically biased away from the observations. In particular, models exhibit too much shortwave cloud radiative warming in association with inter-annual poleward shifts of the Hadley circulation edge latitude. Models also tend to locate their climatological circulations too far equatorward in comparison to the observations. We present evidence to suggest that the systematic model bias in the position of the climatological circulation might explain the bias in cloud-circulation coupling, as well as might

constitute an emergent constraint on the model response to increasing CO_2 concentrations.

In Chapter 4, we verify the mechanism derived from the correlative analysis of fully-coupled global climate models in Chapter 3 through targeted numerical simulations using an idealized model of the global climate. While previous work has highlighted model uncertainty related to cloud thermodynamic changes, we demonstrate that much of the model biases in the coupling between mid-latitude clouds and the general circulation as well as the model spread in the mid-latitude shortwave cloud radiative feedback are in fact a result of the biases in the model representation of the location of the present-day circulation. Thus, an improved representation of the large-scale atmospheric circulation in models can lead to a substantial improvement in the representation of model clouds in the present day climate and more confident predictions of cloud changes in the future climate.

In Chapter 5, we conclude with a summary of our findings and a presentation of the questions that remain to be addressed in future work.

Chapter 2

Quantifying observed linkages between clouds and the general circulation of the atmosphere:

The Hadley circulation as a key dynamical indicator

2.1 Introduction

Maximal incoming solar radiation near the equator induces a thermally-direct convective circulation, the Hadley circulation, which is key for the transport of heat, angular momentum, and moisture from the tropics to the extra-tropics. Synoptic-scale baroclinic waves tap into the potential energy available from the differential heating between the equator and the pole, continue the poleward transport of heat, momentum, and moisture, and drive a westerly mid-latitude jet. These aspects of the general circulation of the atmosphere characterize both the short-term surface weather conditions – the Hadley circulation helps to set the extent of the sub-tropical minimum in precipitation (e.g. Hu and Fu 2007), the regions of large baroclinic wave activity help to set the mid-latitude precipitation maximum (e.g. Bender, Ramanathan, and Tselioudis 2012), etc. – and the long-term climate state.

The general circulation of the atmosphere also helps to determine whether clouds develop and what are their properties. Broadly, the regions of mean downward atmospheric motions associated with, for example, the descending branch of the Hadley circulation, are conducive to the formation of low-level clouds such as stratocumulus and cumulus, while the regions of mean upward atmospheric motions associated with, for example, the cold

fronts along the storm tracks are conducive to the formation of high-level clouds such as cumulonimbus. Conversely, clouds, by trapping longwave radiation and reflecting solar radiation, play a key role in the radiative budget of the Earth and influencing the thermal structure of the atmosphere.

The latitudinal structure of the net radiative energy budget drives a circulation which sets the dynamical conditions for the formation of clouds which, in turn, modify the energy budget. Understanding the complex mutual interactions among clouds, their radiative effects, and the general circulation of the atmosphere remains a major open question in scientific knowledge of the present-day climate and a leading source of uncertainty for predictions of future climate (see e.g. Bony and Dufresne 2005; Trenberth and Fasullo 2010; Bony et al. 2015).

A priori, one might hypothesize that changes in the characteristics of the general circulation would directly induce changes in clouds and their radiative properties that are important for determining the global-mean climate feedback onto CO_2-forced warming. For example, with more intense extra-tropical storms, one might expect to see deeper and brighter clouds (Tselioudis and Rossow 2006). However, the future intensity and frequency of extra-tropical storms are not robustly predicted by climate models (Geng and Sugi 2003; Booth, Wang, and Polvani 2013).

The robust dynamical climate changes that are predicted in response to increasing CO_2 concentrations include a poleward shift of the tracks of storms (Yin 2005; Barnes and Polvani 2013), and a poleward expansion of the tropical circulation (Hu and Fu 2007; Lu, Vecchi, and Reichler 2007; Lu, Deser, and Reichler 2009). With a poleward shift of atmospheric circulation, one might expect a concomitant poleward shift of cloudiness, the net radiative effect of which would be akin to pulling back the curtain of clouds and letting in more sunlight (see Chapter 1 and Bender, Ramanathan, and Tselioudis 2012; Tselioudis and Konsta 2017) – a positive cloud radiative feedback. The majority of climate models

included in the Intergovernmental Panel on Climate Change Fifth Assessment Report produce a positive mid-latitude cloud radiative feedback (Boucher et al. 2013). However, more recent modeling studies reveal diverse model behavior with respect to cloud and radiation changes with shifts of the eddy-driven jet in the Southern Hemisphere (Grise et al. 2013; Kay et al. 2014; Grise and Polvani 2014b).

Previous work has focused primarily on analyzing model cloud behavior that is known to be biased, has concentrated on the summertime Southern Hemisphere, and has been concerned mainly with eddy-driven jet shifts (see Chapter 1). Extensive satellite-retrieval observations of the climate system over the last 30 years and comprehensive reanalysis datasets provide an opportunity to examine cloud-dynamics interactions beyond the summertime Southern Hemisphere and using a broader array of metrics for the general circulation than the eddy-driven jet. We here emphasize that we perform a comprehensive observational analysis: we synthesize and advance the previous piecemeal approaches by instead surveying all seasons and all mid-latitude ocean basins; and, we incorporate and extend the results from previous studies who focus on one metric for the dynamics and one metric for the clouds by instead assessing the correlations among as broad of an array of dynamical indices that we believe measure the mid-latitude circulation and all the parameters of clouds and their properties available from satellite-retrievals.

Studying how clouds, their radiative effects, and dynamics mutually covary on inter-annual time scales can be a useful tool for understanding the nature and mechanisms of their interaction, and for producing meaningful constraints for model evaluation. In this chapter, we use satellite observations and reanalysis data to perform an extensive analysis of the inter-annual relationships among mid-latitude clouds, their radiative effects, and the latitudinal position of the general circulation. We describe in detail the data and methodology in Section 2.2. In Sections 2.3 and 2.4 we discuss the results from the analysis of the correlations among multiple dynamical indices and a suite of cloud and radiation properties. We

expand on the previous literature by adding the Hadley circulation to the list of dynamical indicators and by exploring the relationships in all ocean basins and seasons. Finally, in Section 2.5 we consider the poleward cloud shifts over the last 30 years in the context of the observed relationships between clouds and atmospheric dynamics.

2.2 Data and Methods

In this section, we describe in detail the data and methods used in this chapter and throughout the remainder of this thesis.

Data

International Satellite Cloud Climatology Project (ISCCP) D2

Satellite-derived observations of cloud properties are taken from the NASA Goddard Institute for Space Studies International Satellite Cloud Climatology Project (ISCCP) D2 (Rossow and Schiffer 1999). The ISCCP-D2 dataset has temporal coverage from July 1983 to December 2009 with three-hourly sampling and spatial resolution of approximately 30 km. Temporally (i.e., monthly) averaged fractional areal cloud cover of larger regions are the product of instantaneous fractional areal cloud cover and the frequency of occurrence.

There are known systematic biases in the dataset that inform our methodological choices. First, the ISCCP-D2 satellites are passive remote sensors, so that their top-down view of high-level clouds may obscure lower-level clouds.

The calibration of the satellite measurements is done against the Earth excluding clouds, rather than with satellite radiometers, under the assumption that the negligible temporal variations of the Earth yield a more accurate calibration target than could the radiometers. Hence, temporal changes of the Earth itself become the satellite error. Additionally, inhomogeneities in instrumentation, such as switching satellites, may result in spurious

long-term trends. Consequently, ISCCP data cannot be used to detect global, long-term, or linear trends. However, regional, short-term, and non-linear changes can be tracked reliably. Nevertheless, some regional discontinuities, or "seams", notably over the Indian Ocean and at times over the North Atlantic, may appear due to observation of adjacent regions by different geostationary satellites (Brest, Rossow, and Roiter 1997).

The ISCCP-D2 dataset is *retrieved* from observed radiative fluxes available from two wavelengths – infrared (IR; 11 μm) and visible (VIS; 0.6 μm) – and is not equivalent to a direct observation. When a pixel is determined to be cloudy, the retrieved IR radiance is compared to the NASA GISS radiative transfer model to calculate the cloud top temperature, and the retrieved VIS radiance is used to calculate the visible optical thickness. Cloud top pressure is calculated from the cloud top temperature using an observed vertical temperature profile. Cloud top pressure or height must be interpreted as a radiative cloud top pressure or height; i.e., the vertical level at which significant cloud mass is first encountered. It is thus biased low.

Total cloud amounts are too low over land by 0.10 (of fractional areal cloud cover) compared directly to matching surface observations (Warren et al. 1986; Warren et al. 1988), less in summer but more in winter. We thus focus on the retrievals over the ocean basins. Upper-level cloudiness is low by 0.05 to 0.10 compared to observations by Stratospheric Aerosol and Gas Experiments (SAGE; Liao, Rossow, and Rind 1995) and by two different analyses of High-Resolution Infrared Sounder (HIRS) data (Jin, Rossow, and Wylie 1996; Stubenrauch et al. 1999) due mostly to non-detection of optically-thin cirrus (Wielicki and Parker 1992). However, the IR retrievals may be a useful proxy for the longwave radiative effect of these high clouds. Polar cloud amounts are too low by 0.15 to 0.25 in summer (Schweiger and Key 1992; Rossow and Garder 1993) and are too high by 0.05 to 0.10 in winter (Curry et al. 1996) compared to surface observations. We therefore restrict our analysis to latitudes between 65°S and 50°N.

ISCCP-FD

We compute the influence of clouds on the radiative energy budget using the cloud radiative effect metric. The cloud radiative effect (CRE) is defined as the clear-sky upwelling radiative flux at TOA minus the all-sky upwelling radiative flux at TOA:

$$CRE = R_{clear} - R_{all} \tag{2.1}$$

for both shortwave (SW) and longwave (LW) radiative fluxes at TOA. Shortwave and longwave clear-sky and all-sky upwelling radiative fluxes at TOA are obtained from the NASA GISS ISCCP-FD data set (Zhang et al. 2004). Data is available at three hour time steps with global coverage on a 2.5 equal-area map (approximately 280 km intervals) and with temporal coverage from July 1983 to December 2009.

The ISCCP-FD dataset is derived from the 2001 NASA GISS GCM radiative transfer model (Hansen et al. 2002; Oinas et al. 2001) using modifications to ISCCP-D1 as the input data. The GISS GCM radiative transfer model defines SW as 0.2 to 5.0 μm and LW as 5.0 to 200.0 μm. Modifications to the ISCCP-D2 input are required due to the treatment of ice, cloud vertical structure, diurnal variations, and cloud inhomogeneities. For the LW fluxes, the GISS GCM does not explicitly model multiple scattering, but does parameterize its effects as corrections to the outgoing TOA flux.

The input satellite-retrieval dataset – ISCCP-D1 – does not sample all of the Earth at every 3-hourly timestep. Empty cells typically account for 15% of all grid boxes. To make ISCCP-FD globally complete, a procedure using a sliding 3-year climatology from ISCCP-D2 is used to fill in any empty cells with the surface properties, such as surface temperature, as well as with the cloud properties for each of the 15 cloud types; e.g. stratocumulus, stratus, cumulonimbus, etc.

We note here that we have also analyzed the TOA radiative fluxes derived from the

Clouds and Earth's Radiative Energy System Energy Balanced and Filled (CERES-EBAF) version 2.7 (Loeb et al. 2012), which is more finely resolved, but covers a much shorter temporal record (between March 2000 and June 2013). The shorter time-series is a serious disadvantage, as we must rely on the robustness of the statistics in our necessarily correlative analysis.

European Centre for Medium-Range Weather Forecasting (ECMWF) Interim Reanalysis (ERA-Interim)

Dynamics (e.g., zonal wind at 850 hPa, zonal-mean meridional wind, pressure vertical velocity at 500 hPa, mean sea level pressure, total precipitation, evaporation) are taken from the European Centre for Medium-Range Weather Forecasting (ECMWF) Interim Reanalysis (ERA-Interim), which produces a multi-variate, globally complete, consistent record of the atmosphere (Dee et al. 2011). In each 12-hour analysis cycle, bias-corrected observations, the majority of which derive from satellites, are combined with the ECMWF Integrated Forecast System output from the previous analysis cycle to initialize a short-range forecast for the next analysis cycle. Although constrained by observational data, reanalysis data are not equivalent to observations, and yet are still affected by the satellite biases and changes in calibration. The representation of climate signals. i.e. trends, in reanalysis is thus affected by changes in the global observing system and by the presence of time-varying biases in models and observations.

The energy balance at the surface boundary is poor, with a global imbalance of 6.9 Wm^{-2}. The imbalance occurs primarily over the oceans and is associated with an increase in net solar radiation there. Kållberg 2011 suggests that the model clouds are the major contributor to the imbalance in surface energy, and are likely to be unrealistic indicators of actual cloudiness. We therefore do not include ERA-Interim clouds in our analysis, although one might consider them to be more internally consistent with the dynamical indicators

derived from ERA-Interim.

NASA Earth Science Program for Modeling, Analysis, and Prediction (MAP) Climatology of Mid-latitude Storminess (MCMS)

The definition of the storm track requires cyclone tracking. We use the NASA MAP (Modelling, Analysis, and Prediction) Climatology of Mid-latitude Storminess (MCMS) cyclone tracking algorithm, which identifies storms in space and tracks them in time. It has been shown that the characteristics of the storm track are sensitive to the choices that must be made in tracking the cyclones (Bauer, Tselioudis, and Rossow 2016). We describe these choices below, as they are likely to limit the generalizability of the results derived therefrom.

The storms which constitute the storm track are sufficiently long-lived extra-tropical synoptic-scale low-pressure weather systems. Cyclones are first identified as sufficiently low local (defined by a critical radius dependent on wavenumber and latitude) minimum in an input sea level pressure (SLP) field. The sea level pressure field is low pass filtered at wavenumber 13 to identify synoptic systems, and is processed only poleward of about 30° to identify extratropical cyclones. Cyclones must meet a local Laplacian criteria. Physically, this means that cyclone centers must be sufficiently vortical, since the relative geostrophic vorticity is proportional to the Laplacian of pressure assuming constant density and the f-plane approximation. Cyclones are also required to be trackable; that is, having a center within the region defined by both the critical radius and the maximum propagation speed from the previous or next time step.

Tracking in time is based on three principles: "change is gradual", "stay the course", and "close is best". Centers with smaller changes in SLP over time are connected together rather than with centers with larger changes in SLP over time. Centers with smaller changes in direction are connected together rather than centers with larger changes in direction.

Centers with smaller changes in distance are connected together rather than centers with larger changes in distance, Tracked storms are required to last more than 24 hours and to have traveled at least 200 km to avoid stationary tracks.

Methodology

Throughout this chapter and the remainder of this thesis, we characterize the latitudinal position of the atmospheric circulation by first taking the zonal mean then performing analysis as opposed to performing analysis on each longitude then zonally averaging. This is done to give more weight to longitudes with larger values of the variable of interest. We also leverage the natural smoothing of integration over differentiation in, for example, our choice of the definition of the mid-latitude eddy-driven jet latitude.

We note that we have tried different methods for defining and computing the following indices, and our results are largely insensitive to the specific choices we have made.

Regional Definitions

Using regionally averaged fields is motivated by the need to analyze the Pacific and Atlantic ocean basins separately in the Northern Hemisphere. We separate our analysis into three broad regions: the Southern Hemisphere, the North Atlantic, and the North Pacific. The North Atlantic is delineated by the longitudinal boundaries 280°E to 360°E and North Pacific is delineated by the longitudinal boundaries 120°E to 240°E, as in Bender, Ramanathan, and Tselioudis 2012.

Edge of the Hadley Circulation

Global The Hadley circulation is canonically defined as a zonal-mean circulation. From the equation of conservation of mass on a sphere with longitude λ and latitude θ, and using

pressure as the vertical coordinate

$$\frac{1}{a\cos\theta}\frac{\partial}{\partial\lambda}u + \frac{1}{a\cos\theta}\frac{\partial}{\partial\theta}\Big(v\cos\theta\Big) + \frac{\partial}{\partial p}\omega = 0 \tag{2.2}$$

we take the zonal mean $[\cdot] \equiv \frac{1}{2\pi}\int_0^{2\pi} \cdot\, d\lambda$ such that Equation 2.2 reduces, by applying periodic boundary conditions in λ and multiplying by the metric term $a\cos\theta$, to

$$\frac{\partial}{\partial\theta}\Big([v]\cos\theta\Big) + \frac{\partial}{\partial p}\Big(a\,[\omega]\cos\theta\Big) = 0 \tag{2.3}$$

We can define a streamfunction ψ by

$$\frac{\partial}{\partial p}\psi = [v]\cos\theta \tag{2.4}$$

$$\frac{\partial}{\partial\theta}\psi = -a\,[\omega]\cos\theta \tag{2.5}$$

such that we satisfy Equation 2.3 identically. Integration of Equation 2.4, assuming $\psi\,(\theta, p = 0) = 0$, yields

$$\psi = \cos\theta\int_0^p [v]\,d\tilde{p} \tag{2.6}$$

With proper scaling, we can interpret $\psi\,(\theta, p)$ as a northward mass flux through latitude θ vertically integrated from pressure level p to TOA ($p = 0$). Scaling pressure by gravitational acceleration g yields mass per unit height by hydrostasy such that $\int_0^p [v]\,\frac{d\tilde{p}}{g}$ is the zonally averaged the northward mass flux integrated from p to TOA. This, multiplied by the circumference of the latitude circle $2\pi a\cos\theta$ yields the total vertically integrated northward mass flux $2\pi a\cos\theta\int_0^p [v]\,\frac{d\tilde{p}}{g}$. Consequently, for physical interpretability, we define

the meridional mass streamfunction Ψ in terms of Equation 2.6

$$\Psi = \frac{2\pi a}{g}\psi \tag{2.7}$$

We define the edge of the Hadley circulation θ_{HC} as the the first latitude from the equator that the mass flux at $500\,\text{hPa}$ changes from poleward to equatorward; i.e. $\Psi\left(\theta_{HC}, p = 500\,\text{hPa}\right) = 0$. The $500\,\text{hPa}$ pressure level is chosen as representative of the free troposphere, away from boundary effects at the tropopause and at the surface. To compute the edge of the Hadley circulation, we linearly interpolate to 0.01° resolution between the two gridpoints where $\Psi\left(\theta_{HC}, p = 500\,\text{hPa}\right)$ changes sign.

Local We express the mass continuity Equation 2.2 as

$$\nabla_p \cdot \mathbf{u} + \frac{\partial}{\partial p}\omega = 0 \tag{2.8}$$

where **u** necessarily represents the divergent component of the horizontal velocity and ∇_p the isobaric gradient operator in spherical coordinates. Following Schwendike et al. 2014 we can define an intermediate velocity potential θ with $\nabla_p\theta \equiv \mathbf{u}$ and a potential function χ with $\Theta = \frac{\partial}{\partial p}\chi$, so that Equation 2.8 becomes

$$\frac{\partial}{\partial p}\left(\nabla_p^2\chi + \omega\right) = 0 \tag{2.9}$$

Taking $\nabla_p^2\chi$ and ω to be 0 at the vertical boundaries, we obtain

$$\nabla_p^2\chi = -\omega \tag{2.10}$$

Given $\omega\left(\theta, \lambda\right)$ with time t and pressure level p fixed, we solve for $\chi\left(\theta, \lambda\right)$ by eigenfunction decomposition. We switch to the latitudinal coordinate $\phi \equiv \sin\theta$ for simplicity. The

eigenfunctions of the ∇_p operator are the spherical harmonic functions $Y_{m,n}(\phi, \lambda)$ with corresponding eigenvalues $-\frac{n(n+1)}{a^2}$. We express

$$\chi = \sum_{m,n} \tilde{\chi}_{m,n} Y_{m,n} \tag{2.11}$$

$$\omega = \sum_{m,n} \tilde{\omega}_{m,n} Y_{m,n} \tag{2.12}$$

where, by orthogonality, the coefficients are given by

$$a_{m,n} = \frac{1}{4\pi} \int_{\lambda=0}^{\lambda=2\pi} \int_{\phi=-1}^{\phi=1} Y^*_{m,n} a(\phi, \lambda)\, d\phi d\lambda \tag{2.13}$$

with $Y^*_{m,n}$ denoting the complex conjugate of $Y_{m,n}$. Substituting Equations 2.11 and 2.12 into Equation 2.10, using linearity, the eigenvalues, and orthogonality, we obtain

$$\tilde{\chi}_{m,n} = \frac{a^2}{n(n+1)} \tilde{\omega}_{m,n} \tag{2.14}$$

so that

$$\chi(\phi, \lambda) = \sum_{m,n} \frac{a^2}{n(n+1)} \frac{1}{4\pi} \int_{\lambda=0}^{\lambda=2\pi} \int_{\phi=-1}^{\phi=1} Y^*_{m,n} \omega(\phi, \lambda)\, d\phi d\lambda\, Y_{m,n}(\phi, \lambda) \tag{2.15}$$

Following Keyser, Schmidt, and Duffy 1989, we define a $\boldsymbol{\psi}$ vector streamfunction

$$\boldsymbol{\psi} \equiv -\nabla_p \chi \tag{2.16}$$

such that

$$\psi_\theta = -\frac{1}{a} \frac{\partial}{\partial \phi} \Big(\chi \cos\theta \Big) \tag{2.17}$$

Using the same scaling argument of the canonical Hadley circulation, we can define a local Hadley circulation

$$\Psi_\theta(\theta, \lambda, p) = -\frac{2\pi a \cos\theta}{g}\psi_\theta\Big|_{\phi\to\theta} \tag{2.18}$$

The regional Hadley circulation $[\Psi_\theta]_{\lambda_1}^{\lambda_2}$ is defined as for an interval of longitudes (λ_1, λ_2)

$$[\Psi_\theta]_{\lambda_1}^{\lambda_2} \equiv \frac{1}{\lambda_2 - \lambda_1}\int_{\lambda_1}^{\lambda_2} \Psi_\theta d\lambda \tag{2.19}$$

The edge of the regional Hadley circulation is defined and computed as it is for the the canonical zonal-mean Hadley circulation. The regional Hadley circulation is used only for analysis of the Northern Hemisphere regions. Since the edge of the regional Hadley circulation is poorly defined in June-July-August (JJA), the canonical zonal-mean edge of the Hadley circulation edge is used.

Edge of the Dry Zone

Given the zonally averaged precipitation minus evaporation $[P - E]$, we define the latitudinal edge of the subtropical dry zone as the first latitude from the equator, poleward of the subtropical minimum, that there is net precipitation; i.e. $[P - E] > 0$. The latitude of the edge of the regional subtropical dry zone is defined using the regionally averaged precipitation minus evaporation $[P - E]_{\lambda_1}^{\lambda_2} = \frac{1}{\lambda_2 - \lambda_1}\int_{\lambda_1}^{\lambda_2} P - E\, d\lambda$.

Eddy-Driven Jet Latitude

We define the latitude $\theta_{u_{850}}$ of the mid-latitude eddy-driven jet as the center of mass of the zonal-mean westerly wind at 850hPa $[u_{850}]$

$$\theta_{u_{850}} = \frac{\int_\Theta [u_{850}]\,\theta\cos\theta\, d\theta}{\int_\Theta [u_{850}]\cos\theta\, d\theta} \tag{2.20}$$

where Θ represents the interval of latitudes for which $[u_{850}] > 0$ and that contain the maximum zonal mean westerly wind. The latitude of the regional eddy-driven jet is defined using the regionally averaged westerly wind $[u_{850}]_{\lambda_1}^{\lambda_2} = \frac{1}{\lambda_2 - \lambda_1} \int_{\lambda_1}^{\lambda_2} u_{850}\, d\lambda$.

We choose the 850hPa pressure level because it is sufficiently far from the surface to avoid topographical effects but sufficiently close to the surface to avoid confounding it with the upper-level angular-momentum conserving sub-tropical jet. This definition takes into account not only the latitude at which the zonal mean westerly wind is maximum, but the width of the eddy-driven jet as well as the sphericity of the Earth.

We note that the results derived from using this definition of the eddy-driven jet seem to be robust against different definitions; e.g. finding the maximum of a quadratic fit to the gridpoint of the maximum u850 and the two adjacent points (Barnes and Polvani 2013; Grise and Polvani 2014b), and against different indices; e.g. the Southern Annular Mode (c.f. Grise et al. 2013), and the Northern Annular Mode/North Atlantic Oscillation (NAM/NAO) (c.f. Li et al. 2014).

Storm Track Latitude

The zonal mean storm density $[SD]$ is defined as the zonal-mean number of occurrences of tracked extra-tropical storms $\left[S_{\text{extratropical}}\right]$ per unit area

$$[SD] = \frac{1}{\cos\theta} \left[S_{\text{extratropical}}\right] \tag{2.21}$$

The latitude θ_{SD} of the extra-tropical storm track is defined as the center of mass of the zonally averaged storm density $[SD]$

$$\theta_{SD} = \frac{\int_\Theta [SD]\, \theta \cos\theta\, d\theta}{\int_\Theta [SD] \cos\theta\, d\theta} = \frac{\int_\Theta \theta \left[S_{\text{extratropical}}\right]\, d\theta}{\int_\Theta \left[S_{\text{extratropical}}\right]\, d\theta} \tag{2.22}$$

which is the center of mass of the number of tracked extratropical storms without taking into account the sphericity of the Earth. Here, Θ is chosen to be the interval of latitudes between 80° and 30° in both hemispheres. This interval of latitudes is chosen to capture the mid-latitudes without the spurious effects at the poles. The latitude of the regional storm track is defined using the regionally averaged storm density. Defining the storm track latitude with the storm density rather than the number of tracked storms thus gives greater weighting to the extra-tropics than to the tropics. This allows for closer representation to the conceptual storm track by providing less weight to regions where one could see tropical storms and more to regions where one expects mid-latitude cyclones.

Cloud Central Latitudes

We define the representative latitudes for each of total, high, middle, and low cloud fraction σ_i to be the center of mass of the zonal-mean cloud fraction over a pre-specified interval of latitudes $\Theta_{i,t}$

$$\theta_{\sigma_i,t} = \frac{\int_{\Theta_i} [\sigma_i]\, \theta \cos\theta \, d\theta}{\int_{\Theta_{i,t}} [\sigma_i] \cos\theta \, d\theta} \tag{2.23}$$

The interval $\Theta_{i,t}$, chosen to capture the mass of the field of interest without effects from poor satellite retrieval over polar regions. For high clouds in particular, we seek to capture the variability due to extra-tropical dynamics and mid-latitude cyclones, and so choose an interval which excludes tropical high clouds. Thus, the central latitude of the cloud fields is derived for the 25-65°N/S regions. The derivation follows the formulation in Bender, Ramanathan, and Tselioudis 2012, who calculate the latitude of the weighted center of mass of the cloud field similarly.

We avoid defining the representative cloud latitude to be the the latitude of maximum cloud fraction for various reasons: peakedness is not always robust, as the cloud field is very noisy and coarsely gridded; peakedness is not always well-defined, especially for low

clouds; and peakedness is not always meaningful, as changes in the latitude of the maximum cloud fraction may not necessarily capture systematic latitudinal changes in the cloud field. For example, removing mass on the equatorward edge of the maximum would not displace the latitude of the peak of the field, whereas it would displace the latitude of the center of mass.

Given the top-down view of the ISCCP satellite, we must estimate the true low cloud cover from the ISCCP low cloud cover (Morcrette and Fouquart 1986; Rozendaal, Leovy, and Klein 1995; Weare 2000). The ISCCP satellites observe three layers of cloud cover: high cloud fraction H_{ISCCP} which is above 440 hPa, middle cloud fraction H_{ISCCP} which is between 680 hPa and 440 hPa, and low cloud fraction L_{ISCCP} which is below 680 hPa. We assume that ISCCP observes well high-topped clouds, so that the true probability of observing a high cloud $P(H) = H_{ISCCP}$. We do not make this assumption about the true probability of observing a middle cloud $P(M)$. By the law of total probability, we have

$$P(M) = P(M \cap \neg H) + P\left(M \mid H\right) P(H) \tag{2.24}$$

We can identify the middle cloud fraction that ISCCP observes $M_{ISCCP} = P(M \cap \neg H)$. We assume random overlap, so that the ratio of the true middle cloud fraction in scenes when high clouds are absent is the same as the ratio of the true low middle cloud fraction to scenes when high clouds are present; i. e. $P(M) = P\left(M \mid H\right)$. Hence,

$$P(M) = \frac{M_{ISCCP}}{1 - H_{ISCCP}} \tag{2.25}$$

Similarly for the true probability of observing a low cloud, we have

$$P(L) = P\left(L \cap \neg(M \cup H)\right) + P\left(L \mid (M \cup H)\right) P\left((M \cup H)\right) \tag{2.26}$$

and identify $L_{ISCCP} = P\left(L \cap \neg(M \cup H)\right)$. We assume random overlap so that $P(L) = P\left(L \mid (M \cup H)\right)$. Expanding $P(M \cup H)$ and the using the random overlap assumption for middle clouds, we have

$$P(L) = \frac{L_{ISCCP}}{1 - M_{ISCCP} - H_{ISCCP}} \tag{2.27}$$

We use the estimated true probability of observing a low cloud $P(L)$ as the true fractional areal low cloud cover in the remainder of this thesis.

We note here that we have also analyzed different cloud properties derived from ISCCP-D2 and ISCCP-FD; e.g. cloud optical depth, cloud top height, cloud top pressure, cloud liquid water path, cloud ice water path, etc., and the results are consistent with those presented herein but do not add significantly enough to the analysis to warrant their inclusion into the already dense tables.

Data Analysis

Monthly data are averaged over a three-month season to account for the seasonal cycle and to ensure signals are dominated by inter-annual variability and not seasonal or sub-seasonal variability. We compute the correlations separately for all four seasons, as the cloud radiative effects are sensitive to the magnitude of the incoming solar radiation. We have also analyzed the inter-annual variability associated with the warm months (e.g. AMJJAS in the NH) and the cold months (e.g. ONDJFM in the NH), and the results are consistent with those herein, but this broad definition of the seasons masks the behavior of the equinoctial seasons (MAM and SON).

The above-defined inter-annual cloud and dynamical indices are de-trended and correlated for each season and each region to summarize the relationships. Seasonal-mean cloud and dynamical variables are linearly regressed on the seasonal-mean cloud and dynamical

indices to examine the spatial responses to a 1° poleward shift of the circulation. Zonal-mean seasonal-mean quantities are also linearly regressed on the indices. Use of regression analysis means that interpretation is limited to arguments of consistency and plausibility. The statistical significance of the correlations and linear regressions is assessed using the Student's *t*-test.

The four key indicators of the position of the atmospheric circulation are correlated with the central latitudes of the low, middle, high cloud field (defined with lids at 680hPa, 440hPa, and 50hPa, respectively) and of the total cloud field from ISCCP-D2 as well as with the mean value of the SW and LW CRE for the mid-latitude region (30-60°N/S) from the ISCCP-FD dataset. The cloud and radiation analysis is performed for the 1984-2009 period.

In order to address issues related to potential ISCCP biases related to satellite zenith angle regional variability, our analysis was repeated using the ISCCP dataset revised by Norris and Evan 2015 that aims to remove such biases. The results of that analysis were almost identical to the ones presented here, suggesting the validity of our methodological choices.

2.3 Case Studies

We begin by presenting maps of the inter-annual relationships between the clouds, and their radiative effects, and two key metrics of the atmospheric circulation. In Figure 21 we show changes in high cloud amount (left column), LW CRE (middle column), and SW CRE (right column) associated with a 1° poleward shift of the mid-latitude eddy-driven jet (top row) and the Hadley circulation edge (bottom row). Figure 21a is for the North Atlantic and Figure 21b is for the Southern Ocean. For both regions we show the DJF season, as these exemplify the results of our study. For the North Pacific, and for the the remaining seasons,

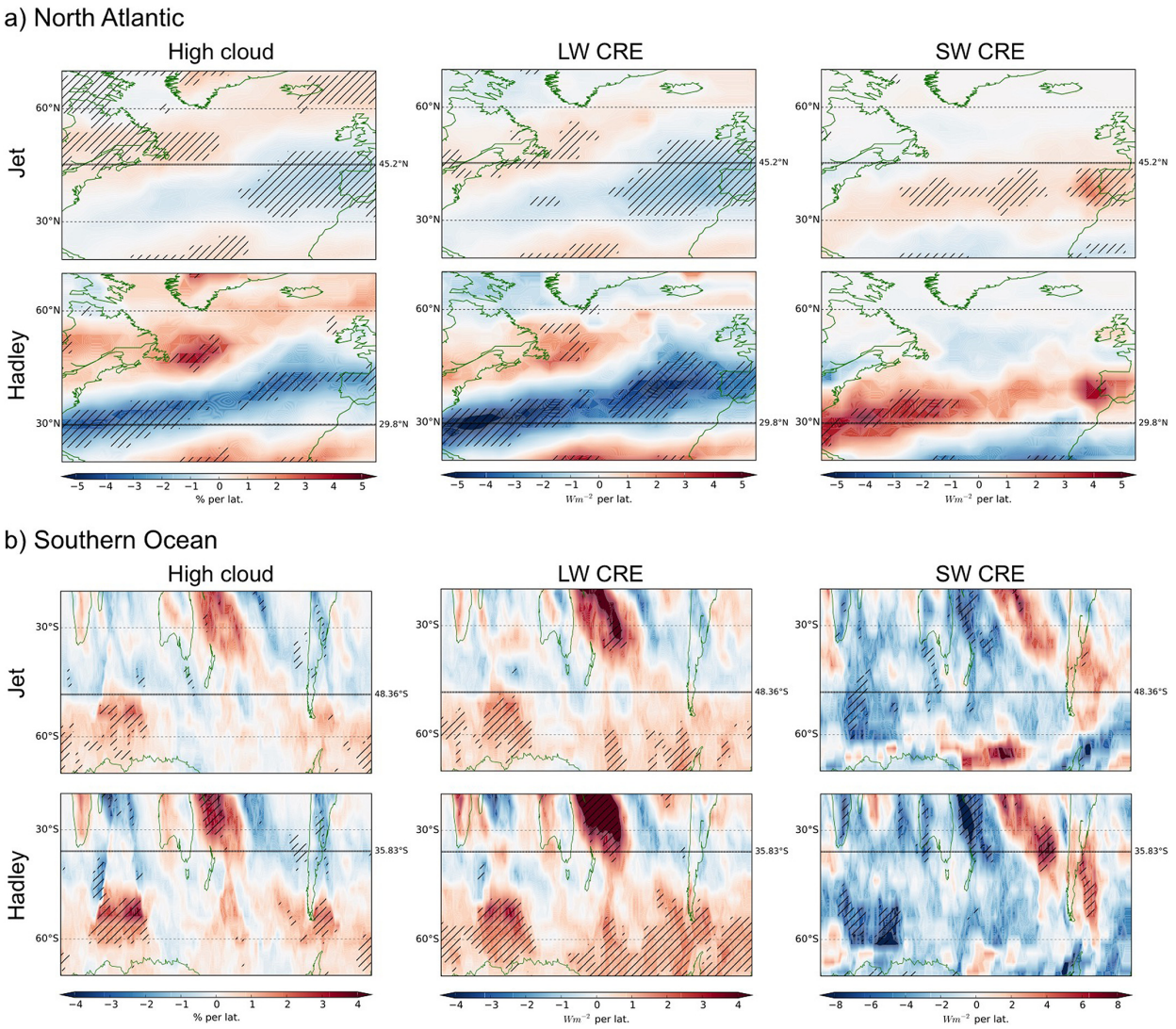

Figure 21: DJF changes in high cloud amount (left column), longwave (LW) CRE (middle column), and shortwave (SW) CRE (right column) for a 1° poleward shift of the mid-latitude eddy-driven jet latitude (top row) and the HC edge latitude (bottom row) for (a) the North Atlantic and (b) the Southern Ocean. Hatching indicates statistical significance at the 95% level. Note the different color scales.

the results will be presented below (in Table).

In wintertime North Atlantic (Figure 21a) high clouds shift consistently with the Hadley circulation and with the storm track, but the shifts show quantitative differences with respect to each. The poleward shifts of the Hadley circulation are associated with more pronounced high cloud decreases in lower midlatitudes, whereas in comparison, the poleward shifts of the mid-latitude eddy-driven jet are associated with more moderate high cloud increases in the higher mid-latitudes and decreases in the lower midlatitudes. The longwave cloud radiative anomalies are consistent with the changes in the high cloud field. Poleward shifts of the Hadley circulation are associated with strong and spatially extensive longwave cloud radiative cooling anomalies in the lower mid-latitudes, whereas in comparison, poleward shifts of the eddy-driven jet are associated with weaker, less spatially extensive longwave cloud radiative anomalies and, in particular, weaker longwave cloud radiative cooling anomalies that are concentrated on the eastern region of the North Atlantic basin. With regard to the shortwave cloud radiative anomalies with shifts of the Hadley circulation and with the jet, they are negligible for both dynamical indices in the higher latitudes (poleward of approximately 45°N), as one might expect from the small wintertime insolation there. In the lower mid-latitudes, however, there are significant shortwave cloud radiative anomalies with poleward shifts of the Hadley circulation and smaller, but non-negligible, shortwave cloud radiative anomalies with poleward shifts of the jet. This is the first observational evidence for positive shortwave cloud radiative anomalies with poleward shifts of the circulation in the wintertime North Atlantic.

The high cloud changes and longwave cloud radiative anomalies presented here are consistent with the results of Li et al. 2014 who use CloudSat/CALIPSO high cloud retrievals and CERES-EBAF radiative fluxes for a 5-year period and correlate them with the NAM index. However, Li et al. 2014 find that the shortwave cloud radiative anomalies associated with a change in the NAM index is a factor 2-3 smaller than the longwave cloud radiative

anomalies everywhere, while our analysis shows this to be true only at the higher latitudes of the basin. This could be due to differences in data sets, the smaller time period that Li et al. 2014 use, or the fact that they use a water vapor and temperature adjusted CRE. Whatever the cause, we note the overall close agreement between our analysis and theirs, which indicates the robustness of the derived relationships between dynamics, clouds, and radiation changes.

In the summertime Southern Ocean (Figure 21b), high clouds shift poleward with inter-annual poleward shifts of both the Hadley circulation and the eddy-driven jet. However, poleward shifts of the Hadley circulation are associated with increases in the high cloud field between 40°S and 60°S and small decreases between 30°S and 40°S, whereas in comparison poleward shifts of the eddy-driven jet are associated with high cloud increases concentrated between 50°S and 60°S and smaller decreases between 30°S and 50°S. Consistently, there are longwave cloud radiative warming anomalies associated with poleward circulation shifts in the higher latitudes and smaller longwave cloud radiatie cooling anomalies between 30°S and about 45°S. On the other hand, surprisingly, poleward shifts of both the Hadley circulation and the eddy-driven jet are associated with extensive shortwave cloud radiative cooling anomalies throughout the mid- and higher latitudes. The only exception seems to be the region east of South America that exhibits significant shortwave cloud radiative warming anomalies. These findings agree with those reported by Grise et al. 2013 and Grise and Polvani 2014b for Southern Ocean cloud and cloud radiative anomalies accompanying inter-annual shifts the eddy-driven jet. This is expected as similar methodologies and the same data sets are used in these two analyses.

2.4 Comprehensive Analysis

The plots in Figure 21 discussed in Section 2.3 offer only a partial, and qualitative, picture of the relationships between shifts of the Hadley circulation and eddy-driven jet and the associated changes in clouds and CRE. To offer a more complete and quantitative picture of the linkages among clouds, their radiative effects, and dynamics, linear correlation analysis is performed between all the dynamical indices and the suite of cloud and radiation properties. The results are summarized in Table 21.

Table 21 displays the correlations between the four indices of the position of the mid-latitude circulation – the latitudes of the Hadley circulation edge, the dry zone edge, the eddy-driven jet, and the storm track – and several cloud variables – the central latitude of the total, high, and low cloud fields, and the mid-latitude (30°S - 60°S) mean shortwave and longwave CRE. Results are shown for all three mid-latitude ocean basins – Southern Hemisphere, North Atlantic, and North Pacific – and for all seasons – DJF, MAM, JJA, SON. The correlations significant at the 95% level are shown in bold type, and they are the ones on which we concentrate here. Positive shortwave and longwave CRE correlations with indices of the position of the circulation indicate anomalous cloud radiative warming associated with poleward shifts of the circulation, and negative correlations indicate anomalous cloud radiative cooling associated with poleward circulation shifts.

We start by considering the correlation of the circulation with the cloud fields. We include the dry zone edge and storm track latitudes in Table 21 for completeness, but focus on the Hadley circulation edge and eddy-driven jet latitudes in our discussion. From Table 21 it can be seen that the only consistent inter-annual correlation between a cloud field property and a dynamical index is the one between the high cloud central latitude and the Hadley circulation edge latitude: poleward expansion of the Hadley circulation is linked to poleward shifts in the high cloud central latitude. This linkage is significant in the Southern

		Southern Hemisphere				North Atlantic				North Pacific			
		HC	P-E	Jet	Storm Track	HC	P-E	Jet	Storm Track	HC	P-E	Jet	Storm Track
DJF	Total (deg)	0.29	**0.41**	0.09	0.34	**0.46**	**0.59**	**0.49**	0.29	0.12	-0.10	-0.37	0.07
	High (deg)	**0.47**	0.33	0.22	0.32	**0.71**	**0.64**	**0.56**	**0.44**	0.34	-0.04	-0.08	0.06
	Low (deg)	-0.35	-0.10	-0.10	-0.06	-0.13	-0.05	-0.05	-0.32	0.05	-0.22	-0.12	-0.03
	SWCRE (Wm^{-2})	**-0.43**	-0.29	**-0.40**	-0.09	**0.52**	**0.49**	**0.58**	**0.46**	0.22	-0.14	-0.11	-0.21
	LWCRE (Wm^{-2})	0.36	0.17	0.20	0.08	**-0.59**	**-0.59**	**-0.50**	-0.18	0.00	0.22	0.03	0.14
MAM	Total (deg)	**0.42**	**0.72**	0.04	-0.14	-0.06	0.06	**-0.43**	-0.34	-0.12	0.14	-0.34	-0.14
	High (deg)	**0.52**	**0.50**	-0.04	0.01	0.06	0.17	0.06	0.22	0.09	**0.70**	0.24	0.18
	Low (deg)	-0.11	0.02	0.18	0.31	-0.22	-0.05	-0.24	**-0.39**	-0.03	-0.06	-0.20	-0.08
	SWCRE (Wm^{-2})	**-0.67**	**-0.39**	-0.19	-0.16	0.06	0.33	-0.04	0.03	0.02	0.30	-0.14	-0.02
	LWCRE (Wm^{-2})	-0.02	-0.18	-0.31	-0.24	0.07	0.05	0.05	-0.08	0.12	-0.18	0.14	-0.03
JJA	Total (deg)	0.20	**0.69**	-0.11	0.19	0.29	**0.59**	-0.04	0.07	0.36	0.11	0.39	0.13
	High (deg)	**0.49**	**0.63**	0.06	**0.45**	**0.52**	0.36	0.13	0.30	**0.40**	0.17	0.25	0.38
	Low (deg)	**-0.41**	-0.09	-0.20	-0.13	-0.16	0.33	-0.08	-0.14	-0.29	0.20	0.15	-0.10
	SWCRE (Wm^{-2})	**-0.41**	-0.12	-0.23	-0.02	-0.02	0.32	0.31	**0.41**	-0.12	0.23	0.35	**0.40**
	LWCRE (Wm^{-2})	0.19	0.05	0.16	0.10	-0.05	-0.17	-0.33	**-0.40**	0.14	-0.20	-0.37	-0.19
SON	Total (deg)	0.01	0.37	-0.30	0.31	-0.17	**0.61**	0.06	0.07	0.19	0.12	0.02	0.19
	High (deg)	**0.56**	**0.47**	0.23	**0.56**	-0.20	**0.49**	0.05	-0.25	0.32	**0.38**	0.27	0.30
	Low (deg)	**-0.47**	0.12	-0.19	**-0.46**	**-0.47**	-0.08	-0.18	0.22	0.11	-0.22	0.04	0.09
	SWCRE (Wm^{-2})	-0.30	-0.25	-0.08	-0.24	0.02	**0.41**	0.06	0.16	0.12	0.05	0.18	0.31
	LWCRE (Wm^{-2})	0.20	0.14	0.07	0.26	**0.55**	0.01	0.02	-0.23	-0.03	0.16	0.07	-0.08

Table 21: Correlation coefficients (R) of the linear regressions between the dynamical indicators – the Hadley circulation edge latitude, the dry zone ($P - E$) edge latitude, the mid-latitude eddy-driven let latitude, and the storm track latitude – and cloud indicators – the central latitudes of total, high, and low cloud and the mean mid-latitude (30°S-60°S) values of longwave (LW) and shortwave (SW) CRE – for all three ocean basins and for all seasons. Bold type indicates regressions significant at the 95% level.

Hemisphere during all seasons, in the North Atlantic during winter and summer, and in the North Pacific during summer. Note that the equatorward shift of the low clouds is likely due to their decrease at the higher mid-latitude regions, which shifts the center of mass of the low cloud field to lower latitudes

Poleward shifts of the mid-latitude eddy-driven jet, in comparison to poleward shifts of the Hadley circulation edge latitude, are associated with significant poleward shifts in the high and total cloud field only in the North Atlantic and only in the winter season. Note how in all other seasons the jet and cloud field correlations are of varying signs and, in general, not statistically significant. We note here that the relationships between clouds and dynamics in the North Pacific may have zonally-asymmetric spatial structures that are masked by the zonal-averaging we have performed (see, e.g. Norris and Iacobellis 2005; Tselioudis, Zhang, and Rossow 2000; Grise and Medeiros 2016)

Next, we turn to the correlation between the dynamics and the cloud radiative effects. The longwave CRE shows significant correlations with both the Hadley circulation edge and the eddy-driven jet latitude only in the wintertime North Atlantic. The shortwave CRE, on the other hand, shows significant correlations with the Hadley circulation in all seasons over the Southern Hemisphere and in the wintertime North Atlantic, and with the jet in the summertime Southern Hemisphere and the wintertime North Atlantic. In the Southern Hemisphere the poleward shift of the Hadley circulation edge is linked to anomalous shortwave cloud radiative cooling in all seasons except Southern spring (SON), while in the wintertime North Atlantic the poleward shift of both the Hadley circulation and the eddy-driven jet latitudes is associated with anomalous shortwave cloud radiative warming. As illustrated in Figure 21, this shortwave cloud radiative warming is found in the lower mid-latitudes, with negligible shortwave cloud radiative anomalies in the higher mid-latitudes due to the low insolation there in the winter season.

Table 21 suggests that the inter-annual shifts in the edge latitude of the Hadley circu-

lation is a key dynamical indicator for understanding inter-annual changes in clouds and their radiative effects. Towards disentangling the relative effects of the poleward shift of the Hadley circulation edge latitude from that of the eddy-driven jet latitude, we display in Table 22 the regression coefficient (m) and correlation coefficient (R) values among those two indices of the position of the mid-latitude circulation and the cloud variables – the central latitude of the total, high, and low cloud fields, and the mid-latitude mean shortwave and longwave CRE. On the top of each panel we report the m and R values for the relationship between the Hadley circulation edge and the eddy-driven jet latitude. Results are again shown for all three mid-latitude ocean basins – Southern Hemisphere, North Atlantic, and North Pacific – and for all seasons – DJF, MAM, JJA, SON. The correlations significant at the 95% level are shown in bold type.

Table 22 shows that in the wintertime North Atlantic, the Hadley circulation edge and the jet latitude are positively and significantly correlated, as they are in the summertime Southern Hemisphere (see also Kang and Polvani 2011). The results in Table 22 suggest that the correlations between the mid-latitude jet latitude and cloud shifts are only robust when the Hadley circulation edge latitude and the jet latitude are significantly correlated with one another. The influence of the mid-latitude jet could be exaggerated during these seasons due to the high correlation between the jet and Hadley circulation metrics. Further, in seasons and ocean basins when the Hadley circulation edge latitude and the eddy-driven jet latitude are not correlated with one another (e.g. the wintertime Southern Hemisphere, the zonal-mean correlation plot of which we display in Figure 22), the Hadley circulation edge latitude remains significantly correlated with the cloud variables, whereas the eddy-driven jet latitude does not. Hence, Tables 21 and 22 seem to suggest that the Hadley circulation rather than the eddy-driven jet is the dominant driver of the cloud shifts.

A question that arises from Tables 21 and 22 is: why are poleward shifts of the Hadley circulation and the eddy-driven jet associated with anomalous shortwave cloud radiative

		Southern Hemisphere				North Atlantic				North Pacific			
DJF		HC (deg)	**m=0.54 R=0.58**		Jet (deg)	HC (deg)	**m=0.15 R=0.57**		Jet (deg)	HC (deg)	m=0.10 R=-0.29		Jet (deg)
		m	R	m	R	m	R	m	R	m	R	m	R
	Total (deg)	0.04	0.29	0.01	0.06	0.11	0.37	**0.04**	**0.52**	0.00	0.01	-0.02	-0.35
	High (deg)	**0.26**	**0.47**	0.12	0.22	**0.65**	**0.65**	**0.14**	**0.56**	0.09	0.10	-0.03	-0.08
	Low (deg)	**-0.15**	**0.44**	-0.08	-0.25	-0.17	-0.36	-0.04	-0.31	-0.05	-0.12	-0.04	-0.24
	SWCRE (Wm^{-2})	**-1.11**	**0.43**	**-0.98**	**-0.40**	**0.55**	**0.39**	**0.21**	**0.58**	-0.15	-0.10	-0.06	-0.11
	LWCRE (Wm^{-2})	0.22	0.36	0.17	0.20	**0.94**	**-0.54**	**0.22**	**0.50**	0.29	0.21	-0.02	-0.03
MAM		HC (deg)	**m=0.761 R=0.581**		Jet (deg)	HC (deg)	**m=0.156 R=0.391**		Jet (deg)	HC (deg)	m=0.297 R=0.301		Jet (deg)
		m	R	m	R	m	R	m	R	m	R	m	R
	Total (deg)	0.06	**0.42**	0.07	0.04	-0.24	-0.06	**-0.05**	**-0.43**	-1.10	-0.12	-0.04	-0.34
	High (deg)	**0.42**	**0.52**	-0.02	-0.04	0.10	0.06	0.02	0.06	0.20	0.09	0.10	0.24
	Low (deg)	**-0.05**	-0.11	0.11	0.18	-0.34	-0.22	-0.06	-0.24	-0.07	-0.03	-0.09	-0.20
	SWCRE (Wm^{-2})	**-0.59**	**-0.67**	0.22	-0.19	0.04	0.06	-0.02	-0.04	0.02	0.02	-0.22	-0.14
	LWCRE (Wm^{-2})	-0.02	-0.02	0.34	-0.31	0.07	0.07	0.02	0.05	0.18	0.12	0.10	0.14
JJA		HC (deg)	m=0.15 R=0.17		Jet (deg)	HC (deg)	m=0.37 R=0.31		Jet (deg)	HC (deg)	m=0.33 R=0.39		Jet (deg)
		m	R	m	R	m	R	m	R	m	R	m	R
	Total (deg)	0.07	0.24	-0.02	-0.01	0.05	0.29	-0.01	-0.08	0.03	0.34	0.02	0.22
	High (deg)	**0.47**	**0.49**	0.04	0.06	**0.12**	**0.52**	-0.04	0.13	**0.09**	**0.40**	0.05	0.25
	Low (deg)	**-0.45**	**0.63**	-0.12	-0.27	-0.02	-0.10	-0.04	-0.15	-0.04	0.28	0.02	0.15
	SWCRE (Wm^{-2})	**-0.47**	**-0.41**	-0.16	-0.23	-0.02	-0.02	0.30	0.31	-0.16	-0.12	0.41	0.35
	LWCRE (Wm^{-2})	0.28	0.19	0.15	0.16	-0.02	-0.05	-0.13	-0.33	0.06	0.14	0.35	-0.37
SON		HC (deg)	**m=0.491 R=0.482**		Jet (deg)	HC (deg)	m=0.385 R=0.171		Jet (deg)	HC (deg)	m=0.467 R=0.309		Jet (deg)
		m	R	m	R	m	R	m	R	m	R	m	R
	Total (deg)	0.00	0.01	-0.04	-0.30	-2.94	-0.17	0.01	0.06	2.75	0.19	0.00	0.02
	High (deg)	**0.31**	**0.56**	0.13	0.23	-2.15	-0.20	0.01	0.05	1.56	0.32	0.07	0.27
	Low (deg)	**-0.27**	**-0.47**	-0.11	-0.19	**-3.64**	**-0.47**	-0.05	-0.18	0.46	0.11	0.01	0.04
	SWCRE (Wm^{-2})	-0.61	-0.30	-0.16	-0.08	0.08	0.02	0.04	0.06	0.26	0.12	0.10	0.18
	LWCRE (Wm^{-2})	0.16	0.20	0.05	0.07	**2.07**	**0.55**	0.01	0.02	-0.08	-0.03	0.05	0.07

Table 22: Regression coefficients (m) and correlation coefficients (R) of the linear regressions between the HC edge and the eddy-driven let latitudes, and the central latitudes of total, high, and low cloud, and the mean mid-latitude (30°S-60°S) values of longwave (LW) and shortwave (SW) CRE for all three ocean basins and for all seasons. Bold type indicates regressions significant at the 95% level. The top panels show the m and R values between the HC edge and the jet latitudes.

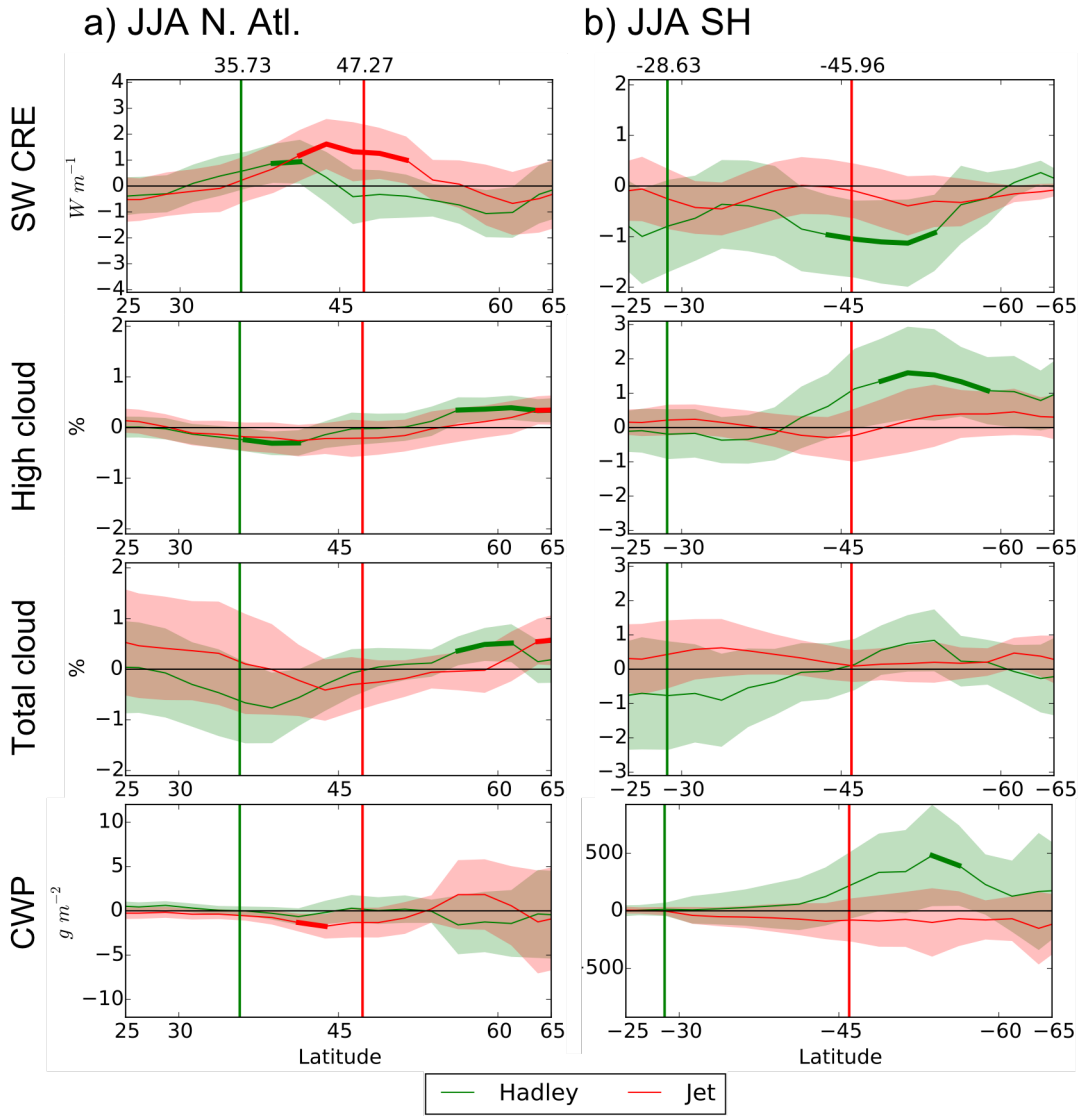

Figure 22: Rregressions on the HC edge (green) and eddy-driven jet (red) latitudes of the shortwave (SW) CRE (top row), the high cloud cover (second row), and the total cloud cover (third row), and cloud liquid water path (CWP= $\int_{P_c}^{P_b} qdp$ where P_c is the cloud top pressure, P_b is the cloud base pressure, and q is the mixing ratio of liquid water) (bottom row) for the JJA season and for (a) the North Atlantic (N. Atl.) and (b) the Southern Hemisphere (SH). Bold lines indicate statistically significant changes, shading the 95% confidence interval, and the vertical lines indicate the climatological position of the HC edge and the eddy-driven jet. Note the different y-axes across columns and across rows.

warming in the lower mid-latitudes of the North Atlantic but anomalous shortwave cloud radiative cooling at similar latitudes in the Southern Hemisphere, despite the consistent poleward shift of the high clouds in both regions? This question is explored in Figure 23, which shows the zonal-mean regression on the Hadley circulation edge (green) and eddy-driven jet (red) latitudes of the shortwave CRE (top row), the high cloud cover (middle row), and the total cloud cover (bottom row), during the DJF season of (a) the North Atlantic and (b) the Southern Hemisphere. Statistically significant changes are indicated by a bold line, while the mean positions of the Hadley circulation edge and the eddy-driven jet are indicated with vertical lines.

In the North Atlantic, one can see in Figure 23a that anomalous shortwave cloud radiative warming of approximately 1 Wm^{-2} and 2 Wm^{-2} in magnitude occurs over the lower mid-latitudes (30°N - 45°N) with poleward shifts of the eddy-driven jet and Hadley circulation latitudes, respectively. Those shortwave cloud radiative warming anomalies correspond to approximately 0.5% and 2% decreases in both high and total cloud in the region. Poleward of about 45°N there are no shortwave cloud radiative warming anomalies, despite moderate but significant high and total cloud increases with poleward shifts of the circulation, probably due to the low value of insolation in this region and season.

In the Southern Hemisphere, in contrast, Figure 23b shows that shortwave cloud radiative cooling anomalies of about 2 Wm^{-2}, for both poleward shifts in the Hadley circulation edge and the eddy-driven jet latitudes, occurs poleward of 45°S, corresponding to a 1% increase in both high and total cloud in the region. It must be noted that a SW cooling of $1Wm^{-2}$ with a corresponding 2% high and total cloud increase also occurs in the winter (JJA) season (Figure 22), even with the low value of insolation. Equatorward of 45°S, however, there are no shortwave cloud radiative warming anomalies despite small but significant decreases in high cloud with the poleward shift of the Hadley circulation edge. This is because the total cloud field does not show significant changes in that region with

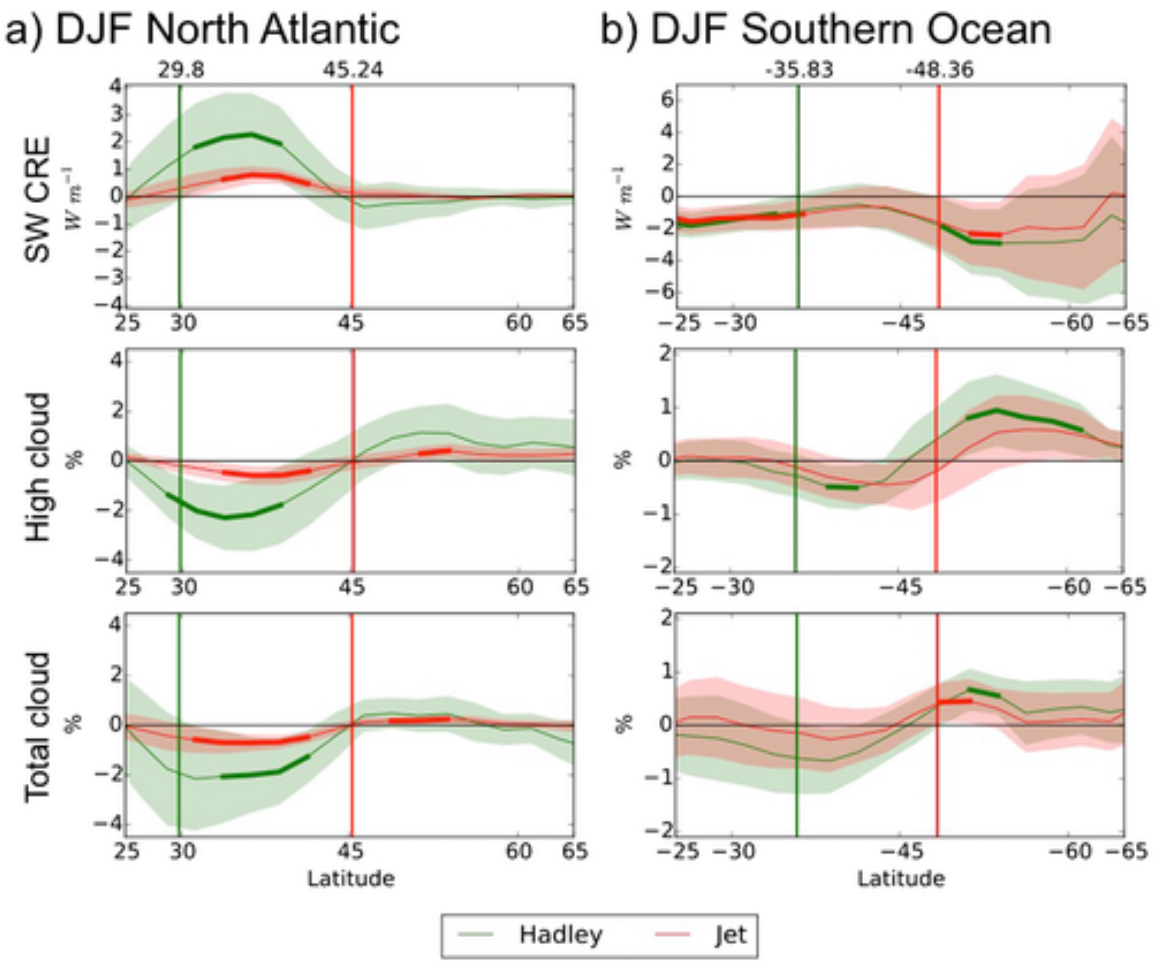

Figure 23: Regressions on the HC edge (green) and eddy-driven jet (red) latitudes of the shortwave (SW) CRE (top row), the high cloud cover (middle row), and the total cloud cover (bottom row), for the DJF season and for (a) the North Atlantic and (b) the Southern Ocean. Bold lines indicate statistically significant changes, shading the 95% confidence interval, and the vertical lines indicate the climatological position of the HC edge and the jet. Note the different y-axes across columns and across rows.

poleward shifts of either the Hadley circulation edge or the eddy-driven jet latitudes (Figure 23b, bottom row).

The lack of total cloud change with poleward circulation shifts in the Southern Hemisphere may be explained by the climatological structure of the Southern Hemisphere cloud field. In that region, low and middle clouds dominate the total cloud amount (e.g. Haynes et al. 2011). In fact, over the Southern Hemisphere, the sum of low and middle clouds is greater than 70% for the entire 30°S - 65°S latitude band, as shown in Figure 24. The only exception to this is, again, a small region east of South America. This implies that poleward shifts in high clouds occur in a background of very high coverage of low and middle clouds. At the same time, that background field of low and middle clouds remains unchanged during poleward shifts of the Hadley circulation edge and the eddy-driven jet latitudes, as depicted in Figure 24. This is why the impact of the high cloud shifts on the total cloud cover, and on the resulting shortwave cloud radiative anomalies, is very small. Note that it is over the North Atlantic as well as over the previously identified exceptional region east of South America, where the low and middle cloud cover is lowest and also where there is anomalous shortwave cloud radiative warming with poleward shifts in the high clouds (Figure 21).

2.5 Trends

The relationships between the latitudinal indicators of the circulation and the cloud type central latitudes derived in Sections 2.3 and 2.4 can be used to re-examine the results of Bender, Ramanathan, and Tselioudis 2012 who report the existence of multi-decadal poleward shifts in the mid-latitude cloud field. In Table 23 we report the regression coefficient (m) and correlation coefficient (R) values for the 1984-2009 trend in the Hadley circulation edge latitude, the mid-latitude eddy-driven jet latitude, and the high and total cloud central

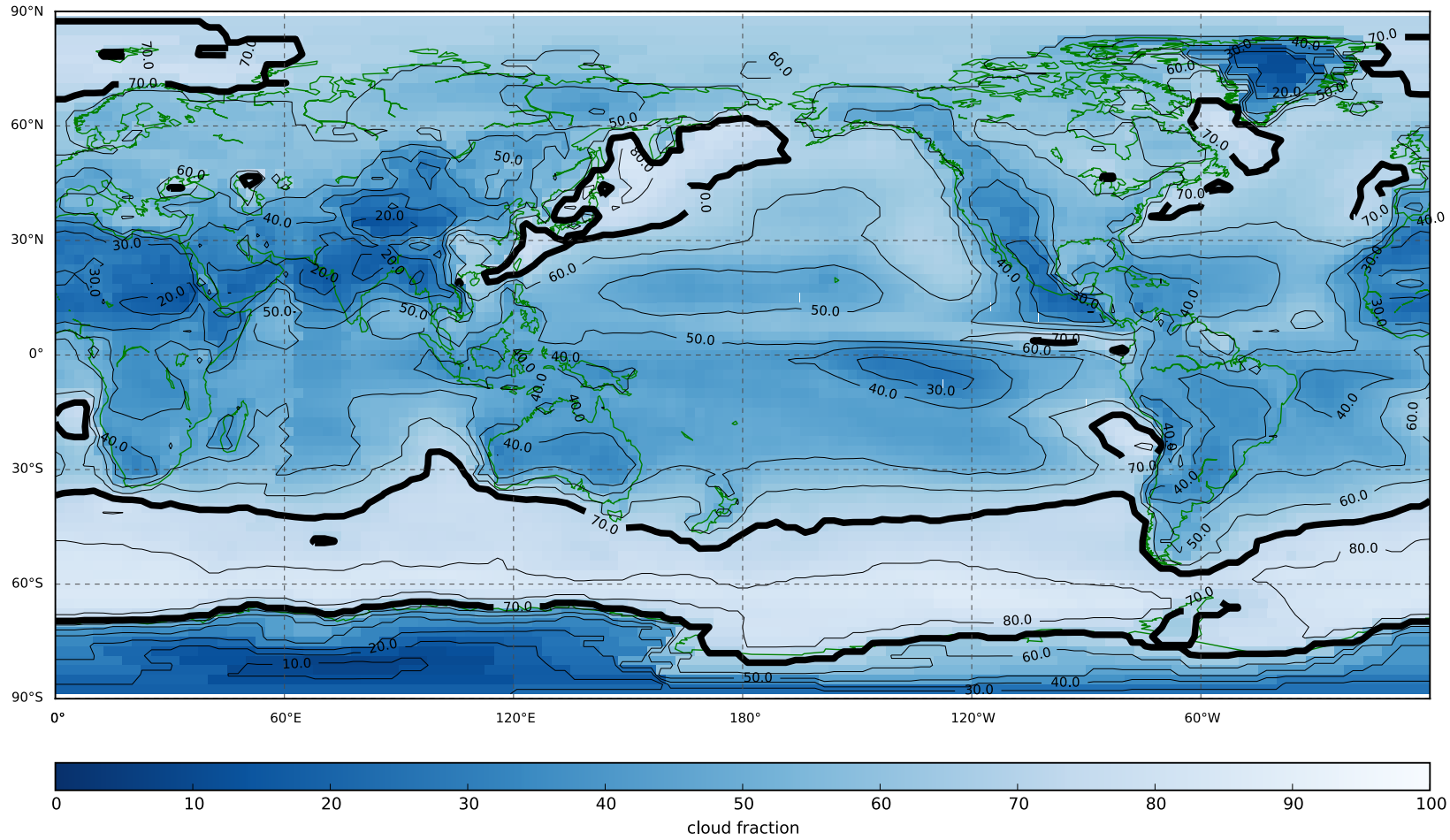

Figure 24: The global climatological cloud cover of the estimated true low plus middle clouds for the DJF season from ISCCP-D2. The thick black line indicates 70% low+middle cloud cover

latitudes. Results are again reported for all the three mid-latitude ocean basins – Southern Hemisphere, North Atlantic, and North Pacific – and for all seasons – DJF, MAM, JJA, SON. The correlations significant at the 95% level are shown in bold type.

In the Southern Hemisphere, both the Hadley circulation edge latitude and the high cloud central latitude have been shifting consistently poleward in all seasons except Southern spring (SON), with comparable rates of about 0.3-0.5° per decade or about 0.8-1.3° in the last 26 years. The Southern Hemisphere eddy-driven jet has shifted poleward at a similar rate only during DJF, but even then the shift is not statistically significant for that specific time period. In the Northern Hemisphere regions, the poleward shifts of the high cloud central latitude are significant only in the North Pacific during summer and autumn, but are not accompanied by corresponding significant shifts in the latitudinal indicators of the circulation. It is likely that any cloud changes in the Northern Hemisphere ocean basins are zonally-asymmetric (see, e.g. Simpson, Shaw, and Seager 2014), and are not likely to be detected in this basin-mean analysis.

Turning now to the total cloud field, it is evident that across almost all ocean basins and seasons, the total cloud central latitude seems to have been shifting poleward, consistent with, e.g. Norris et al. 2016. The poleward shift in the total clouds is likely a robust response to increasing CO_2 concentrations. Given the consistent poleward shifts in the total cloud field, do we also find a positive cloud curtain feedback (Tselioudis and Konsta 2017)? In Figure 25 we display for each season the 25-year trends (following Norris et al. 2016) in the zonal-mean shortwave CRE from ISCCP-FD, such that positive trends indicate anomalous shortwave cloud radiative warming and hence likely a positive cloud radiative feedback while negative trends indicate anomalous shortwave cloud radiative cooling and hence likely a negative cloud radiative feedback. We find evidence for a positive cloud radiative feedback in the Northern Hemisphere, consistent with the results from Sections 2.3 and 2.4. However, it seems that there is no observational evidence for a positive cloud

		Southern Hemisphere		North Atlantic		North Pacific	
DJF		m	R	m	R	m	R
	Total (deg)	**-0.01**	**-0.86**	**0.01**	**0.51**	0.01	0.36
	High (deg)	**-0.05**	**-0.84**	0.02	0.24	0.00	-0.05
	HC (deg)	**-0.05**	**-0.48**	0.04	0.25	-0.01	-0.11
	Jet (deg)	-0.03	-0.26	0.04	0.12	0.01	0.06
MAM		m	R	m	R	m	R
	Total (deg)	**-0.02**	**-0.82**	**0.02**	**0.55**	0.00	0.16
	High (deg)	**-0.04**	**0.75**	0.03	0.33	0.03	0.33
	HC (deg)	**-0.06**	**-0.46**	-0.01	-0.07	-0.02	-0.07
	Jet (deg)	-0.01	-0.10	-0.03	-0.09	0.01	0.03
JJA		m	R	m	R	m	R
	Total (deg)	**-0.02**	**-0.81**	**0.04**	**0.79**	**0.02**	**0.60**
	High (deg)	**-0.05**	**-0.75**	0.02	0.34	**0.04**	**0.66**
	HC (deg)	**-0.03**	**-0.43**	0.07	0.27	0.07	0.27
	Jet (deg)	0.01	**0.12**	-0.07	-0.31	-0.02	-0.07
SON		m	R	m	R	m	R
	Total (deg)	**-0.01**	**-0.85**	**0.02**	**0.52**	**0.01**	**0.58**
	High (deg)	**-0.04**	**-0.59**	0.01	0.29	**0.04**	**0.59**
	HC (deg)	-0.02	-0.12	0.16	0.32	0.04	0.12
	Jet (deg)	0.01	0.09	0.07	0.31	-0.04	-0.18

Table 23: Regression coefficients (m) and correlation coefficients (R) of the linear trends for the central latitudes of total and high cloud as well as for the HC edge and the eddy-driven let latitudes, for all three ocean basins and for all seasons. Bold type indicates regressions significant at the 95% level.

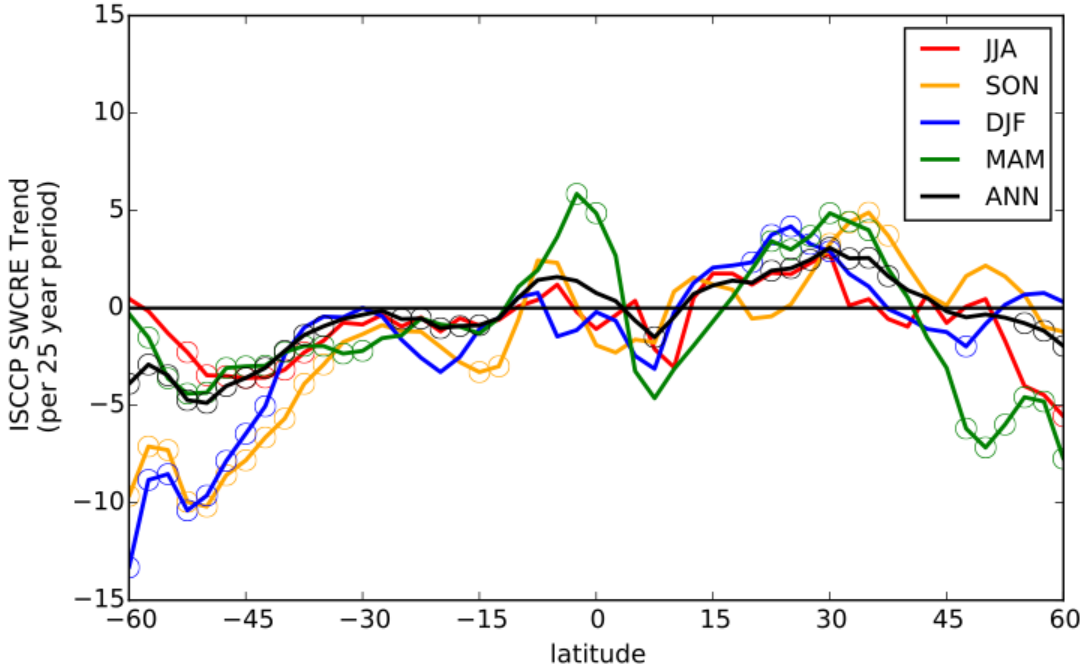

Figure 25: Trend in the annual-mean (black) and seasonal-mean (colors) zonal-mean ISCCP-FD shortwave cloud radiative effect (SWCRE, Wm^{-2}) over 1983-2009. Circles indicate trend significance at the 95% confidence level. All trends are relative to the 60°S-60°N mean change.

radiative feedback in the Southern Hemisphere despite the requisite poleward shifts in the total and high cloud field – we instead find anomalous shortwave radiative cooling in most seasons. We reconcile this result for the Southern Hemisphere with the contrasting predictions from global climate models (see, e.g. Figure 14) in the next chapter.

2.6 Summary

The results presented in this chapter show that the inter-annual, de-trended, poleward shifts of the Hadley circulation edge latitude correlate significantly with the poleward shifts in the high cloud central latitude in almost all basins and seasons. The inter-annual, de-trended,

poleward shifts of the mid-latitude eddy-driven jet, on the other hand, correlate significantly with shifts in the high cloud central latitude only in the wintertime North Atlantic. This seems to be because while in most basins and seasons, poleward shifts in both the Hadley circulation edge and eddy-driven jet latitudes are associated with increases in high cloud amount at the higher midlatitude regions, the poleward shifts in the Hadley circulation edge latitude also reduce high cloud amounts in the lower midlatitude regions (Figures 21 and 23), and the combined change produces consistently significant correlations between the Hadley cell edge and high cloud central latitude shifts. In the North Atlantic winter season, poleward shifts in the high cloud central latitude associated with poleward shifts of either Hadley circulation edge or eddy-driven jet are, in turn, associated with anomalous shortwave cloud radiative warming, as cloud cover increases in a region of low values of insolation but decreases in a region of much higher values of insolation. However, in the Southern Hemisphere and in all seasons, poleward shifts of high clouds associated with poleward Hadley circulation edge shifts are associated with weak anomalous shortwave cloud radiative cooling in the higher latitudes but no shortwave cloud radiative anomalies in the lower mid-latitudes. This seems likely to be due to the fact that in the lower mid-latitude regions, where low and middle clouds show amounts of 70% or greater, the shifts in the high cloud produce negligible shortwave cloud radiative anomalies.

This chapter concentrates on the cloud and radiation anomalies associated with dynamical shifts that may be caused by natural variability patterns, such as the El Niño-Southern Oscillation or the Pacific Decadal Oscillation, or by anthropogenic influences, such as ozone depletion or greenhouse gas warming. The results from this analysis suggest that the observed multi-decadal Southern Hemisphere cloud field shifts are more likely related to tropical expansion than to a poleward shift in the storm tracks. This result, along with the strong correlations of the Hadley cell edge with the midlatitude high cloud field, highlights a prominent role of the Hadley circulation in affecting mid-latitude cloud and indicates that

tropical expansion, rather than shifts in the eddy-driven jet, might be the more important driver of mid-latitude cloud radiative feedbacks. We explore this further in the next chapter.

Chapter 3

Quantifying modeled linkages between clouds and the general circulation of the atmosphere:

The Hadley circulation as an emergent constraint on the model responses to increasing carbon dioxide

3.1 Introduction

Clouds and their radiative properties co-vary with the large-scale circulation of the atmosphere, as discussed in Chapter 2, and all are projected to co-evolve in the future with increasing CO_2 concentrations. There is strong evidence that increasing concentrations of atmospheric greenhouse gases will also contribute to poleward shifts in the atmospheric circulation (e.g. Kushner, Held, and Delworth 2001; Yin 2005; Lu, Vecchi, and Reichler 2007; Hu and Fu 2007; Barnes and Polvani 2013), but the future changes in clouds and their radiative properties remain unclear and account for most of the model uncertainty in projections of the future climate (e.g. Andrews et al. 2012; Vial, Dufresne, and Bony 2013; Webb, Lambert, and Gregory 2013). A dominant source of the model uncertainty is tropical and sub-tropical low clouds and their shortwave cloud radiative effects (SWCRE) (e.g. Bony and Dufresne 2005), but extra-tropical cloud and shortwave radiation biases have also been linked to the uncertainty in the model response to increasing CO_2 concentrations (e.g. Trenberth and Fasullo 2010; Grise, Polvani, and Fasullo 2015). Quantifying the effects of

poleward circulation shifts on extra-tropical clouds and their shortwave radiative properties may therefore help to constrain the large inter-model spread in the equilibrium climate sensitivity. That is, we re-frame the global-mean climate feedback parameter in Equation **??**, in particular the especially uncertain shortwave TOA radiative response due to clouds R_{SWCRE}, from a dependence on the highly uncertain cloud changes $\frac{\partial R_{SWCRE}}{\partial x_{cloud}}\Big|_{\bar{T}_s} \frac{\Delta x_{cloud}}{\Delta T_s}$, analysis of which has only gone so far in helping to reduce the model uncertainty in equilibrium climate sensitivity ΔT_s, to a dependence on the more reliably predicted changes in the atmospheric circulation $\frac{\partial R_{SWCRE}}{\partial x_{dyn}}\Big|_{\bar{T}_s} \frac{\Delta x_{dyn}}{\Delta T_s}$. Which dynamical feedback parameter x_{dyn} should we use?

Despite emphasis on the relationship between clouds and the mid-latitude eddy-driven jet, for which results vary greatly by season, ocean basin, and model (Bender, Ramanathan, and Tselioudis 2012; Grise et al. 2013; Kay et al. 2014; Li et al. 2014; Grise and Polvani 2014b; Grise and Medeiros 2016), observations actually show that the inter-annual variability in mid-latitude clouds and their radiative effects correlates more consistently and more robustly with poleward shifts in the Hadley circulation edge latitude than with shifts in the eddy-driven jet latitude (see Chapter 2), especially in the Southern Hemisphere. The eddy-driven jet may shift the centers of the extra-tropical storms and their clouds, but the increase in static stability N^2 associated with the shifts in the subsiding branch of the Hadley circulation limits the development of high clouds on the equatorward flank of the storm tracks (Frierson, Lu, and Chen 2007; Kang and Lu 2012; Grise and Polvani 2016; see also Equation 4.4). Poleward shifts of the Hadley circulation edge latitude more effectively inhibit high clouds in the greatly insolated lower mid-latitudes ($\sim$28°S-$\sim$48°S) than do shifts in the the eddy-driven jet latitude, and so is more likely to be associated with the shortwave radiative response due to future change in clouds (see Chapter 2).

In this chapter, then, we examine the implications of using the Hadley circulation edge latitude as our dynamical feedback parameter; i.e. $x_{dyn} = \theta_{HC}$. We examine the inter-

annual relationship between the lower mid-latitude shortwave cloud radiative effect and the Hadley circulation edge latitude in Coupled Model Intercomparison Project phase 5 (CMIP5) models, with a focus on the Southern Hemisphere where the observational results are especially robust. This chapter is structured as follows. In Section 3.2 we describe the data and methods used. We motivate the analysis in Section 3.3. In Section 3.4 we examine the model spread in the co-variability between the Hadley circulation edge latitude θ_{HC} and the shortwave cloud radiative anomalies ($\frac{\partial R_{SWCRE}}{\partial \theta_{HC}}$). In Section 3.5 we relate the model spread in the linkage between HC-SWCRE to model biases in the climatological Hadley circulation. In Section 3.6 we show that these biases in the model climatologies imprint onto the spread in model's predictions of the climate response to increasing CO_2. We summarize our results in Section 3.7.

3.2 Data and Methods

Data

The observational radiative flux data used in this study are the monthly-mean top-of-atmosphere radiative fluxes derived from the International Satellite Cloud Climatology Project (ISCCP-FD; Zhang et al. 2004). We present the results using the dataset adjusted for satellite zenith angle and drift biases by Norris and Evan 2015, but use of the unadjusted dataset did not show significant differences in the derived relationships. The dataset covers the period July 1983 to December 2009, but only years with the entire DJF season available are analyzed; i.e. December 1983 to February 2009. Over this period, the monthly-mean meridional wind data from the European Centre for Medium-Range Weather Forecasts (ECMWF) Interim Re-Analysis (ERA-Interim; Dee et al. 2011) are used to calculate the mass stream function (see Section 2.2 for details).

Model radiative fluxes and dynamical variables are obtained from the monthly-mean

output from 22 CMIP5 models (Taylor, Stouffer, and Meehl 2012), as listed in Table 31. We present the analysis of two sets of model output: 1) the pre-industrial (PI) control runs and 2) the abrupt quadrupling of the concentration of CO_2 (abrupt4$\times CO_2$) runs. We also analyzed the historical runs, but we use the pre-industrial control run variability because 1) it is unforced, 2) the cloud changes from varying global temperature are minimal, and 3) the length of integration (between 300 and 1156 years) yields a robust statistical analysis. The results are similar when the historical runs of the models are analyzed. To avoid biasing the results with one model, only the first ensemble member ("r1i1p1") from each model is used. The equilibrium climate sensitivity (ECS) of each model is taken from Forster et al. 2013 (see Table 1, sixth column), although the ECS from Extended Table 1 of Sherwood, Bony, and Dufresne 2014 was also used and actually yield greater correlation strength between the summertime Southern Hemisphere Hadley circulation edge latitude and ECS (R=0.54, m=1.48). We present the results of the correlations with Forster et al. 2013 for a more conservative estimate of the robustness of our results and for consistency with the literature (e.g. Grise and Polvani 2014b; Caldwell, Zelinka, and Klein 2018). The shortwave TOA radiative response due to clouds R_{SWCRE} is defined for each model as the difference in SWCRE between the atmosphere-"equilibrated" (first 50 years removed) abrupt $4\times CO_2$ run and the pre-industrial control run climatology.

Methods

The Hadley circulation (HC) edge latitude is computed by linearly interpolating to 0.01° resolution the first latitude from the equator where the atmospheric meridional mass stream-function changes sign from poleward to equatorward in the mid-troposphere (500 hPa) (see Section 2.2 for details). The shortwave cloud radiative effect (SWCRE) is defined as the top-of-atmosphere upwelling clear-sky SW radiation (i.e., rsutcs) minus the top-of-atmosphere upwelling all-sky SW radiation (i.e., rsut) (see Section 2.2 for details).

To remove intra-seasonal variability, de-seasonalized monthly-mean data are averaged over the DJF season. To examine inter-annual co-variability, the de-trended SWCRE time series are linearly regressed onto the de-trended Hadley circulation edge latitude time series. We refer to the shortwave cloud radiative anomalies associated with a 1° poleward shift of the Hadley circulation edge latitude as the HC-SWCRE, or $\frac{\partial R_{SWCRE}}{\partial x_{dyn}}\Big|_{\bar{T}_s}$. Positive values of the HC-SWCRE indicate anomalous shortwave cloud radiative warming with poleward Hadley circulation edge shifts, and negative values of the HC-SWCRE indicate anomalous shortwave cloud radiative cooling with poleward HC edge shifts. Regionally-averaged quantities are computed by first linearly interpolating to 0.01° horizontal resolution and then averaging over the point-by-point values. Statistical significance and confidence intervals are determined using two-tailed Student's *t*-tests as well as boot-strapping.

In this chapter, we focus on results for the Southern Hemisphere, and in particular the summer (DJF) season when insolation and the shortwave cloud radiative effect is maximized at Southern mid-latitudes (Figure 31). Observations show that the linkage between clouds and the Hadley circulation is relatively consistent across seasons in the Southern Hemisphere (see Chapter 2), especially when compared to the Northern Hemisphere (see Chapter 2 and Grise and Medeiros 2016), in which the models are surprisingly consistent with one another and with observations. For example, note in Figure 32 that all models exhibit shortwave cloud radiative warming anomalies in the lower mid-latitudes with poleward shifts in Hadley circulation, as do the observations (Figure 21), and note the relatively small range in climatological Hadley circulation edges (approximately 27°N-30°N) and the agreement with the observations (approximately 30°N). We will show that this agreement across models and between models and observations does not hold in the Southern Hemisphere. Still, analysis for all ocean basins and all seasons as well as for the annual-mean was performed and those results are also discussed.

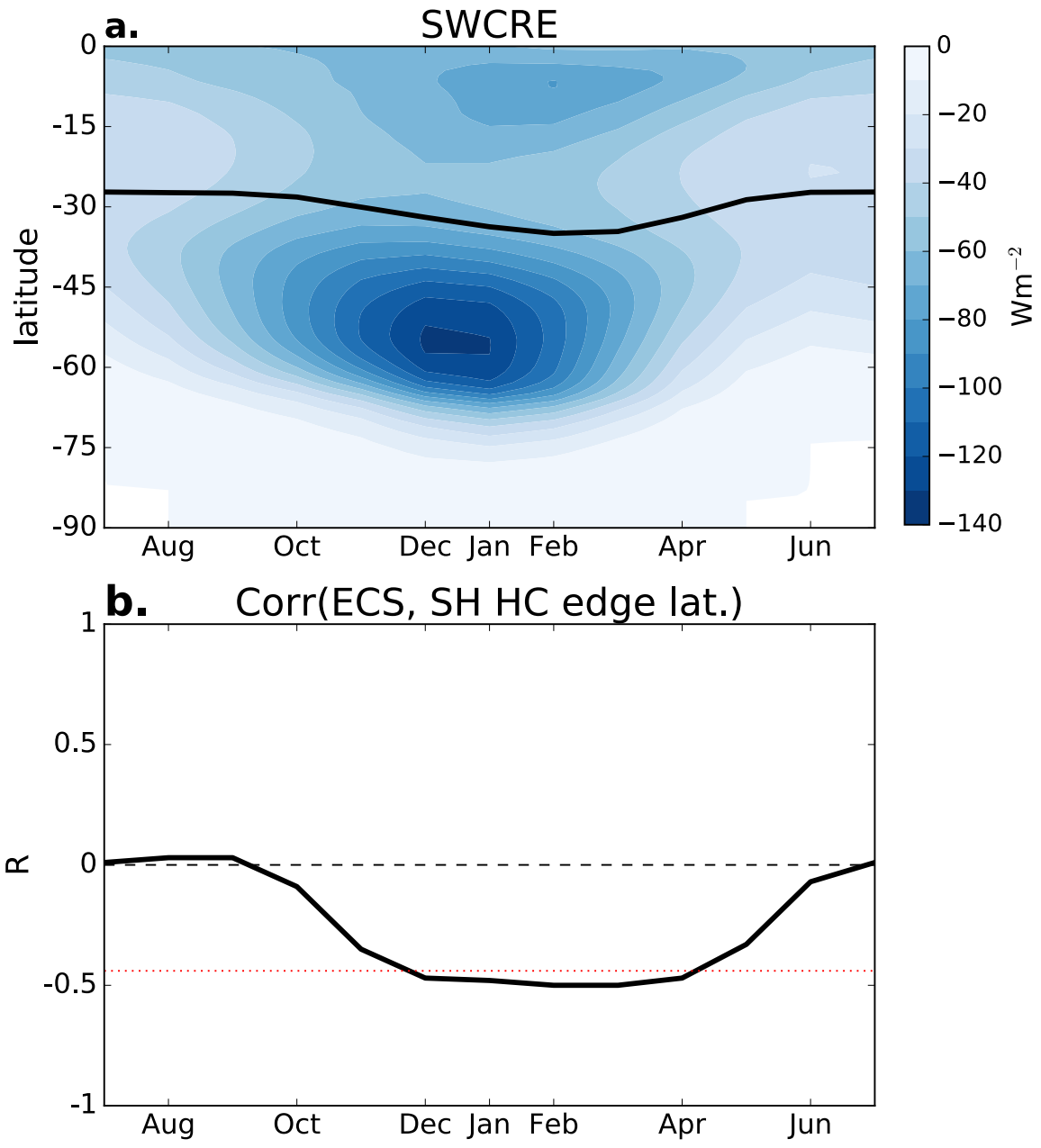

Figure 31: (a) The CMIP5 multi-model mean seasonal cycle of (colors) shortwave cloud radiative effect in Wm^{-2} and (black line) the latitude of the SH HC edge. (b) The seasonal cycle of the correlation coefficient (R) between the latitude of the SH HC and the ECS taken from Forster et al. 2013. The red dashed line demarcates the critical R value beyond which the correlations are statistically significant according to the Student's *t*-test. Note that the seasonality of the correlation between the HC edge and ECS matches that of the HC edge and the SWCRE.

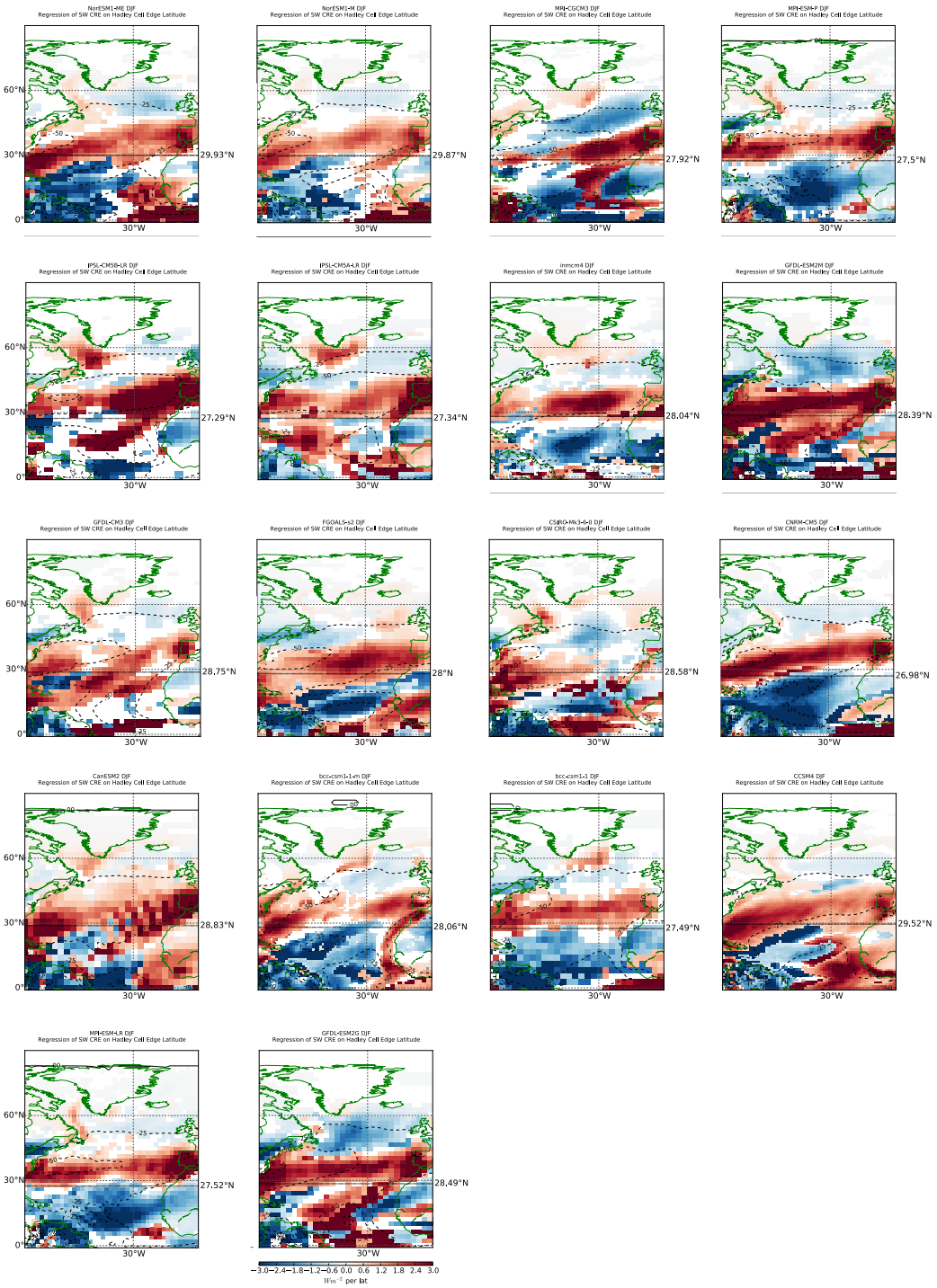

Figure 32: The (colors) spatial pattern of the slope (m) between the inter-annual local HC edge latitude and SWCRE in DJF North Atlantic for 18 CMIP5 models. Red (blue) indicates anomalous SW cloud radiative warming (cooling) with poleward shifts in the local HC. Contours denote climatological values of SWCRE. Dashed contours indicate negative values . The bold horizontal dotted line depicts the climatological local HC edge.

3.3 Motivation

By way of motivation, we first examine the CMIP5 models' shortwave cloud radiative response to increasing CO_2 in order to identify regions of strong model response. The $4\times CO_2$-forced shortwave cloud radiative response is displayed in Figure 33 (top) for summer (DJF), which dominates the annual-mean response in the Southern Hemisphere due to maximum insolation. Analysis for other seasons was performed and results were consistent but weaker in magnitude. During DJF, the major consistent shortwave cloud radiative response is what appears to be a dipole pattern in the Southern mid-latitudes: at high latitudes, defined as where the multi-model mean shortwave cloud radiative response is negative ($\sim$48°S-90°S), there is anomalous shortwave cloud radiative cooling; at lower mid-latitudes (thick-dashed vertical lines in Figure 33 top), defined as where the multi-model mean shortwave cloud radiative response is positive ($\sim$28°S-$\sim$48°S), there is anomalous shortwave cloud radiative warming. Note that this dipole behavior is also present, but of smaller magnitude, in the annual-mean $4\times CO_2$-forced shortwave cloud radiative responses (Figure 34). It is important to note this because the equilibrium climate sensitivity is an annual-mean quantity, although it may influenced by climate feedback processes which might act preferentially during particular seasons.

The relationship between the model uncertainty in the shortwave cloud radiative response in each of the two regions – the high latitudes and the lower mid-latitudes – and the model spread in the values of the equilibrium climate sensitivity is explored in the bottom of Figure 33. The model spread in the high-latitude shortwave cloud radiative response (left panel), does not correlate significantly with the model spread in equilibrium climate sensitivity, and any relationship would not be directly causal as models with higher values of equilibrium climate sensitivity tend also to have stronger shortwave cloud radiative cooling responses (c.f. Tan, Storelvmo, and Zelinka 2016). In the lower mid-latitudes, however,

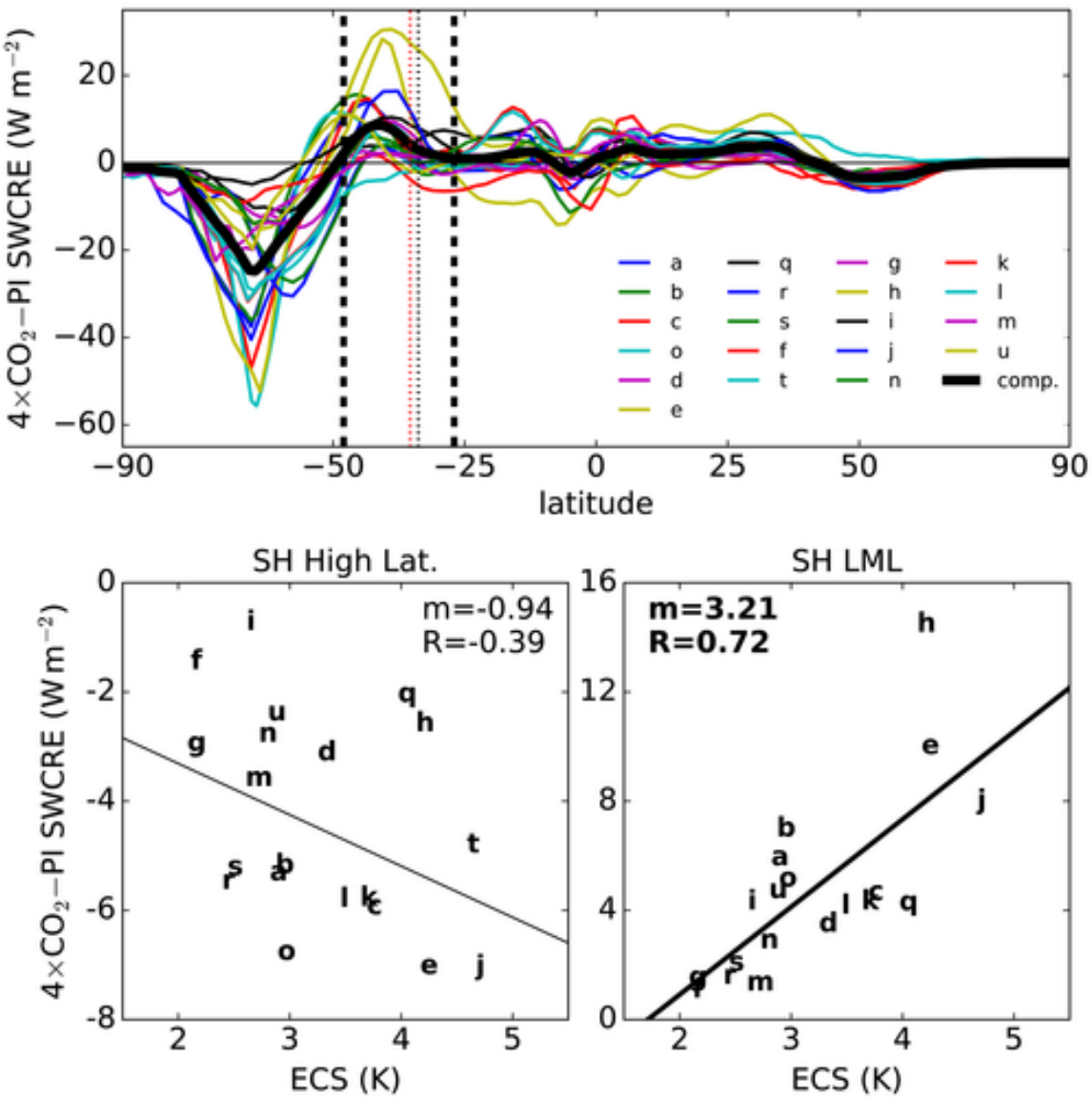

Figure 33: (top) The change in zonal-mean SWCRE for each CMIP5 model from the pre-industrial (PI) control climatology to the atmosphere-"equilibrated" $4\times CO_2$ climatology for DJF. Positive (negative) values correspond to anomalous shortwave cloud radiative warming (cooling). (bottom) Least-squares linear regressions of the inter-model spread in ECS on the inter-model spread in the shortwave cloud radiative response averaged over the (left) higher mid-latitudes and over the (right) LML (lower mid-latitudes). The LML is confined between the two thick-dashed vertical lines. The multi-model mean climatological HC edge latitude is depicted for the PI runs with a black thin-dashed line and for the $4\times CO_2$ runs with a red thin-dashed line. Each line and data point corresponds to one model (see Table 31 for model labels) Regressions statistically significant at the 95% confidence level, assessed using the Student's *t*-test, are denoted by thicker regression lines and bold coefficients.

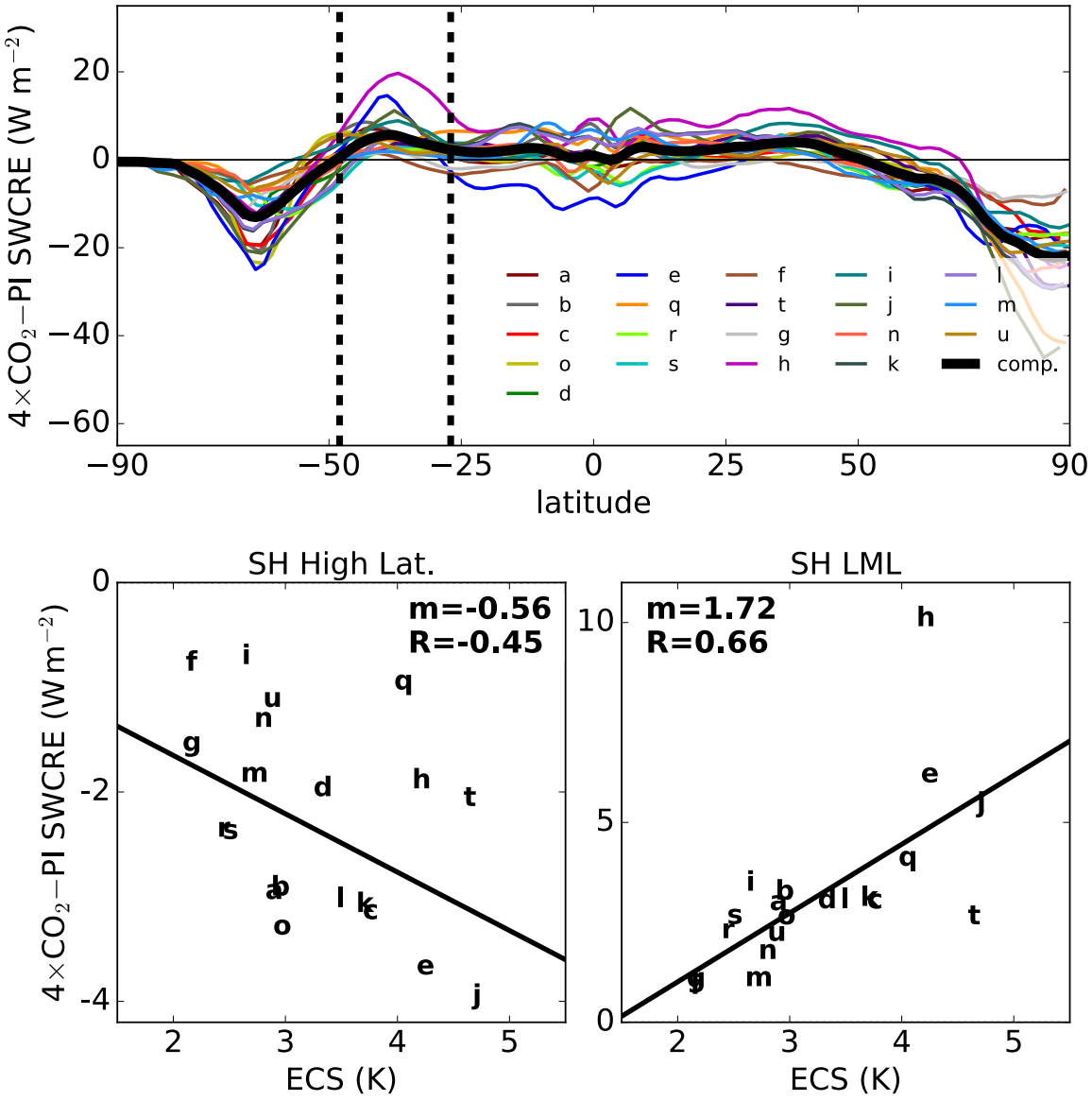

Figure 34: same as Figure 33, but for annual-mean values rather than DJF-mean values.

the correlation between the model spread in the shortwave cloud radiative response and in equilibrium climate sensitivity is statistically significant (right panel), such that models with higher values of equilibrium climate sensitivity tend also to have stronger shortwave cloud radiative warming responses (see also Figure 7 of Grise, Polvani, and Fasullo 2015). Note that this correlation persists when the annual mean responses are analyzed (Figure 34). The high latitude response has been studied extensively and is attributed to a thermodynamic cloud phase radiative feedback – with increasing CO_2, the melting isotherm which intersects the surface near 55°S shifts southward and melts ice cloud into more reflective liquid cloud (see Chapter 1 and, e.g. Kay et al. 2014; Storelvmo, Tan, and Korolev 2015; Ceppi, Hartmann, and Webb 2016). We might explain this negative correlation as models which exhibit more global-mean warming tend also to "melt" more of their ice clouds into more reflective liquid clouds.

We focus our analysis in this chapter on the lower mid-latitudes, where a mechanism for the shortwave cloud radiative response has not yet been established. A potential mechanism is the poleward shift of the Hadley circulation edge, since its subsiding branch terminates within the lower mid-latitudes, near 34°S in the CMIP5 multi-model mean pre-industrial climatology (thin black line in Figure 33 top), and since the observations (see Chapter 2) show that the mid-latitude clouds and their shortwave radiative effects are strongly correlated with meridional shifts in the Hadley circulation edge on inter-annual timescales. To date, no study has investigated whether the inter-annual variability of the mid-latitude clouds and their shortwave radiative effects are related to the Hadley circulation in models. If it is, this relationship could be predictive of the models' shortwave cloud radiative response to increasing CO_2 and ultimately the models' global-mean surface warming response.

3.4 Model Spread in HC-SWCRE Linkage

We begin our analysis by comparing in Figure 35 the spatial structure of the inter-annual HC-SWCRE co-variability for the observations (a) with that of the CMIP5 multi-model mean (b). In the observations (see Chapter 2), the HC-SWCRE relationship in the lower mid-latitudes of the Southern Hemisphere is mostly negative and dominated by anomalous shortwave cloud radiative cooling. We note two exceptions: the previously identified (see Chapter 2) region of anomalous shortwave cloud radiative warming east of South America, and what we interpret as an intrusion of anomalous shortwave cloud radiative warming from the tropics in the eastern South Pacific, likely associated with southward and westward shifts of the South Pacific Convergence Zone (SPCZ) and the deep convective clouds there. In contrast to the observations, the CMIP5 multi-model mean spatial pattern of the HC-SWCRE, while showing a weak cooling in the central Pacific associated with shifts of the SPCZ, is dominated by pronounced and zonally-symmetric shortwave cloud radiative warming anomalies.

We compare the above spatial structure of the inter-annual HC-SWCRE co-variability with the CMIP5 multi-model mean spatial pattern of the $4\times CO_2$-forced shortwave cloud radiative response in Figure 35c. The co-location of the CMIP5 multi-model mean region of anomalous shortwave cloud radiative warming associated with unforced Hadley circulation edge shifts (red in Figure 35b) with the region of the shortwave cloud radiative warming response to $4\times CO_2$ forcing (Figure 35c) suggests a contribution to the shortwave cloud radiative warming response from the $4\times CO_2$-forced poleward expansion of the Hadley circulation edge. Note that the spatial correlation between the two patterns is statistically significant (R = 0.53). The question, then, is: to what extent is the CMIP5 multi-model mean HC-SWCRE relationship representative of individual model behavior? To answer this question, we next examine the inter-model spread in the HC-SWCRE relationship about

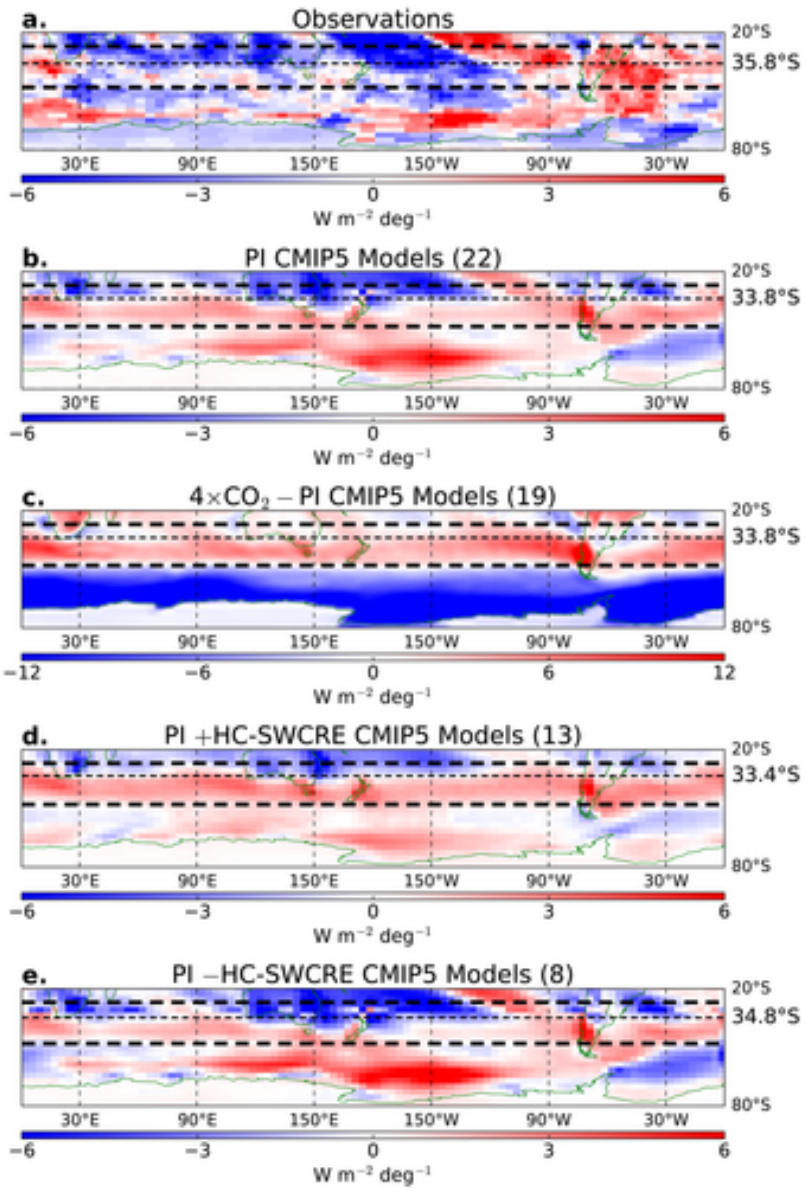

Figure 35: DJF least squares linear regressions of the SH HC edge latitude on the SH SWCRE for (a) ISCCP-FD and ERA-Interim, (b) the CMIP5 pre-industrial multi-model mean, (d) only the +HC-SWCRE models, and (e) only the −HC-SWCRE models. Units in (a), (b), (d), and (e) are Wm^{-2} per 1° poleward shift in the HC. Displayed in parentheses near the panel label is the number of models used in the composite. The LML is confined between the two thick-dashed horizontal lines, and the mean climatological HC edge latitude is depicted with thin-dashed horizontal lines, with mean value to the right. (c) The multi-model change in SWCRE for CMIP5 from the pre-industrial (PI) control climatology to the atmosphere-"equilibrated" $4\times CO_2$ climatology for DJF. Positive (negative) values correspond to anomalous shortwave cloud radiative warming (cooling). The PI HC edge latitude is depicted with gray thin-dashed horizontal lines, and the $4\times CO_2$ HC edge is depicted with black thin-dashed lines, with mean value to the right.

the multi-model mean.

The magnitude of the HC-SWCRE regression coefficients averaged over the lower mid-latitudes for each of the 22 CMIP5 models used are listed in Table 31, along with the values from the observational analysis (Chapter 2). We average over the lower mid-latitudes because of the zonal structure exhibited by both the unforced HC-SWCRE co-variability (Figure 35b) and the $4\times CO_2$-forced shortwave cloud radiative response (Figure 35c). There is a large inter-model spread in the pre-industrial HC-SWCRE (third column), with the majority of CMIP5 models exhibiting positive HC-SWCRE values indicating lower mid-latitude mean shortwave cloud radiative warming anomalies with poleward shifts of the Hadley circulation edge. We designate those models "+HC-SWCRE" models in contrast to models which we designate "−HC-SWCRE" models that exhibit lower mid-latitude mean shortwave cloud radiative cooling anomalies with poleward shifts of the Hadley circulation edge. We note that this is similar to the Type I/II classification of Grise and Polvani 2014b in both methodology and model categorization. Still, even within each subset of models, the HC-SWCRE values vary by an order of magnitude, from about $+0.15\ Wm^{-2}degree^{-1}$ to about $+1.5\ Wm^{-2}degree^{-1}$ in the +HC-SWCRE models, and from about $-0.10\ Wm^{-2}degree^{-1}$ to about $-1.0\ Wm^{-2}degree^{-1}$ in the −HC-SWCRE models.

Beyond regression coefficients, the strength of the correlation as measured by the correlation coefficient also varies across models — in only one model (MIROC5) the lower mid-latitude shortwave cloud radiative anomalies seem independent of shifts in the Hadley circulation edge, whereas in all other models the correlation is statistically significant, with some correlation coefficients as high as 0.90 (fourth column in Table 31). Thus, in almost all models, as in observations, shortwave cloud radiative anomalies seem to be robustly associated with inter-annual shifts in the Hadley circulation edge; however, the sign of those shortwave cloud radiative anomalies averaged over the lower mid-latitudes is highly

	Name	4×CO_2 HC Edge Shift	HC Edge Lat	LML HC-SWCRE	HC-SWCRE *R*	LML mean ω500	LML HC-ω500	ECS
Observations		-	−35.83	−0.69	-0.41	−3.23	−0.48	-
+HC-SWCRE Models								
a	bcc-csm1-1	−1.49	−33.01	1.00	0.69	5.75	2.05	2.82
b	bcc-csm1-1-m	−2.34	−35.01	0.39	0.33	6.91	1.06	2.87
c	CanESM2	−3.44	−33.25	0.67	0.65	6.33	2.08	3.69
d	CNRM-CM5v	−1.02	−33.55	0.34	0.47	6.30	2.52	3.25
e	FGOALS-s2	−3.17	−30.74	0.96	0.83	4.25	3.74	4.17
f	GISS-E2-R	−1.41	−32.98	0.16	0.32	5.58	2.11	2.11
g	inmcm4	−1.14	−35.31	0.21	0.24	5.63	0.62	2.08
h	IPSL-CM5A-LR	−3.91	−30.41	1.66	0.88	3.60	4.87	4.13
i	IPSL-CM5B-LR	−1.08	−30.73	0.67	0.59	3.16	3.50	2.61
j	MIROC-ESM	−0.52	−31.48	1.33	0.78	4.37	3.37	4.67
k	MPI-ESM-LR	−1.32	−33.80	0.31	0.39	7.53	3.05	3.63
l	MPI-ESM-P	−1.33	−33.76	0.39	0.42	7.54	3.01	3.45
m	MRI-CGCM3	−1.01	−34.18	0.15	0.4	5.53	1.90	2.60
	Mean	−1.78	−32.94	0.63	-	5.58	2.61	3.24
Neutral Model								
n	MIROC5	−1.40	−34.68	0.00	0.03	6.23	2.03	2.72
−HC-SWCRE Models								
o	CCSM4	−1.38	−36.71	−0.54	-0.45	7.05	0.23	2.89
p	CSIRO-Mk3-6-0	−2.36	−34.26	−0.99	-0.59	-	-	4.08
q	GFDL-CM3	−1.55	−34.09	−0.10	-0.15	7.32	3.15	3.97
r	GFDL-ESM2G	−1.35	−35.53	−0.54	-0.37	6.64	1.51	2.39
s	GFDL-ESM2M	−1.28	−34.77	−0.41	-0.26	6.34	2.17	2.44
t	HadGEM2-ES	−3.23	−33.63	−0.22	-0.17	6.27	1.51	4.59
u	NorESM1-M	−1.42	−36.23	−0.54	-0.43	6.72	0.80	2.80
v	NorESM1-ME	-	−36.16	−0.66	-0.46	6.83	0.51	-
	Mean	−1.80	−35.17	−0.50	-	6.74	1.41	3.31
	Multi-model Mean	−1.79	−33.79	0.20	-	5.98	2.19	3.26

Table 31: Listing and characteristics of the CMIP5 models used in this chapter. Values in the first through sixth columns are calculated for DJF SH. The units of the first column are degrees latitude, where negative values correspond to poleward shifts. The units of the second column are degrees latitude, where negative values correspond to SH. The units of the third column are $Wm^{-2}degree^{-1}$. The fourth column displays the correlation coefficients (R) of the correlation between the HC edge latitude and the LML SWCRE. The units of the fifth column are $hPaday^{-1}$, and of the sixth column $hPaday^{-1}degree^{-1}$. Equilibrium climate sensitivity values are taken from Table 1 of Forster et al. 2013.

variable across models.

To examine the spatial distribution of the shortwave cloud radiative anomalies in the two subsets of model, we plot the HC-SWCRE relationship separately for the composite of +HC-SWCRE models (Figure 35d) and for the composite of −HC-SWCRE models (Figure 35e). Unlike the observations, both model classes, including the −HC-SWCRE models, show a zone of consistent shortwave cloud radiative warming anomalies on the poleward flank of the lower mid-latitudes (between approximately 35°S-45°S). In each of the −HC-SWCRE models (see also Figure 41 in Chapter 3) and in their multi-model mean (Figure 35d), this zone of shortwave cloud radiative warming anomalies is narrower than in each of the +HC-SWCRE models (see also Figure 41 in Chapter 3) and their multi-model mean (Figure 35e). The −HC-SWCRE models show a more meridionally extensive region of shortwave cloud radiative cooling anomalies on the equatorward flank of the lower mid-latitudes (between approximately 25°S-35°S), primarily due to a stronger shift in the SPCZ in the central Pacific. Note here that we have repeated the analyses performed in this study but excluding the Pacific signal, and despite its being of large amplitude, it did not change our conclusions.

In both subsets of models, the patches of cooling on the equatorward flank of the lower mid-latitudes extend approximately to the latitude of the climatological Hadley circulation edge (thin dashed lines). With the −HC-SWCRE models having on average a more poleward (or wider) climatological Hadley circulation (with an edge latitude of 34.8°S) compared to the more equatorward (or wider) climatological Hadley circulation of the average +HC-SWCRE model (with an edge latitude of 33.4°S), the −HC-SWCRE models therefore exhibit a larger area of shortwave cloud radiative cooling anomalies. This suggests that the model representation of the linkage between shortwave cloud radiative anomalies and the shifts of the Hadley circulation edge on inter-annual timescales may be connected to the climatological position of the Hadley circulation in each model. We quantify this in

the next section.

3.5 Model Biases in Climatological Hadley Circulation

Figure 36 (top) correlates the inter-model spread in pre-industrial climatological latitude of the Hadley circulation with that of the lower mid-latitude HC-SWCRE. Although we partition the models into two subsets in Table 31 for ease of discussion, the behavior of the models is actually continuous – models with narrower climatological Hadley circulations exhibit more positive values of HC-SWCRE, and models with wider climatological Hadley circulations exhibit more negative values of HC-SWCRE. The −HC-SWCRE models agree better with with observations (gray lines and envelope) as measured by both the climatological Hadley circulation edge latitude and HC-SWCRE; in contrast, none of the +HC-SWCRE models lies within the uncertainty of the observed HC-SWCRE relationship, and most exhibit unrealistically narrow Hadley circulations in comparison to the observations. This suggests that the model representation of the unforced co-variability between inter-annual shifts of the Hadley circulation edge latitude and shortwave cloud radiative anomalies in the lower mid-latitudes may be tied to where models place the latitude of the Hadley circulation in their respective climatologies. We next explore the physical mechanisms of why the shortwave cloud radiative anomalies associated with poleward shifts in the Hadley circulation edge seem to link so robustly to the climatological position of the Hadley circulation edge in models.

Since mid-latitude cloud radiative properties and vertical structure relate to the mid-tropospheric vertical velocity (e.g. Tselioudis and Jakob 2002), we examine the relationship between the Hadley circulation edge latitude and mid-tropospheric vertical velocity, i.e. ω at 500 hPa, in the lower mid-latitudes. The inter-model spread in the climatological position of the Hadley circulation correlates strongly with the inter-model spread in the

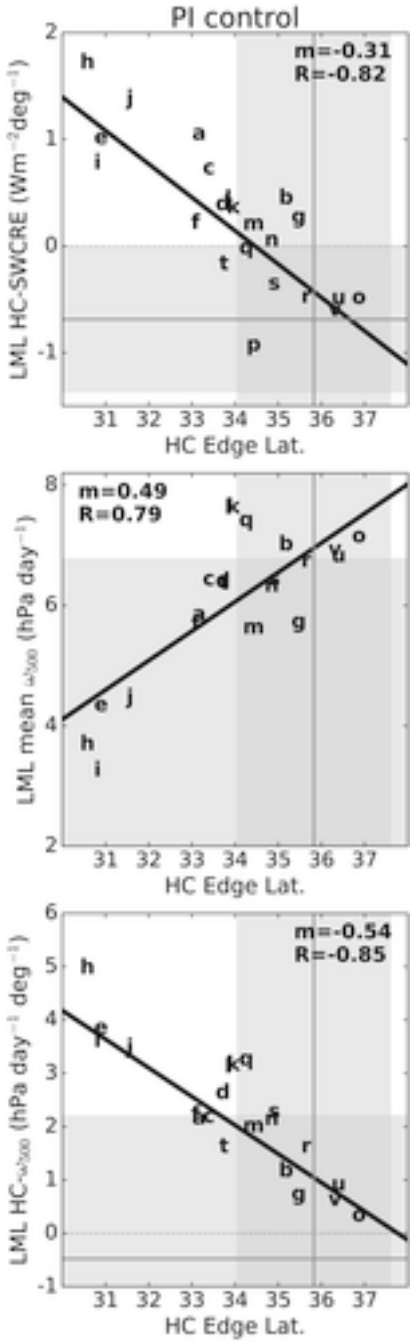

Figure 36: Least-squares linear regressions on the inter-model spread in climatological DJF SH HC edge latitude of the inter-model spread in DJF SH (top) LML HC-SWCRE, (center) climatological mean pressure vertical velocity at 500 hPa (ω500) averaged over the LML, and (bottom) LML HC-ω500. Each data point corresponds to one model (see Table 31 for model labels). Regressions statistically significant at the 95% confidence level, assessed using a Student's *t*-test, are denoted by thick lines and bold coefficients (all are significant). Gray lines represent observed values (derived from ISCCP-FD and ERA-Interim), and gray shading represents the 95% confidence interval thereof.

strength of the climatological mean vertical velocity in the lower mid-latitudes (Figure 36 center): models with narrower Hadley circulations seem to exhibit weaker climatological subsidence in the lower mid-latitudes whereas models with wider Hadley circulations seem to exhibit stronger climatological subsidence in the lower mid-latitudes. With poleward shifts of the Hadley circulation edge, the subsidence strengthens in the lower mid-latitudes of all models (Table 31 and Figure 36 bottom), and the inter-model spread in the climatological position of the Hadley circulation correlates well with the increase in vertical velocity associated with poleward shifts of the Hadley circulation, as measured by the regression coefficient HC-ω_{500}, or $\frac{\partial \omega_{500}}{\partial \theta_{HC}}\Big|_{\bar{T}_s}$ (Figure 36 bottom). Models with narrower climatological Hadley circulations and weaker mean subsidence in the lower mid-latitudes tend to experience a stronger subsidence increase as the Hadley circulation edge shifts poleward than models with wider climatological Hadley circulations and stronger mean subsidence in the lower mid-latitudes, which tend to experience weaker subsidence increases as the Hadley circulation edge shifts poleward.

We can model the dependence of $\frac{\partial \omega_{500}}{\partial \theta_{HC}}\Big|_{\bar{T}_s}$ on θ_{HC} by assuming a particular meridional structure for ω_{500}, which we represent as a Fourier series as a function of both latitude θ and the Hadley cell edge latitude θ_{HC}:

$$\omega_{500}\left(\theta;\theta_{HC}\right) \equiv \sum_{j=-\infty}^{\infty}\sum_{k=-\infty}^{\infty} c_{j,k} e^{ij\omega\theta} e^{ik\omega\theta_{HC}} \tag{3.1}$$

where the $c_{j,k}$ are the complex constant Fourier coefficients of ω_{500}. Then, the meridional average $\langle\cdot\rangle$ over the lower mid-latitudes, defined to be the zone $[\theta_{max}, \theta_{min}]$, is

$$\langle\omega_{500}\rangle = \sum_{j=-\infty}^{\infty}\sum_{k=-\infty}^{\infty} \langle c_{j,k} e^{ij\omega\theta}\rangle e^{ik\omega\theta_{HC}} = \sum_{j=-\infty}^{\infty}\sum_{k=-\infty}^{\infty} \langle c_{j,k} e^{ij\omega\theta}\rangle \left[\cos k\omega\theta_{HC} + i \sin k\omega\theta_{HC}\right] \tag{3.2}$$

Using the small angle approximation, valid for sufficiently small θ_{HC} with relative error e

bounded by $|e| \leq \frac{\theta_{HC}^2}{6}$ (with $e < 11\%$ for $\theta_{HC} = 45°$), we have

$$\langle \omega_{500} \rangle \approx \sum_{j=-\infty}^{\infty} \sum_{k=-\infty}^{\infty} \langle c_{j,k} e^{ij\omega\theta} \rangle \left[1 - \frac{(k\omega)^2}{2} \theta_{HC}^2 + ik\omega\theta_{HC} \right] \tag{3.3}$$

and the sensitivity to shifts in the Hadley circulation edge latitude

$$\frac{\partial \langle w_{500} \rangle}{\partial \theta_{HC}} \approx \sum_{j=-\infty}^{\infty} \sum_{k=-\infty}^{\infty} \langle c_{j,k} e^{ij\omega\theta} \rangle \left[ik\omega - (k\omega)^2 \theta_{HC} \right] \tag{3.4}$$

Hence, the sensitivity of the lower mid-latitude mean vertical velocity to shifts in the Hadley circulation edge latitude $\frac{\partial \langle w_{500}(\theta) \rangle}{\partial \theta_{HC}}$ is approximately linearly related to the Hadley circulation edge latitude θ_{HC}, as we have shown empirically (bottom of Figure 36 and Table 31). Note that the approximate linearity between the two quantities remains unchanged when a $\cos\theta$ area weighting is used because the θ_{HC} terms may be taken out of the meridional average $\langle \cdot \rangle$. This relationship should also be invariant to the timescale of analysis (e.g. monthly, inter-annually, climatologically, etc.) and therefore should apply to both the inter-annual co-variability between the vertical velocity in the lower mid-latitudes and the Hadley circulation edge latitude within models as well as the spread across models in the climatological $\omega 500$ in the lower mid-latitudes and the Hadley circulation edge latitude, all else being equal.

Physically, poleward shifts in the Hadley circulation edge seem to extend the influence of the strong sub-tropical subsidence into the lower mid-latitudes. In models with narrower climatological Hadley circulations, this induces anomalously strong subsidence in a region which climatologically experiences weak subsidence; i.e. a big "kick". This likely results in a strong decrease in cloud cover and hence may explain the strong shortwave cloud radiative warming anomalies that are exhibited. On the other hand, in models with wider climatological Hadley circulations and climatologically strong subsidence in the

lower mid-latitudes, the poleward shifts in the Hadley circulation edge induce relatively weak subsidence anomalies. This likely results in only small changes to the cloud field and hence may explain the relatively small shortwave cloud radiative warming anomalies that are exhibited. In the observations (Chapter 2), however, there are actually shortwave cloud radiative cooling anomalies with inter-annual poleward shifts in the Hadley circulation edge, likely because the real-world clouds may not be as univariately dependent on subsidence anomalies as are the model clouds (see also Grise and Medeiros 2016). What are the implications of this model bias in the representation of clouds and circulation in the present-day for the model projections of future climate?

3.6 Forced Response

The analysis of the CMIP5 pre-industrial control runs presented so far shows that the unforced poleward shifts of the Hadley circulation edge are robustly associated with anomalous shortwave cloud radiative warming on the poleward flank of the lower mid-latitudes on inter-annual timescales (Figure 35). We now examine whether this association is also found in the CMIP5 models' response to $4\times CO_2$ forcing. First Figure 37 (top) shows the correlation between the inter-model spread in the HC-SWCRE co-variability with the inter-model spread in the $4\times CO_2$ shortwave cloud radiative warming response in the lower mid-latitudes. The plot indicates that the magnitude of the shortwave cloud radiative anomalies in the lower mid-latitudes with unforced shifts in the Hadley circulation edge seems to predict well the magnitude of the shortwave cloud radiative warming response to quadrupling CO_2 concentrations (as noted in Grise and Polvani 2014b, see their Figure 11). We have also shown that the inter-annual co-variability between shortwave cloud radiative anomalies and the edge of the Hadley circulation is strongly related to the climatological position of the Hadley circulation edge. We therefore correlate the inter-model spread in the

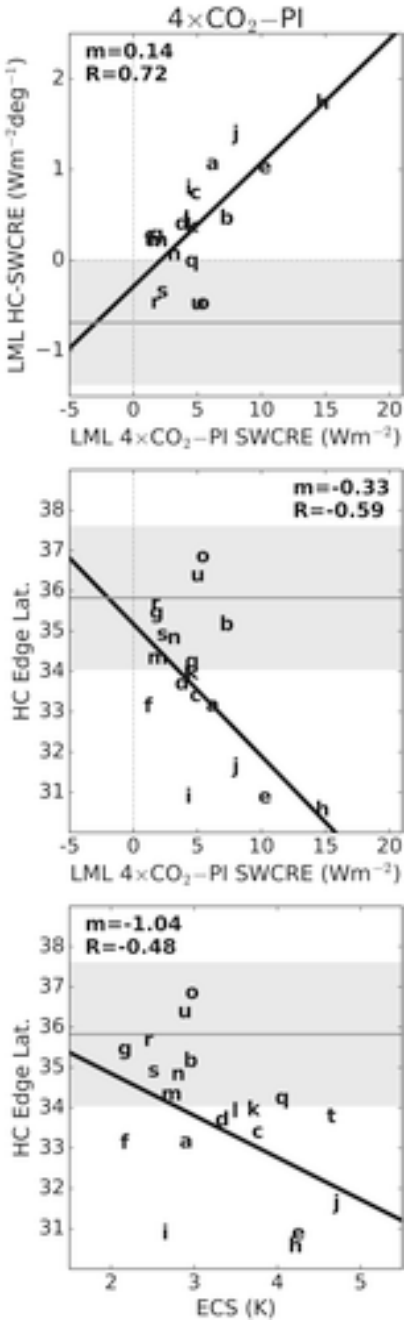

Figure 37: Least-squares linear regressions on the inter-model spread in LML averaged $4\times CO_2-PI$ SWCRE of the inter-model spread in (top) LML HC-SWCRE and (center) inter-model spread in climatological DJF SH HC edge latitude. (bottom) Least squares linear regression on the inter-model spread in equilibrium climate sensitivity of the inter-model spread in climatological DJF SH Hadley cell edge latitude. Each data point corresponds to one model (see Table 31 for model labels). Regressions statistically significant at the 95% confidence level, assessed using the Student's *t*-test, are denoted by thick lines and bold coefficients (all are significant). Gray lines represent observed values (derived from ISCCP-FD and ERA-Interim), and gray shading represents the 95% confidence interval thereof.

$4\times CO_2$-forced shortwave cloud radiative warming response in the lower mid-latitudes with the inter-model spread in the climatological latitude of the Hadley circulation edge (Figure 37 middle). It is clear that the climatological Hadley circulation edge latitude is strongly correlated with the shortwave cloud radiative response to $4\times CO_2$ forcing in the lower mid-latitudes. Therefore, this relationship could be an emergent constraint that directly links the shortwave cloud radiative response to the climatological Hadley circulation extent via the influence of atmospheric dynamics on cloud radiative effects described herein and in Chapter 2.

Finally, given the strong correlation between the shortwave cloud radiative response in the lower mid-latitudes with the inter-model spread in the values of equilibrium climate sensitivity (Figure 31b), we correlate the inter-model spread in equilibrium climate sensitivity with the inter-model spread in the climatological latitude of the Hadley circulation (Figure 37 bottom). We find that the correlation between the climatological Hadley circulation edge latitude and ECS is weaker than that between the climatological Hadley circulation edge latitude and the shortwave cloud radiative response, but still statistically significant. Models with wider climatological Hadley circulations, which more closely resemble the observations, tend to exhibit lower values of ECS than models with narrower Hadley circulation, which less closely resemble the observations. This relationship between the climatological Hadley circulation edge and ECS is likely mediated by the inter-model spread in cloud-circulation coupling in both unforced and CO_2-forced runs (Figure 37). That is, the ECS

$$\begin{aligned} \Delta T_s &\sim \left.\frac{\partial R_{SWCRE}}{\partial \omega_{500}}\right|_{\bar{T}_s} \left.\frac{\partial \omega_{500}}{\partial \theta_{HC}}\right|_{\bar{T}_s} \frac{\Delta \theta_{HC}}{\Delta T_s} \\ &\sim \left.\frac{\partial R_{SWCRE}}{\partial \omega_{500}}\right|_{\bar{T}_s} \theta_{HC} \frac{\Delta \theta_{HC}}{\Delta T_s} \end{aligned} \tag{3.5}$$

One can assess the sensitivity of shortwave cloud radiative anomalies to changes in subsidence $\left.\frac{dR_{SWCRE}}{d\omega_{500}}\right|_{\bar{T}_s}$ as we have done here or with a cleaner analysis in which one takes

into account the changes in, for example, the strength of the boundary inversion (see e.g. Myers and Norris 2013; Myers and Norris 2016; Grise and Medeiros 2016). We here argue that since $\frac{d\omega_{500}}{\theta_{HC}}\Big|_{\bar{T}_s} \sim \theta_{HC}$, $\frac{d\omega_{500}}{\theta_{HC}}\Big|_{\bar{T}_s}$ is time-scale invariant and hence should hold for both the recent past and for the future. We note that Equation 3.5 is also consistent with Figure 3c of Grise and Polvani 2014a who find a strong correlation between ECS ΔT_s and the dynamical sensitivity of the Hadley circulation $\frac{\Delta\theta_{HC}}{\Delta T_s}$ to increasing CO_2 concentrations.

Thus, the results presented in this section seem to indicate that the climatological Hadley circulation edge latitude may be a "promising" emergent constraint (Klein and Hall 2015). Models with narrower Hadley circulations exhibit stronger subsidence increases in the lower mid-latitudes and stronger shortwave cloud radiative warming anomalies with unforced poleward shifts of the Hadley circulation edge, and thus warm more with CO_2-forced poleward shifts of the Hadley circulation. This relationship constitutes an admittedly less robust but still statistically significant and physically motivated emergent constraint that links ECS to the climatological pre-industrial Hadley circulation extent, although accurately assessing the statistical significance of emergent constraints is difficult (Caldwell et al. 2014).

3.7 Summary and Discussion

We document a robust inter-annual relationship between shortwave cloud radiative anomalies and poleward shifts in the Hadley circulation in the summertime (DJF) Southern Hemisphere. All CMIP5 models exhibit anomalous shortwave cloud radiative warming in the lower mid-latitudes with poleward shifts in the Hadley circulation edge. In many models ($+$HC-SWCRE models) the anomalous shortwave cloud radiative warming dominates the the entire lower mid-latitude zone, while in a few other models ($-$HC-SWCRE models) there are also intrusions of shortwave cloud radiative cooling from the tropics. The inter-

model spread in the representation of the linkage between clouds and circulation seems to arise from the inter-model spread in representation of the large-scale circulation itself, particularly in where models place the climatological Hadley circulation edge. In models with narrower climatological Hadley circulations, poleward shifts in the Hadley circulation edge transition the lower mid-latitudes from a regime of weak subsidence to one of strong subsidence, likely resulting in decreased cloud cover and hence anomalous shortwave cloud radiative warming. In models with wider climatological Hadley circulations, poleward shifts in the Hadley circulation edge keep the lower mid-latitudes in a regime of strong subsidence, and the shortwave cloud radiative warming anomalies are small (Figure 35). The key finding here is that the CO_2-forced shortwave cloud radiative response in the lower mid-latitudes seems to be correlated with model biases in the climatological position of the Hadley circulation edge. This is consistent with previous studies which find a strong link between model biases in shortwave cloud radiative effects and the model climatology (Trenberth and Fasullo 2010; Grise, Polvani, and Fasullo 2015; Siler, Po-Chedley, and Bretherton 2018). In particular, models with climatological HC edge latitudes closer to the observations show a weaker shortwave cloud radiative warming response and tend to have smaller values of ECS.

Our analysis of the linkage between clouds and the circulation brings forward two main issues: 1) how changes in the large-scale circulation imprint on the subsidence, i.e. $\frac{d\omega_{500}}{x_{dyn}}\Big|_{\bar{T}_s}$, and 2) how changes in the large-scale subsidence imprint on clouds and their radiative effects, i.e. $\frac{dR_{SWCRE}}{d\omega_{500}}\Big|_{\bar{T}_s}$. Regarding the latter, the same increase in subsidence may affect clouds differently depending on the model microphysics scheme (Storelvmo, Tan, and Korolev 2015; Ceppi, Hartmann, and Webb 2016). In this chapter, we have examined the former with respect to the Hadley circulation, i.e. $x_{dyn} = \theta_{HC}$, and have shown that model biases in Hadley circulation edge location affect the magnitude of the subsidence anomalies with Hadley circulation edge shifts $\frac{d\omega_{500}}{\theta_{HC}}\Big|_{\bar{T}_s} \sim \theta_{HC}$. The model behavior is a continuous

function of the climatological location of the Hadley circulation. However, this might also be connected to the representation of clouds in the models, as the climatological cloud radiative effects may help determine the location of the large-scale atmospheric circulation (Ceppi et al. 2012; Ceppi, Zelinka, and Hartmann 2014; Siler, Po-Chedley, and Bretherton 2018). It must be noted also that this thesis focuses on the effects of the latitudinal shifts of the circulation. Changes in the strength of the circulation may produce different cloud radiative responses that can have contrasting effects on model climate sensitivity (see, e.g. Su et al. 2014).

We note further here that the results from our emergent constraint differ from previous studies which generally indicate that models which match some observational constraint tend to have higher values of ECS. However, those previous studies have not used our observational constraint, for which we have outlined a plausible physical mechanism. Of course, we do not argue that our observational constraint is a necessarily better metric. We acknowledge that ECS is influenced by a variety of processes that produce feedbacks, and that no singular metric will, or even can, constrain it. Previous studies examine, for example, the depth and intensity of the HC and its embedded monsoonal circulation, lower tropospheric mixing, the double ITCZ bias, and the seasonal cycle of marine boundary layer cloud. Our results are not contradictory but complementary, as neither previous studies nor the current one claims or can claim to assess the full extent of ECS influences.

Our findings nevertheless highlight that inter-model differences in the cloud-dynamics coupling may be due, not only to model biases in thermodynamics (e.g. Tan, Storelvmo, and Zelinka 2016) or the representation of clouds (e.g. Grise and Medeiros 2016), but also to inter-model differences in the climatological large-scale atmospheric circulation itself. Although the models' representations of clouds and their radiative effects still need to be improved and the biases in cloud microphysical schemes still need to be addressed, advancing our understanding of the linkages between cloud and the general circulation of the

atmosphere may come from a more realistic model representation of the circulation itself. In the next chapter, we demonstrate how this can be achieved.

Chapter 4

Understanding observed and modeled linkages between clouds and the general circulation of the atmosphere:

A numerical experiment to test the proposed Hadley circulation explanation

4.1 Introduction

The large-scale atmospheric circulation and temperature help to determine whether and which type of clouds form. Clouds, in turn, impact the atmospheric conditions. This coupling among clouds, dynamics, and thermodynamics is highly uncertain and contributes to the model uncertainty in how clouds will feed back onto the response of the climate system to increasing concentrations of CO_2 (e.g. Bony et al. 2015; Voigt and Shaw 2015). The cloud radiative feedbacks remain the single largest source of the model uncertainty for projections of future climate (e.g. Andrews et al. 2012; Vial, Dufresne, and Bony 2013; Webb, Lambert, and Gregory 2013; Qu et al. 2014). While it is now believed that the cloud radiative feedback is positive in the tropics (e.g. Ceppi et al. 2017), the sign and the strength of the cloud radiative feedback in the mid-latitudes remains unclear (Boucher et al. 2013).

Previous work has examined the especially uncertain shortwave cloud radiative feedback in the mid-latitudes as a function of dynamics and of thermodynamics. The prevailing hypothesis, articulated in the 5th Assessment Report of the International Panel on Climate

Change, has been a dynamical one – that poleward shifts of the mid-latitude eddy-driven jet should be associated with anomalous shortwave cloud radiative warming because clouds should shift to higher latitudes with lower insolation and reflect less sunlight (Boucher et al. 2013). However, the existence and magnitude of this interaction between the jet and the clouds, and its impact on the shortwave cloud radiative effect (SWCRE), has been found to depend on ocean basin, season, and climate model (see Chapter 2 and Bender, Ramanathan, and Tselioudis 2012; Grise et al. 2013; Kay et al. 2014; Li et al. 2014; Grise and Polvani 2014b). For example, Grise and Polvani 2014b analyze the inter-annual co-variability between the mid-latitude jet and shortwave cloud radiative anomalies across the mid-latitudes ($30°$S-$60°$S) in the summertime (DJF) Southern Hemisphere. They find two classes of models among phase 5 of the Coupled Model Intercomparison Project (CMIP5): the Type I models (analogous to our "warming" or $+$HC-SWCRE models in Chapter 3) exhibit strong shortwave cloud radiative warming anomalies in the mid-latitudes with poleward shifts in the eddy-driven jet latitude, whereas the Type II (analogous to our "cooling" or $-$HC-SWCRE models in Chapter 3) models exhibit only small shortwave cloud radiative anomalies in the mid-latitudes with poleward shifts in the eddy-driven jet latitude and agree better with observations than do Type I models. Extending this work, Grise and Medeiros 2016 suggest that the difference between the Type I models and the Type II models in their representations of the co-variability between clouds and the eddy-driven jet lies in the different sensitivities of model low clouds to subsidence anomalies. Increased subsidence in the lower mid-latitudes on the equatorward flank of the storm track accompanies poleward shifts of the eddy-driven jet in all models and in the observations. The low clouds in the Type I models are, however, too univariately dependent on the lower mid-latitude subsidence anomalies, compared to the low clouds in the Type II models and in the observations which depend on the anomalies in the strength of the inversion of the planetary boundary layer together with those in the vertical velocity.

Not only is the association between clouds and the jet highly complex, other studies have shown that the mid-latitude shortwave cloud radiative feedback is associated primarily with changes in thermodynamics and not with changes in dynamics (Storelvmo, Tan, and Korolev 2015; Kay et al. 2014; Wall and Hartmann 2015). These results have been interpreted to indicate that model biases in clouds and radiation are due to model biases in small-scale cloud microphysics, which global models must parameterize and which are sparsely observed, and not in large-scale dynamics, which models resolve explicitly (Ceppi and Hartmann 2015). In particular, a well-documented model bias in the parameterization of cloud processes involves the handling of mixed-phase (ice and liquid) clouds (Cesana et al. 2015). At sufficiently cold temperatures (between 0°C and -40°C) in the atmosphere, ice and supercooled liquid water can exist simultaneously, but global climate models tend to underestimate the amount of supercooled liquid cloud compared to the amount of ice cloud because of the difficulties in representing microphysical processes like ice nucleation (McCoy et al. 2015; Tan, Storelvmo, and Zelinka 2016; McCoy et al. 2016), and because of the difficulties in providing observational constraints on the abundance of supercooled liquid clouds (Cesana et al. 2015; Morrison et al. 2012). It has been noted, perhaps related to model biases in mixed-phase clouds (Kay et al. 2016), that the inter-model differences in the shortwave cloud radiative anomalies with poleward shifts in the eddy-driven jet may be attributable to different model parameterizations of shallow convection and moist turbulence, which may affect the strength of the turbulent entrainment of dry free tropospheric air into the boundary layer, etc., and hence the sensitivity of low clouds to jet shifts (see Park and Bretherton 2009; Bretherton and Park 2009; Gettelman, Kay, and Shell 2012; Sherwood, Bony, and Dufresne 2014; Kay et al. 2014; Wall and Hartmann 2015).

The challenges of parameterizing and observationally constraining cloud microphysics in a global climate model suggest the need for a large-scale handle on the problem of more accurately representing model clouds in the mid-latitudes. Our analysis of the observations

(Chapter 2) shows that the inter-annual mid-latitude cloud amount and shortwave cloud radiative anomalies correlate with the edge latitude of the large-scale Hadley circulation, more so than with the eddy-driven jet latitude. Further, one might more readily associate the subsidence anomalies identified by Grise and Medeiros 2016 as critical to model biases in clouds with shifts in the edge latitude of the Hadley circulation rather than with shifts in the eddy-driven jet latitude. That is, the dynamics of the Hadley circulation may be a convenient bridge between the thermodynamics of the tropics and eddy-driven jet dynamics of the extra-tropics, because subsidence strengthening and subsidence-induced warming accompany poleward shifts in the Hadley circulation edge latitude, especially in the lower mid-latitudes identified by Grise and Medeiros 2016. In fact, about half of the full shortwave cloud radiative response in the lower mid-latitudes to $4\times CO_2$ forcing can be predicted from the unforced poleward expansion of the Hadley circulation (Figure 41) in the summertime Southern Hemisphere.

Further highlighting the importance of the Hadley circulation for the mid-latitude clouds and their shortwave cloud radiative effects, we demonstrate in Chapter 3 that model differences in the latitude of the climatological edge of the Hadley circulation correlate with differences in the mid-latitude shortwave cloud-radiative response to increasing CO_2 concentrations and with equilibrium climate sensitivity. Specifically, we find that in CMIP5 models, the climatological position of the Hadley circulation in the Southern Hemisphere is strongly linked to the mid-latitude shortwave cloud response to increasing CO_2 there. With forcing by abrupt quadrupling of the concentration of CO_2, models with unrealistically narrow climatological Hadley circulations exhibit strong shortwave cloud radiative warming responses, which in turn correlates with high values of equilibrium climate sensitivity, whereas models with more realistic climatological Hadley circulations exhibit weak shortwave cloud radiative warming responses, which in turn correlates with lower values of equilibrium climate sensitivity

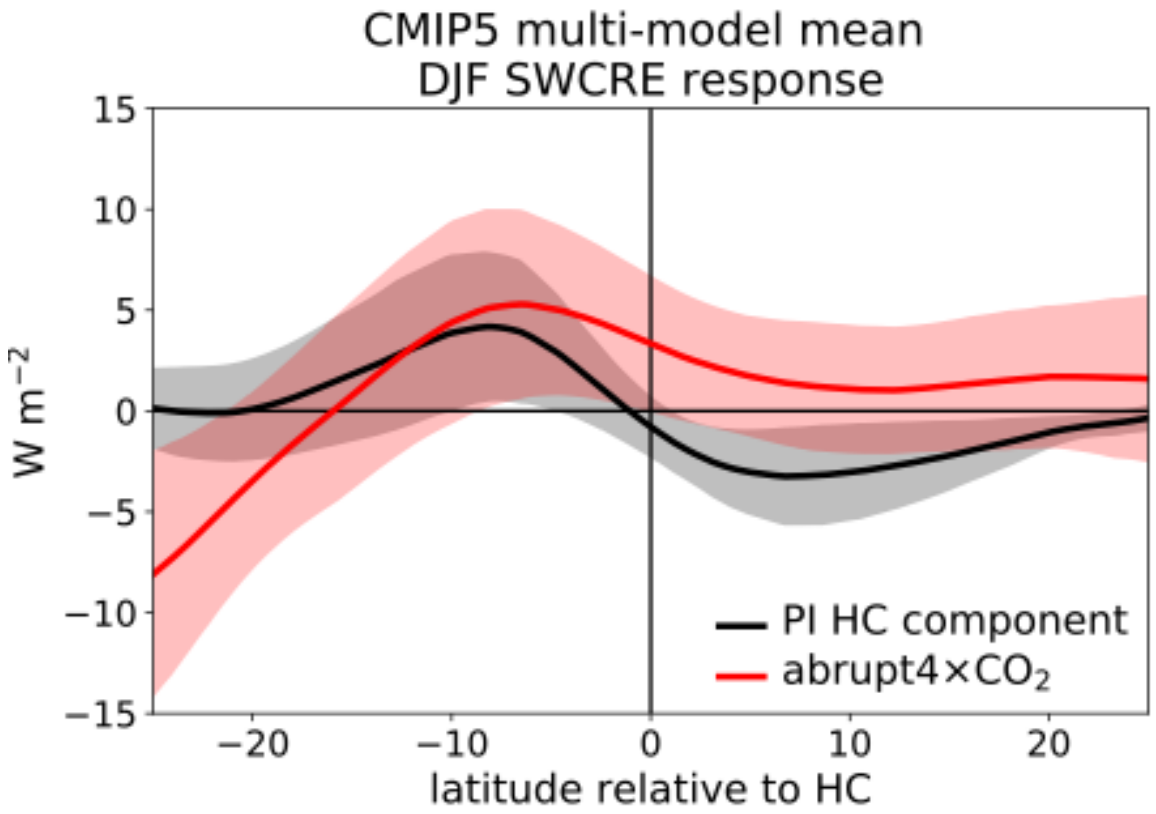

Figure 41: Predicted and actual SWCRE response to $4\times CO_2$ in the SH. The multi-model mean (thick red line) and standard deviation (red shading) of the change in zonal-mean SWCRE from the pre-industrial control climatology to the atmosphere-"equilibrated" (first 50 years excluded) $4\times CO_2$ climatology. The predicted multi-model mean (thick black line) and standard deviation (gray shading) in $4\times CO_2$ zonal-mean SWCRE change computed as the each model's predicted HC edge latitude shift in response to $4\times CO_2$ forcing multiplied by the HC-SWCRE regression. Both the actual and predicted SWCRE responses are plotted as a function of latitude relative to each model's pre-industrial control climatological HC edge, and are area-weighted.

The results of Chapter 3 suggest that the model biases in the large-scale Hadley circulation correlate with the model biases in clouds and their radiative effects. In this chapter, we address this hypothesis through simulations with a single global climate model in a simplified configuration. We vary only the climatological edge of the Hadley circulation using different values of near-surface friction but keep everything else, including the cloud schemes, the same. We emphasize that our use of a single model eliminates a priori the attribution of our results to differences in the parameterization of mixed-phase cloud processes, shallow convection, moist turbulence, etc., and that any differences that we see across our simulations must be attributed to the changes we have imposed on the large-scale circulation. Our use of a simplified configuration eliminates a priori any confounding of our results by zonal asymmetries, e.g. the presence of land or the use of a non-canonical regional Hadley circulation.

Our idealized aquaplanet simulations using one global climate model allows us to demonstrate explicitly in Sections 4.3 and 4.4 that the magnitude of the shortwave cloud radiative anomalies in the mid-latitudes that accompany poleward shifts in the Hadley circulation edge does indeed depend on the climatological position of the Hadley circulation in a manner consistent with the spread across CMIP5 models (Chapter 3). We show in Section 4.5 that the impact of the Hadley circulation operates via subsidence and its control on the amount of low-level clouds. We further show in Section 4.5that the CMIP5 model biases in their representation of the relationship between the Hadley circulation and SWCRE are consistent with the simulations presented here and that about half of the biases across the CMIP5 models can be explained by biases in the Hadley circulation. This demonstrates that improving the large-scale dynamics in models can help to improve the representation of clouds in climate models and therefore help to reduce the model uncertainty in equilibrium climate sensitivity.

4.2 Data and Methods

Data

We use the monthly-mean output from the pre-industrial (PI) control runs ("r1i1p1") and from the last 100 years of the abrupt4$\times CO_2$ runs for all available CMIP5 models (Taylor, Stouffer, and Meehl 2012). We use reanalysis data for the circulation from ERA-Interim (Dee et al. 2011), and satellite retrieval data for the radiative fluxes from ISCCP-FD (Zhang et al. 2004), and for the clouds from ISCCP-D2 (Rossow and Schiffer 1999). We focus on the Southern Hemisphere; because of maximal insolation, we analyze the summer season (DJF). To highlight the cloud-circulation coupling without forcing or other confounding variables, we analyze the pre-industrial control runs. We define the Hadley cell (HC) edge as the latitude of the first zero-crossing of the mid-tropospheric (500 hPa) meridional mass streamfunction. The shortwave cloud radiative effect (SWCRE) is the difference between the all-sky and clear-sky top-of-atmosphere outgoing solar radiation. For more details, see Section 2.2.

To measure the co-variability between clouds and the circulation, we define two metrics: 1) the HC-SWCRE, defined as the regression at each latitude of the inter-annual summer-mean time-series of the SWCRE onto the time series of the Hadley circulation edge latitude (see Section 2.2), and 2) the HC-SWCRE index, computed by averaging the HC-SWCRE over a zone 10 degrees poleward and 5 degrees equatorward of each model's climatological Hadley circulation edge latitude to capture the shortwave cloud radiative anomalies associated with poleward shifts in the edge latitude of the Hadley circulation. Our results are insensitive to the choice of metric or region (Figure 42). The zone 10 degrees poleward and 5 degrees equatorward of each model's climatological Hadley circulation edge latitude, which we refer as the lower mid-latitudes (LML), spans $\sim$30°S-45°S in the multi-model mean, similar to the $\sim$28°S-48°S zone used in Chapter 3. That the results are similar

regardless of the choice of region suggests robustness.

Model

We perform aquaplanet simulations with the ECHAM6 atmosphere general circulation model (Stevens et al. 2013), which is the atmospheric component of the MPI-ESM Earth system model used for CMIP5 (Giorgetta et al. 2013). The model is integrated in T63 resolution (approximately $1.875° \times 1.875°$) with 47 vertical levels and is run for 30 years. We exclude the first 10 years of spin-up in our analysis. All boundary conditions are zonally-symmetric. Insolation is set to perpetual January conditions, and we analyze only the summer hemisphere.

We introduce artificial Rayleigh drag on the zonal wind (u), $\partial_t u = -u/\tau$, in the lower troposphere (between the surface and 700 hPa) to control the position of the climatological Hadley circulation edge following Chen, Held, and Robinson 2007. The Rayleigh drag maximizes near the surface and decays linearly to zero with decreasing pressure up to 700 hPa. We vary the Rayleigh drag strength τ^{-1} from 0 to 2.0 day^{-1} in intervals of 0.5 day^{-1}. Increasing the drag causes an equatorward shift in the edge latitude of the Hadley circulation (Chen, Held, and Robinson 2007).

Increasing surface drag has been shown to shift equatorward the latitude of the *eddy-driven jet* (Chen, Held, and Robinson 2007). By way of explanation for the effect of drag on the latitude of the *Hadley circulation edge*, we recall that the summertime Hadley circulation, in comparison to the cross-equatorial wintertime Hadley circulation, is far from angular-momentum conserving (Walker and Schneider 2006). With an edge latitude farther poleward than the cross-equatorial wintertime Hadley circulation, the summertime Hadley circulation is more strongly influenced by mid-latitude eddies (Schneider and Bordoni 2008; Bordoni and Schneider 2010; Kang and Polvani 2011; Kang and Lu 2012). Hence, we use the Held 2000 metric for the Hadley circulation edge latitude, namely that the

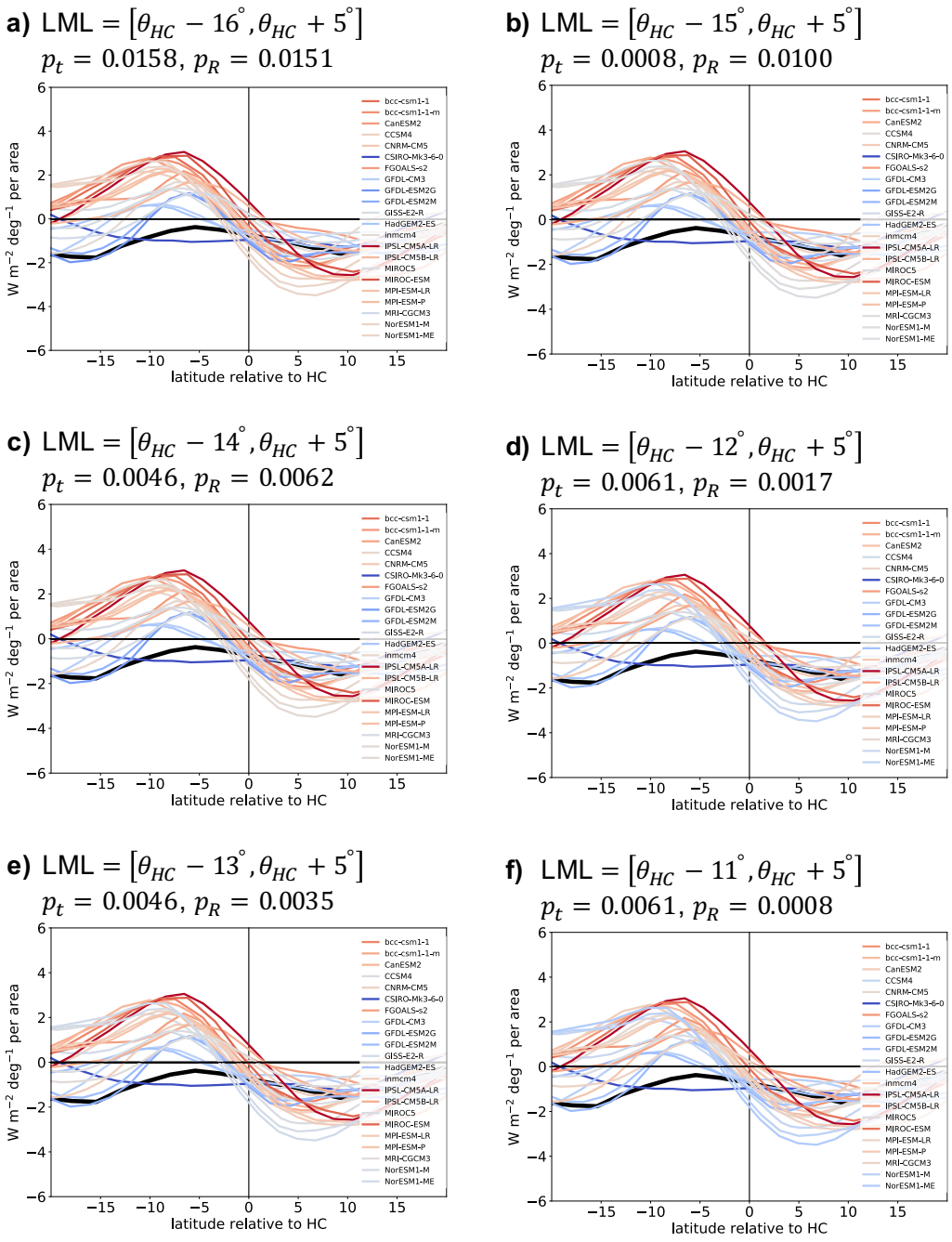

Figure 42: The results of a sensitivity analysis performed against choice of the LML zone. Displayed is the area-weighted HC-SWCRE regressions of each of the CMIP5 models as a function of relative latitude from the climatological HC edge.The definition of the LML relative to the climatological Hadley circulation edge latitude $\theta_H$is listed in the panel title. Also listed is the p-value of the Student's *t*-test for the difference between the means of the climatological Hadley circulation edges of the two groups (blue models v. red models) as p_t, and the p-value of the correlation between the model spread in climatological HC edge latitude and the model spread in HC-SWCRE index as p_R.

Hadley circulation terminates approximately at the latitude where the sub-tropical upper-tropospheric jet first becomes baroclinically unstable. A minimal model that includes this behavior might be the two-layer quasi-geostrophic model of the atmosphere (Phillips 1951; Vallis 2017), in which the criteria for the onset of baroclinic instability is that the vertical shear between the zonal-wind of the top layer u_{top} and the zonal-wind of the bottom layer u_{bot} be sufficiently strong, i.e. at least:

$$u_{top} - u_{bot} > \frac{N^2 H^2}{4} \cdot \frac{\beta}{f_0^2} \tag{4.1}$$

where N^2 is the constant stratification, H is the depth of the troposphere, $\beta = \frac{2\Omega}{a}\cos\theta$ is the beta parameter and $f_0 = 2\Omega\sin\theta$ is the Coriolis parameter. Assuming that we had made the β-plane approximation at θ_{HC}, we can estimate the latitude at which the two terms in Equation 4.1 become comparable in magnitude

$$u_{top} - u_{bot} \sim \frac{N^2 H^2}{4} \cdot \frac{\frac{2\Omega}{a}\cos\theta_{HC}}{4\Omega^2 \sin^2\theta_{HC}} \tag{4.2}$$

Using the small-angle approximation, which is valid near the equator (but admittedly less so in the sub-tropics and lower mid-latitudes),

$$u_{top} - u_{bot} \sim \frac{N^2 H^2}{8a\Omega} \cdot \frac{1 - \frac{1}{2}\theta_{HC}^2}{\theta_{HC}^2} \tag{4.3}$$

and thus

$$\theta_{HC} \sim \left[\frac{\frac{N^2 H^2}{8a\Omega}}{\left(u_{top} - u_{bot}\right) + \frac{N^2 H^2}{16a\Omega}} \right]^{\frac{1}{2}} \tag{4.4}$$

Assuming that the imposition of the low-level Rayleigh drag decreases u_{bot} more than it decreases u_{top}, we have an increase in the shear $u_{top} - u_{bot}$ and hence a decrease or equatorward shift in θ_{HC}.

The ECHAM6 atmosphere model is coupled to a thermodynamic, 10 meter deep slab ocean. The ocean "q-flux" for each of the five runs is computed from surface fluxes saved from each of five companion fixed-SST simulations, in which we use the corresponding value of Rayleigh drag and a variant of the Qobs-SST profile (Williamson et al. 2012), but shifted 15° latitude southward:

$$T_{\mathrm{s}}(\phi) = \begin{cases} 0°\mathrm{C}, & |\phi| \geq \phi_0 \\ 27°\mathrm{C} \cdot \left[1 - \frac{1}{2}\sin^2\left(\frac{\pi}{2}\frac{\phi-\phi_{\max}}{\phi_0+\phi_{\max}}\right) - \frac{1}{2}\sin^4\left(\frac{\pi}{2}\frac{\phi-\phi_{\max}}{\phi_0+\phi_{\max}}\right)\right], & -\phi_0 < \phi \leq \phi_{\max} \\ 27°\mathrm{C} \cdot \left[1 - \frac{1}{2}\sin^2\left(\frac{\pi}{2}\frac{\phi-\phi_{\max}}{\phi_0-\phi_{\max}}\right) - \frac{1}{2}\sin^4\left(\frac{\pi}{2}\frac{\phi-\phi_{\max}}{\phi_0-\phi_{\max}}\right)\right], & \phi_{\max} < \phi \leq \phi_0 \end{cases} \tag{4.5}$$

where $\phi_0 = 60^\circ$ latitude, and $\phi_{\max} = -15^\circ$ latitude. These "q-fluxes" act as an idealized ocean circulation and maintain the interactive slab-ocean SSTs close to the fixed-SST values. It is important to perform these simulations with interactive slab-ocean SSTs because we expect that most of the shortwave cloud radiative anomalies will act on the sea surface since the atmosphere itself is approximately transparent to shortwave radiation.

4.3 Motivation

We begin by demonstrating in Figure 43 that we have reproduced the inter-model spread in cloud-circulation coupling across the fully-coupled CMIP5 models that we have analyzed in Chapter 3 but by using the spread across our simulations which differ only in their climatological Hadley circulations and which were derived from a single, simplified model. We first display the CMIP5 model biases in mid-latitude clouds, radiation and dynamics from Chapter 3 in a more illustrative way. Using monthly-mean output from CMIP5 pre-industrial control runs, we present in Figure 43a the HC-SWCRE, defined as the regression between the inter-annual zonal-mean SWCRE and the edge latitude of the Hadley circula-

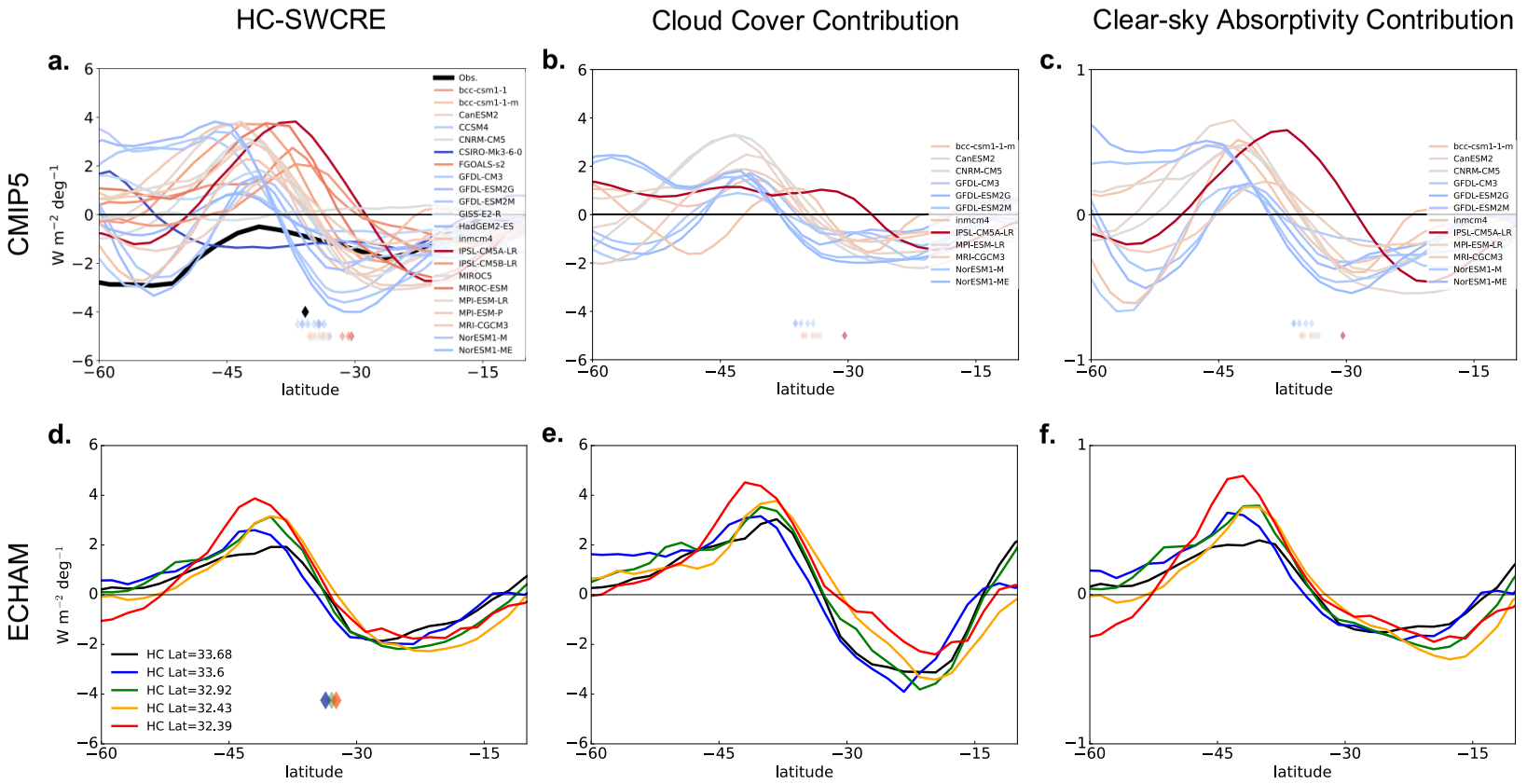

Figure 43: Impact of HC edge shifts on mid-latitude SWCRE. Least-squares linear regression coefficients of the zonal-mean SWCRE against the SH HC edge latitude (left) for (a) CMIP5 models where the DJF-mean values are used, and for (d) the ECHAM6 aquaplanet simulations. The CMIP5 models are colored red for positive LML HC-SWCRE indices and blue for negative LML HC-SWCRE indices. The ECHAM6 simulations are colored according to their climatological HC edge latitude and LML HC-SWCRE maxima. The diamonds display the climatological HC edge latitude, and are colored correspondingly. In (a) the climatological HC edge latitudes of the blue models are displayed above those of the red models for clarity. We display in the thick black line in (a) the observed HC-SWCRE regression derived from ERA-Interim and ISCCP-FD. Decomposition of the full HC-SWCRE regression (a, d) into the SWCRE changes due to cloud cover (b, e), and changes in clear-sky absorptance (c, f) using the approximate partial radiative perturbation method of Taylor et al. 2007, for all models for which data was available. Note the differences in y-axis scales across columns.

tion. From this HC-SWCRE regression, we construct the HC-SWCRE index by averaging the HC-SWCRE regression coefficients over the lower mid-latitudes (see Section 4.2). This index, whose magnitude we use to color the models in Figure 43a, separates models that generally exhibit anomalous shortwave cloud radiative warming in the lower mid-latitudes with poleward shifts in the Hadley circulation edge latitude (positive HC-SWCRE index or "warming" models, in red) from models that generally exhibit anomalous shortwave cloud radiative cooling in the lower mid-latitudes with poleward HC edge shifts (negative HC-SWCRE index or "cooling" models, in blue), similar to the Type I/II classification of Grise and Polvani 2014b.

All models (except CSIRO-Mk3-6-0) display a dipole in the HC-SWCRE with anomalous shortwave cloud radiative cooling in the sub-tropics ($\sim$15°S-30°S) and anomalous shortwave cloud radiative warming in the lower mid-latitude ($\sim$30°S-45°S; LML). As discussed in Chapters 2 and 3, the observations (thick black line in Figure 43a) do not exhibit a dipole in HC-SWCRE, but rather exhibit weak shortwave cloud radiative cooling anomalies throughout the mid-latitudes. In the CMIP5 models, little systematic difference exists between the warming and the cooling models in the shortwave cloud radiative anomalies they exhibit with poleward shifts of the Hadley circulation in the sub-tropics. However, the magnitude of the shortwave cloud radiative warming anomalies in the lower mid-latitudes with poleward shifts of the Hadley circulation is, on average, larger in the warming models than in the cooling models. Furthermore, the climatological position of the Hadley circulation edge (diamonds in Figure 43a) is farther equatorward on average in the warming models than in the cooling models (see Chapter 3) as revealed by the Student's *t*-test (p =0.0083). Hence, we here refer to the warming models as models with narrow Hadley circulations and to the cooling models as models with wide Hadley circulations. The overall model spread in the maxima of the mid-latitude shortwave cloud radiative warming anomalies with poleward Hadley circulation shifts is about 4 $Wm^{-2}degree^{-1}$ (from about 4 $Wm^{-2}degree^{-1}$

to about 0 $Wm^{-2}degree^{-1}$, with the observations at about -0.5 $Wm^{-2}degree^{-1}$), and the model spread in the climatological Hadley circulation edge latitude is about 6° latitude (from about 30°S to about 36°S, with the observations at about 36°S).

4.4 Results from Aquaplanet Simulation

In Chapter 3 we report a strong correlation between the HC-SWCRE index and the climatological position of the Hadley circulation edge in CMIP5 models. This correlation suggests that the model bias in clouds and radiation is linked to the model bias in dynamics. However, since that correlation was derived across different models, it could also arise from inter-model differences in, for example, cloud schemes. To show that the correlation reported in Chapter 3 does indeed arise from a systematic impact of the circulation on clouds, we here perform a set of five simulations with the ECHAM6 model (Stevens et al. 2013), used in aquaplanet setup with zonally-symmetric Southern summer boundary conditions and coupled to a thermodynamic slab ocean. We introduce different values of boundary layer drag to vary the climatological HC edge between 33.7°S and 32.4°S.

In the bottom row of Figure 43, we repeat the analysis for the plots in the top row but for our different ECHAM6 aquaplanet simulations rather than for the CMIP5 models. Figure 43d shows the HC-SWCRE in the five ECHAM6 aquaplanet simulations. Consistent with Chapter 3 and Figure 43a, the mid-latitude maxima in shortwave cloud radiative anomalies with poleward shifts in the Hadley circulation edge is smaller for simulations with wider Hadley circulations than for simulations with narrower Hadley circulations. With the HC-SWCRE maximum varying by 2 $Wm^{-2}degree^{-1}$ between the five simulations, we can reproduce about half of the CMIP5 model spread in mid-latitude HC-SWCRE solely by changing the climatological circulation: the cloud scheme is identical in all five ECHAM6 aquaplanet simulations. That is, by pushing the climatological Hadley circulation edge

latitude towards its observed position, our aquaplanet model exhibits less of the unrealistic warming (or Type I) model behavior and more of the observed cooling (or Type II) model behavior: hence, we have achieved turning a biased warming or Type I model into a more realistic cooling or Type II model.

4.5 Mechanisms of Cloud-Circulation Coupling

We now analyze the aquaplanet simulations and the CMIP5 models in greater detail to understand the mechanisms involved, and to ensure that we have removed the biases for "physical" reasons rather than spurious ones. We first ask: How does the climatological HC latitude affect the cloud-circulation coupling? To answer this question, we use the approximate partial radiative perturbation method of Taylor et al. 2007 with a single-layer radiative transfer model. We decompose the HC-SWCRE into contributions from changes in cloud cover, cloud and clear-sky albedo, and cloud and clear-sky atmospheric absorptivity. This method estimates the contributions to the change between two states in the net TOA shortwave radiative flux $\Delta Q = \Delta S\,(1-A) - S\Delta A$ by the change in insolation ΔS (which we expect to be non-negligible only when examining changes in, e.g., solar and/or orbital forcing) and more importantly by the change in planetary albedo ΔA. We idealize this with a single-layer atmosphere which scatters radiation passing through it with scattering coefficient γ, but absorbs radiation only on the first pass of the incident ray with absorptance $1-\mu$, and with a surface with albedo α (see Figure 44). Then we can express the planetary albedo as $A = \mu\gamma + \mu\alpha\,(1-\gamma)^2\,\frac{1}{1-\alpha\gamma}$. One can tease out the shortwave cloud radiative effects from the shortwave clear-sky radiative effects by computing separately the planetary albedo using the net TOA shortwave radiative fluxes during clear-sky conditions and during cloudy conditions, so that $A = (1-C)\,A_{clr} + C A_{cld}$ where C is cloud fraction.

For the approximate partial radiative perturbation analysis, we take as the control state

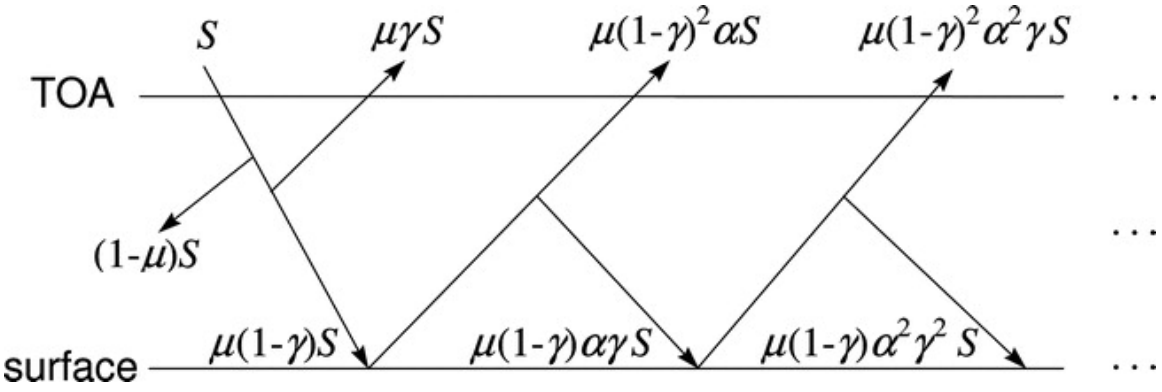

Figure 44: Schematic representation of a simple one-layer shortwave radiation model showing fluxes passing through the atmosphere and being partially reflected on each pass, where S is the insolation, α surface albedo, γ atmospheric scattering coefficient, and $(1-\mu)$ atmospheric absorptance. Wavelengths that are readily absorbed by the atmosphere are assumed to be completely removed on the first pass, and the atmosphere is transparent to other wavelengths. Taken from Figure 1 of Taylor et al. 2007

the composite of years when the Hadley circulation edge latitude is anomalously equatorward (θ^e_{HC}) and as the perturbed state the composite of years when the Hadley circulation edge latitude is anomalously poleward (θ^p_{HC}), normalizing by the difference in Hadley circulation edge latitude between the two states. We exclude the middle 20% of years as neutral Hadley circulation edge latitude years, but note that our results are insensitive to the exclusion of the middle 0%, 5%, 10%, and 15%. We compute the radiative perturbation as the average of the forward and backward substitutions of the control and perturbed fields (see Colman 2003). For example,

$$\begin{aligned}\Delta A_C = &\frac{1}{\theta^p_{HC} - \theta^e_{HC}} \frac{1}{2} \left(\left[A\left(C_{\theta^p_{HC}}, x_{\theta^e_{HC}}\right) - A\left(C_{\theta^e_{HC}}, x_{\theta^e_{HC}}\right) \right] + \right. \\ &\left. \left[A\left(C_{\theta^p_{HC}}, x_{\theta^p_{HC}}\right) - A\left(C_{\theta^e_{HC}}, x_{\theta^p_{HC}}\right) \right] \right)\end{aligned} \tag{4.6}$$

The decomposition (Figure 43b,c,e,f) reveals that the HC-SWCRE predominantly arises from changes in cloud fraction, with smaller contributions from changes in clear-sky atmo-

spheric absorptivity. This clear-sky absorptivity contribution is likely due to less absorption of shortwave radiation absorbed by water vapor associated with anomalously strong subsidence. The contribution by changes in cloud albedo and cloud absorptivity (not shown) is two orders of magnitude smaller than the contribution by changes in cloud fraction, indicating that differences in the lower mid-latitude HC-SWCRE across both the ECHAM6 simulations and the CMIP5 ensemble do not result from thermodynamic cloud phase changes highlighted in previous studies as important for the cloud radiative effect at higher latitudes Ceppi, Hartmann, and Webb 2016; Ceppi and Hartmann 2015; Wall and Hartmann 2015. Rather, the changes in SWCRE due to Hadley circulation shifts and that due to thermodynamic phase changes are likely two independent processes that may both be important for the cloud radiative response to warming. That is, the "dipole" of CO_2-forced shortwave cloud radiative cooling response in the higher latitudes and the shortwave cloud radiative warming in the lower mid-latitudes may not be produced by one coherent climate feedback process but may actually emerge as the results of multiple, perhaps independent climate processes.

Figure 45d compares, across the five ECHAM6 simulations, the total cloud cover response to poleward Hadley circulation edge shifts. We see that the total cloud cover in the lower mid-latitudes decreases more simulations with narrower Hadley circulations than in simulations with wider Hadley circulations. The observations (thick black line in Figure 45a), on the other hand, exhibit relatively weaker reductions in total cloud cover than do the models. The observed decrease in total cloud cover but slight increase in shortwave cloud reflection (thick black line in Figure 43a) can be explained by a reduction in high cloud but a compensation by low clouds in shortwave reflection (see Chapter 2). The ECHAM6 results (Figure 45d) on the spread in total cloud cover decreases with poleward Hadley circulation edge shifts resemble the CMIP5 results as well (Figure 45a): for models with a narrow Hadley circulation (red lines) one sees more cloud cover reduction in the lower mid-

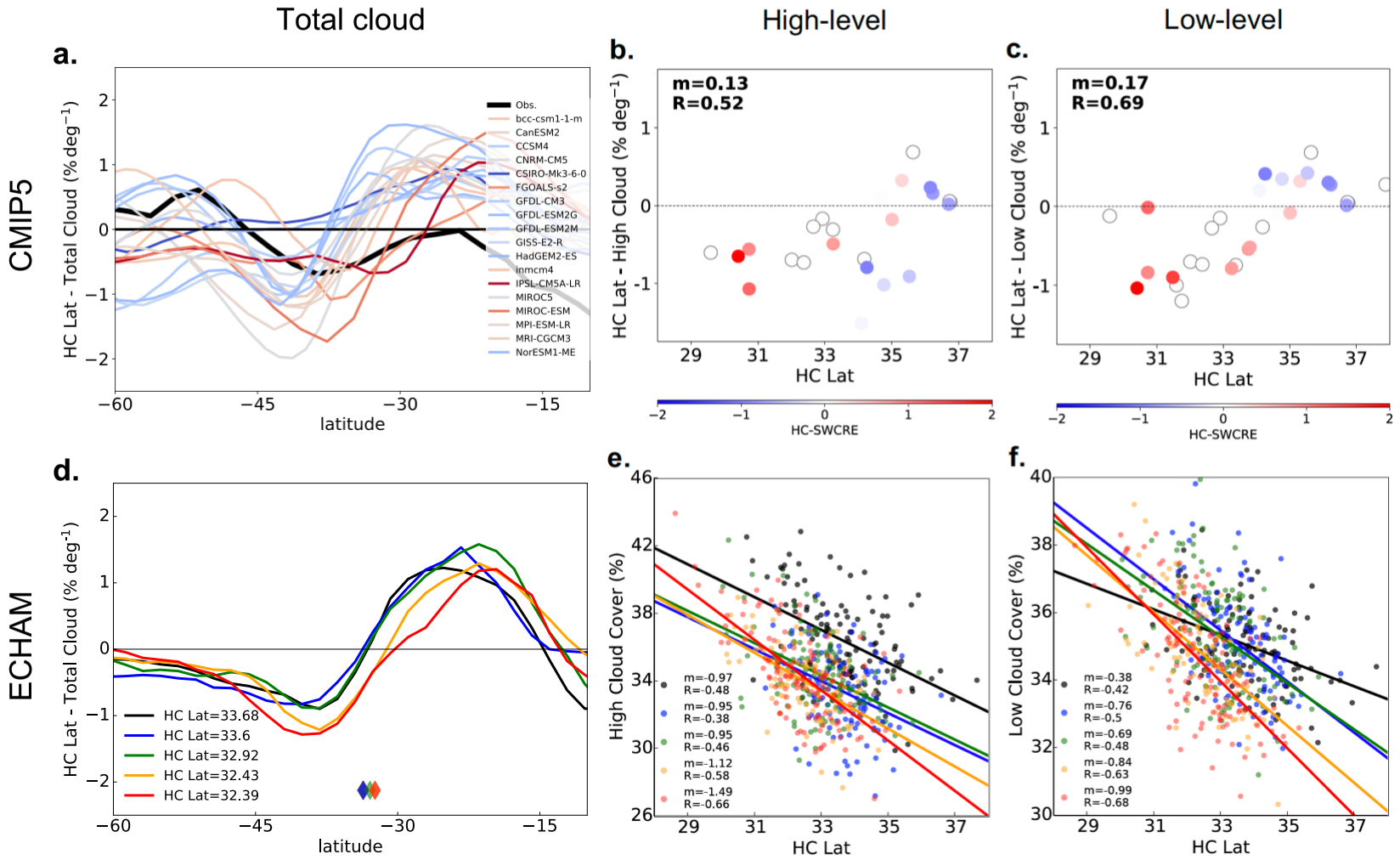

Figure 45: Mid-latitude cloud changes with HC edge shifts. As in Figure 43a,d but for the least-squares linear regression coefficients of the zonal-mean total cloud cover against the SH HC edge latitude (A) for CMIP5 models and (d) for ECHAM6 simulations. We display in the thick black line in (a) the observed HC-total cloud cover regression derived from ERA-Interim and ISCCP-D2. Least-squares linear regression of (b, e) the LML high-level ($\leq$ 400 hPa) cloud cover and (c, f) the LML low-level ($\geq$ 775 hPa) cloud cover against the SH HC edge latitude. The regression coefficient (m) and correlation coefficient (R) are displayed. Each point in (b, c) represents one month in the aquaplanet integration, and each point in (e, f) represents one model, colored according to its LML HC-SWCRE index. Models without HC-SWCRE data are denoted by open circles.

latitudes with poleward Hadley circulation edge shifts than for models with a wide Hadley circulation (blue lines), as revealed by the Student's *t*-test (p =0.0433). Such an association of the lower mid-latitude cloud cover with poleward Hadley circulation edge shifts does not exist in the sub-tropics (15°S-30°S), consistent with Figures 43a,d which shows that the climatological Hadley circulation edge does not correlate with the magnitude of the sub-tropical HC-SWCRE minima.

We next decompose the total cloud cover response to poleward shifts of the Hadley circulation into contributions from high-level clouds (vertically integrated between 400 hPa and the tropopause) and low-level clouds (vertically integrated between 1000-775 hPa). We present this in Figure 45b,c,e,f, where we correlate the lower mid-latitude (Figure 45b,e) high-level and (Figure 45c,f) low-level cloud cover with the Hadley circulation edge. Consistent with our previous observational and modeling results (Chapters 2 and 3), poleward Hadley circulation shifts reduce high-level cloud cover, but the magnitude of this reduction is largely independent of the climatological Hadley circulation edge: in Figure 45b the correlation ($R \approx 0.5$) is only moderately strong, and in Figure 45e the slopes (m) are similar across runs. Poleward Hadley circulation shifts also reduce low-level cloud cover, but, for these clouds, the magnitude of the reduction does depend more strongly on the climatological Hadley circulation edge than does the magnitude of the reduction of high-level clouds: in Figure 45c the correlation ($R \approx 0.70$) is strong, and in Figure 45f. the slopes (m) flatten as the climatological Hadley circulation widens. That is, the reduction of low-level cloud cover with poleward Hadley circulation shifts is larger in models with narrower Hadley circulations than in models with wider Hadley circulations. The fact that the Hadley circulation edge impacts the the linkage between clouds and the circulation in the mid-latitudes via low-level clouds agrees with previous work (e.g. Kay et al. 2014; Grise and Medeiros 2016).

The magnitude of the mid-latitude cloud cover reduction with poleward Hadley circu-

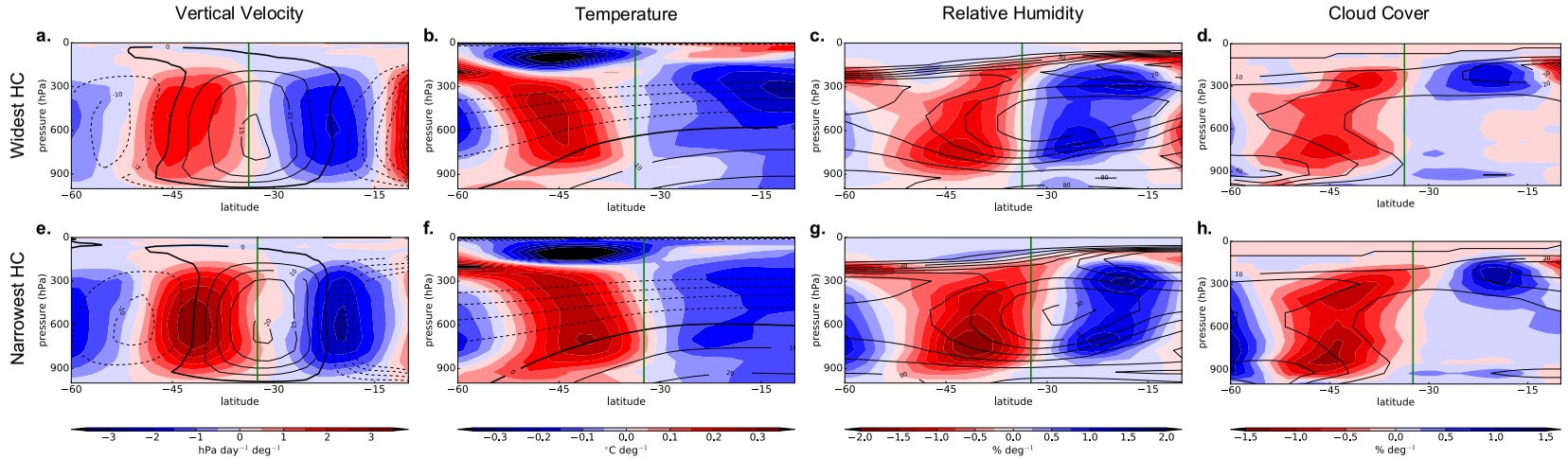

Figure 46: Dynamic and thermodynamic changes with HC edge shifts. In colors are the least-squares linear regression coefficients of the zonal mean pressure vertical velocity (ω) (left), atmospheric temperature (center left), relative humidity (center right) and cloud cover (right) for the ECHAM6 aquaplanet simulations with the most poleward (widest) climatological HC edge latitude (a, b, c, d) and the most equatorward (narrowest) climatological HC edge latitude (e, f, g, h). The climatological HC edge latitude is denoted by a green vertical line. In contours are the corresponding climatological values. In (a, e) the 0 $hPa\,day^{-1}$ contour is bold and in (b, f) the 0°C contour is bold.

lation shifts is tied to the magnitude of the mid-latitude subsidence strengthening accompanying the poleward Hadley circulation edge shift. To show this, we compare in Figure 46 the ECHAM6 aquaplanet simulation with the widest Hadley circulation (top row) with the aquaplanet simulation with the narrowest Hadley circulation (bottom row). We regress on the inter-annual Hadley circulation edge latitude time-series the time-series of vertical velocity (Figure 46a, e), atmospheric temperature (Figure 46b, f), and relative humidity (Figure 46c, g). We also show the differences in cloud cover in Figure 46d, g. The corresponding climatologies are shown with contours, with the climatological edge latitudes of the Hadley circulation denoted by green vertical lines. In both simulations, poleward shifts in the Hadley circulation result in stronger mid-latitude subsidence, stronger subsidence warming, and reductions in relative humidity. We can model the influence of shifts in the Hadley circulation edge latitude on cloud cover C by assuming that there exists some correspondence between the large-scale cloud cover and the large-scale relative humidity. For example, the particular cloud cover parameterization of ECHAM6 explicitly relates the two; i.e.,

$$C = 1 - \sqrt{1 - \frac{RH - RH_0}{RH_s - RH_0}} \tag{4.7}$$

where RH_0 is a threshold relative humidity for cloud cover formation and $RH_s \sim 1$ is the saturation relative humidity (Giorgetta et al. 2013; Sundqvist, Berge, and Kristjánsson 1989). However, we generally expect that, regardless of the details of the parameterization, regions of relatively low relative humidity are less likely to experience cloud cover than regions of relatively high relative humidity, which are more likely to experience cloud cover. That is, we expect:

$$\frac{\partial C}{\partial \theta_{HC}} \sim \frac{\partial RH}{\partial \theta_{HC}} = \frac{\partial RH}{\partial T} \cdot \frac{\partial T}{\partial \omega_{500}} \cdot \frac{\partial \omega_{500}}{\partial \theta_{HC}} \tag{4.8}$$

where the relative humidity $RH = \frac{e}{e_s}$ is the ratio of the vapor pressure of water vapor e to

the saturation vapor pressure of water vapor e_s, both of which depend only on temperature T. Then we have, by the Clausius-Clapeyron relation for e_s and the ideal gas law for e assuming adiabaticity,

$$\frac{\partial RH}{\partial \theta_{HC}} = RH \left[\left(\frac{C_v}{R_v} + 1 \right) \frac{1}{T} - \frac{L_v e_s}{R_v T^2} \right] \cdot \frac{\partial T}{\partial \omega_{500}} \cdot \frac{\partial \omega_{500}}{\partial \theta_{HC}} \tag{4.9}$$

Then, for standard near-surface atmospheric values for C_v, R_v, T, L_v, and $e_v s$, the thermodynamic term $\frac{dRH}{dT}$ is negative, indicating a decrease in relative humidity with warming. We can identify $\frac{\partial T}{\partial \omega_{500}}$ as the adiabatic warming due to increased subsidence, and we have previously identified in Equation 3.4 that $\frac{\partial \omega_{500}}{\partial \theta_{HC}} \sim \theta_{HC}$ (in the lower mid-latitude mean, at least).

Importantly, we find that all of the responses in Equation 4.8 are larger in the narrowest Hadley circulation simulation than in the widest Hadley circulation simulation: that is, the subsidence strengthening $\frac{\partial \omega_{500}}{\partial \theta_{HC}}$ is larger in the simulation with the narrower Hadley circulation; the warming $\frac{\partial T}{\partial \omega_{500}} \frac{\partial \omega_{500}}{\partial \theta_{HC}}$ is larger in the simulation with the narrower Hadley circulation; the relative humidity reduction $\frac{\partial RH}{\partial \theta_{HC}} = \frac{\partial RH}{\partial T} \cdot \frac{\partial T}{\partial \omega_{500}} \cdot \frac{\partial \omega_{500}}{\partial \theta_{HC}}$ is larger in the simulation with the narrower Hadley circulation; and, the cloud cover reduction $\frac{\partial C}{\partial \theta_{HC}}$ is larger in the simulation with the narrower Hadley circulation. This is consistent with our claim that $\frac{\partial \omega_{500}}{\partial \theta_{HC}} \sim c - \theta_{HC}$ for some constant c in Equation 3.4. The shortwave cloud radiative warming anomalies, then, are consistent with reductions in cloud cover throughout the atmospheric column but especially at low-levels, which is evident by the maximum in warming and in drying that we see in and just above the boundary layers (approximately 700 hPa) in Figure 46, although we cannot discount other mechanisms such as boundary layer drying due to free tropospheric warming (e.g. Sherwood, Bony, and Dufresne 2014).

Thus, the cloud cover decrease associated with poleward Hadley circulation shifts is produced by a large-scale reduction in relative humidity. Poleward expansion of the Hadley

circulation on inter-annual time-scales is associated with strengthened subsidence in the lower mid-latitude region. This strengthened subsidence induces a subsidence warming that, by Clausius-Clapeyron, "burns" away clouds by a concomitant decrease in relative humidity, all else being equal. There are other mechanisms which may govern the inter-annual variability of low cloud cover, but these may not necessarily be associated with poleward Hadley cell expansion, which is our focus here. It therefore should be qualitatively independent of how a model parameterizes clouds, and should be a robust model behavior.

Having shown that the reduced cloud cover with poleward Hadley circulation shifts is caused by strengthened subsidence, we now tie the magnitude of that subsidence strengthening to the climatological Hadley circulation edge latitude. Models with wider climatological Hadley circulations exhibit weaker mid-latitude meridional vertical velocity gradients, and thus smaller subsidence strengthening, smaller subsidence warming, and smaller cloud cover reductions for the same 1° poleward Hadley circulation edge shift than models with narrower climatological Hadley circulations. Simply put, models with a narrower Hadley circulation tend also to exhibit a tighter Hadley circulation that yields greater sensitivities of subsidence and cloud cover for a given 1° shift in the edge latitude of the Hadley circulation. In Figure 47a, we quantify the relationship between the climatological Hadley circulation edge and the meridional gradient in vertical velocity that underlies this mechanism. We plot the climatological difference in vertical velocity in the mid-troposphere (500 hPa) between 30°S and 45°S against the sensitivity of the lower-mid-latitude mean vertical velocity to poleward Hadley circulation edge latitude shifts; i.e. HC-ω or $\frac{\partial\langle\omega_{500}\rangle}{\partial\theta_{HC}}$. In both the mid- (500 hPa; dots) and lower (775 hPa; stars) troposphere, poleward Hadley circulation edge shifts lead to stronger subsidence in models with larger meridional gradients in vertical velocity. Therefore, across the ECHAM6 simulations, the differences in the mid-latitude HC-SWCRE are linked to the differences in the climatological Hadley circu-

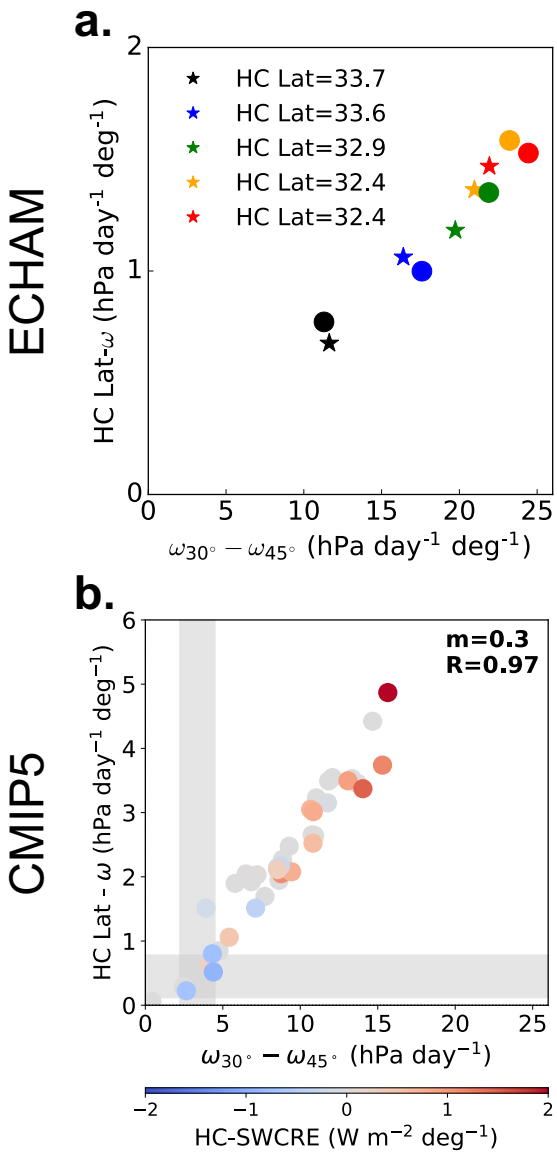

Figure 47: Relationship between climatological LML meridional vertical velocity gradient and LML subsidence increase with poleward HC shift. Scatter plot of the climatological LML mean pressure vertical velocity (ω) gradient, computed as the difference between ω at 30°S and 45°S at 775 hPa (stars) and at 500 hPa (dots) against the least-squares linear regression coefficient (HC-ω regression) of the LML mean ω at the corresponding pressure level against the HC edge latitude for (a) each of the ECHAM6 simulations and (b) at 500 hPa for CMIP5 models. The regression coefficient (m) and correlation coefficient (R) are displayed. Models are colored according to their HC-SWCRE index, and models without HC-SWCRE data are denoted by gray circles. The 95% confidence interval using the Student's *t*-test on observed values derived from ERA-Interim is denoted by gray shading.

lation edge via the connection of the latter to the climatological meridional vertical velocity gradients. Again, the ECHAM6 results (Figure 47a) resemble the biases across CMIP5 models (Figure 47b). Specifically, the spread across CMIP5 models in the climatological meridional vertical velocity gradients is strongly correlated with the model spread in the subsidence increase in the lower mid-latitudes with poleward Hadley circulation shifts (Figure 47b dots; $R = 0.97$) and with the model spread in HC-SWCRE index (Figure 47b colors; $R = 0.81$). Recalling Equation 3.2

$$\langle \omega_{500} \rangle = \sum_{j=-\infty}^{\infty} \sum_{k=-\infty}^{\infty} \langle c_{j,k} e^{ij\omega\theta} \rangle e^{ik\omega\theta_{HC}} \tag{4.10}$$

with the meridional average over the zone $[\theta_{max}, \theta_{min}]$ as $\langle \cdot \rangle = \frac{1}{\theta_{max} - \theta_{min}} \int_{\theta_{min}}^{\theta_{max}} \cdot d\theta$, we have

$$\langle \omega_{500} \rangle = \frac{1}{\theta_{max} - \theta_{min}} \sum_{j=-\infty}^{\infty} \sum_{k=-\infty}^{\infty} \frac{1}{ij\omega} \left[c_{j,k} e^{ij\omega\theta} \Big|_{\theta_{min}}^{\theta_{max}} e^{ik\omega\theta_{HC}} \right. \tag{4.11}$$

and the sensitivity to the shifts in the Hadley circulation edge latitude

$$\frac{\partial \langle \omega_{500} \rangle}{\partial \theta_{HC}} = \frac{1}{\theta_{max} - \theta_{min}} \sum_{j=-\infty}^{\infty} \sum_{k=-\infty}^{\infty} \frac{k}{j} \left[c_{j,k} e^{ij\omega\theta} e^{ik\omega\theta_{HC}} \Big|_{\theta_{min}}^{\theta_{max}} \right. \tag{4.12}$$

Here we assume that the shifts in the Hadley circulation do not substantially change the structure of the vertical velocity but merely shift the existing profile, i.e. $\frac{\partial \langle \omega_{500} \rangle}{\partial \theta_{HC}} \approx \alpha \frac{\partial \langle \omega_{500} \rangle}{\partial \theta}$ for some constant of proportionality α so that

$$\frac{\partial \langle \omega_{500} \rangle}{\partial \theta_{HC}} \approx \frac{1}{\theta_{max} - \theta_{min}} \sum_{j=-\infty}^{\infty} \sum_{k=-\infty}^{\infty} \alpha \left[c_{j,k} e^{ij\omega\theta} e^{ik\omega\theta_{HC}} \Big|_{\theta_{min}}^{\theta_{max}} \right. \tag{4.13}$$

Therefore we have

$$\frac{\partial \langle \omega_{500} \rangle}{\partial \theta_{HC}} \approx \frac{\alpha}{\theta_{max} - \theta_{min}} \left[\omega_{500} \left(\theta_{max}; \theta_{HC} \right) - \omega_{500} \left(\theta_{min}; \theta_{HC} \right) \right] \tag{4.14}$$

so that the the sensitivity of the lower mid-latitude mean ω_{500} is proportional to the lower mid-latitude meridional gradient of vertical velocity. Note here that using a $\cos\theta$ area weighting does not change the linearity between the two quantities, but does result in a different scaling factor and the addition of a constant term. Empirically, it would appear that this relationship between the sensitivity of lower mid-latitude subsidence to shifts in the Hadley circulation edge is more accurately predicted from the climatological vertical velocity gradients than from the climatological Hadley circulation edge latitude since we find a stronger correlation ($R = 0.97$) between $\frac{\partial\langle\omega_{500}\rangle}{\partial\theta_{HC}}$ and $\omega_{500}\left(\theta_{max}\right) - \omega_{500}\left(\theta_{min}\right)$ across models than we do for the correlation ($R = -0.85$) between $\frac{\partial\langle\omega_{500}\rangle}{\partial\theta_{HC}}$ and θ_{HC} across models.

4.6 Summary and Discussion

We have demonstrated that model errors in the simulation of the present-day large-scale atmospheric circulation lead to substantial model errors in how changes in the circulation impact mid-latitude clouds and their radiative effects. Combining idealized aquaplanet simulations of one atmosphere general circulation model with an analysis of the multi-model CMIP5 ensemble, we show that the meridional gradient in the mid-latitude mid-tropospheric vertical velocity controls how shifts in the Hadley circulation edge impact the mid-latitude shortwave cloud radiative effect. Because the meridional gradient in vertical velocity is strongly tied to the latitude of the climatological Hadley circulation edge, we have here identified a mechanism that explains the correlation previously reported in Chapter 3.

Our results suggest that model biases in the climatology of large-scale atmospheric dynamics influence the mid-latitude shortwave cloud radiative response. We demonstrate this explicitly in Figure 48, where we correlate the CMIP5 model bias in the meridional vertical velocity gradient with the lower mid-latitude shortwave cloud radiative response, computed

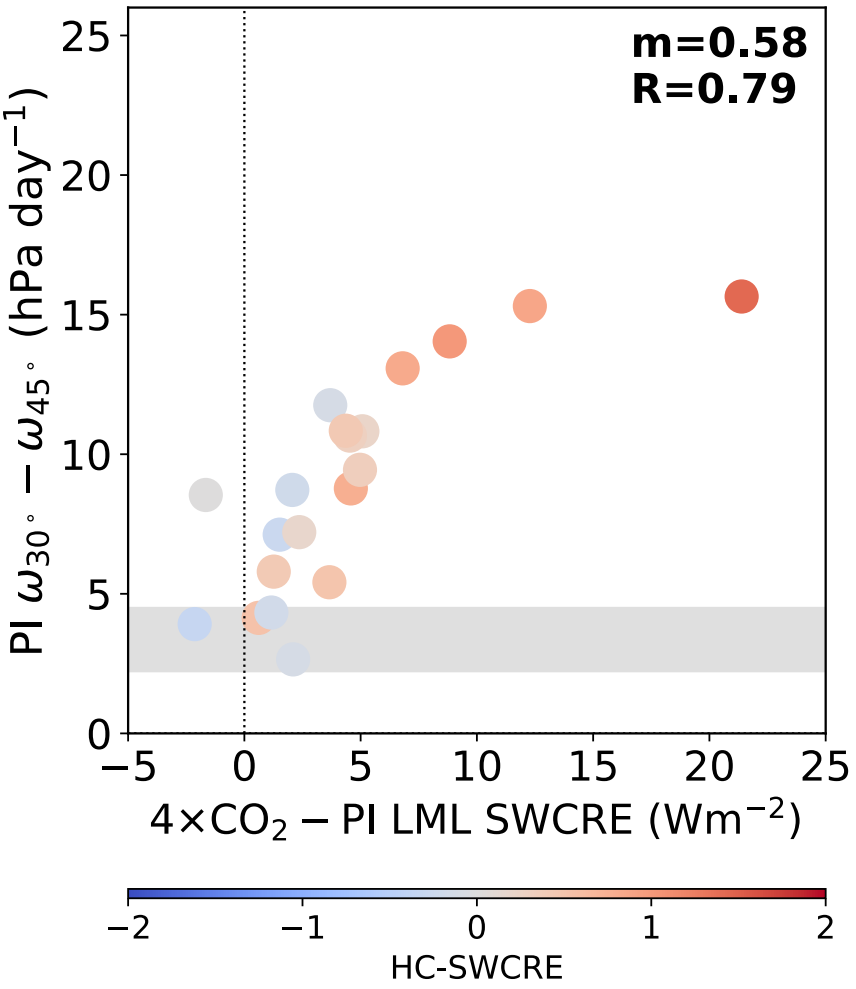

Figure 48: Relationship between climatological meridional vertical velocity gradient and lower-midlatitude shortwave cloud radiative response. Scatter plot of the climatological lower-mid-latitude (30°S-45°S) mean gradient of pressure vertical velocity (ω) at 500 hPa against the lower mid-latitude shortwave cloud feedback for CMIP5 models. The regression coefficient (m) and correlation coefficient (R) are displayed. Models are colored according to their HC-SWCRE index, and models without HC-SWCRE data are denoted by gray circles. The 95% confidence interval using the Student's *t*-test on observed values derived from ERA-Interim is denoted by gray shading.

as the $4\times CO_2-$PI SWCRE in the lower mid-latitudes. The strong correlation suggests that the biases in the models' control circulation project forward onto the model uncertainty in the climate change response. Previous work has shown that uncertainties in the mid-latitude shortwave cloud radiative response in models are due primarily to biases in cloud microphysics (e.g. Tan, Storelvmo, and Zelinka 2016). These and our results are not contradictory. First, we examined the shortwave cloud radiative anomalies and response in the lower mid-latitudes (30°S to 45°S) to changes of the Hadley circulation, whereas previous work focused on the shortwave cloud radiative response in the higher latitudes (poleward of 45°S) to changes of the eddy-driven jet. Second, there are two model biases to address — 1) biases in the sensitivity of small-scale cloud processes and how they respond to changes in environmental conditions, and 2) biases in how clouds are affected by changes in the large-scale circulation and its impact on large-scale atmospheric temperature. Operating on the large-scale via bulk cloud physics, the second bias, which we highlight here, should be independent of small-scale cloud processes.

Unfortunately, climate models continue to exhibit consistent biases in the simulation of the large-scale circulation. This is especially true in the Southern Hemisphere, where in most models the mid-latitude eddy-driven jet and the Hadley circultation edge are too close to the equator (e.g. Ceppi et al. 2012). In our aquaplanet simulations we show that as we push the climatological Hadley circulation edge closer to the observed value, the sensitivity of shortwave cloud radiative anomalies in the mid-latitudes to poleward shifts in the Hadley circulation becomes more realistic. In our most biased simulation the HC-SWCRE sensitivity is $4\,W\,m^{-2}$, and in our least biased simulation the sensitivity is $2\,W\,m^{-2}$. Observations suggest a small negative HC-SWCRE sensitivity during the Southern Hemisphere summer season (Chapter 2). Thus, our results indicate that about half of the biases in the mid-latitude cloud-circulation coupling and their impact on cloud-radiative effects can be removed by improving the climatological atmospheric circulation. Although the represen-

tations of clouds and their radiative effects still need improvement in models, and deficiencies in cloud microphysical schemes must still be addressed, our results offer a promising and perhaps orthogonal way to improve climate models beyond approaches targeting small-scale cloud physics. One such way may involve improved model representations of low-level drag, as highlighted here as well as in, for example, Pithan et al. 2016.

Chapter 5

Conclusion

5.1 Introduction

Understanding mid-latitude clouds and their impact on Earth's radiative energy balance is critical to reduce the persisting model uncertainty in the response of the climate system to increasing concentrations of greenhouse gases. While previous work has highlighted the model uncertainty related to thermodynamic changes in clouds, which require a detailed understanding of sparsely-observed small-scale cloud physics, we have demonstrated here that much of the model biases in the linkage between mid-latitude clouds and the general circulation of the atmosphere as well as the model uncertainty in the mid-latitude cloud radiative response to increasing CO_2 concentrations are in fact a result of the model biases in the representation of the present-day circulation. This shows that improving the model representation of the large-scale atmospheric circulation, which today's climate models can resolve explicitly and on which there are robust observational constraints, can lead to a substantial improvement in the model representation of present-day clouds and increased confidence in model projections of future cloud changes, irrespective of the uncertainties in small-scale cloud physics. We have shown this with three main approaches.

First, we have performed a comprehensive analysis of the observed linkages among clouds, their radiative effects, and the general circulation of the atmosphere in Chapter 2, and have found that the key dynamical indicator for mid-latitude cloud and cloud radiative anomalies on inter-annual time-scales is the Hadley circulation. Second, in Chapter 3 we

have evaluated the representation of the linkages among mid-latitude clouds, their radiative effects, and the general circulation in a suite of fully-coupled global climate models, and have found an emergent constraint – the climatological position of the Hadley circulation – on the model uncertainty in projections of the shortwave cloud radiative response to increasing concentrations of CO_2. Third, we have performed numerical experiments with an idealized aquaplanet model of the global climate in Chapter 4, and have demonstrated that the model biases in the representation of the position of the climatological circulation not only contribute to the model biases in the linkage between cloud and the circulation, but also imprint onto the model uncertainty in the cloud radiative response to increasing CO_2 concentrations.

In this chapter, we summarize and discuss our results. We conclude with a presentation of the questions that remain open, and directions for future work.

5.2 Summary and Discussion

Observations

Previous work on the coupling between mid-latitude clouds and the circulation has focused on analyzing biased model cloud behavior, has concentrated on one season or region, and has been concerned almost exclusively with shifts in the mid-latitude eddy-driven jet. We have advanced the scientific knowledge on the cloud radiative feedback by documenting in Chapter 2 a comprehensive observational survey across all three ocean basins and across all seasons of the linkages between the latitudinal shifts of a broad array of metrics for the atmospheric circulation available from the comprehensive European Centre of Medium-Range Weather Forecasts Interim reanalysis data set (ERA-Interim; Dee et al. 2011) and all of the mid-latitude cloud and cloud radiative properties that have been retrieved from the extensive satellite observations of the climate system by the NASA GISS International Satellite

Cloud Climatology Project (ISCCP) D2 (Rossow and Schiffer 1999) and FD (Zhang et al. 2004) over the last 30 years.

To determine the effects of the inter-annual variability in the latitudinal position of the circulation on mid-latitudes cloud properties for each ocean basin and for each season, we have regressed the time-series of key indices of cloud radiative properties on the time-series of key dynamical indicators. The cloud indices that we have examined include the total, high, and low cloud central latitude and the mid-latitude ($30^\circ - 60^\circ$) mean shortwave (SW) and longwave (LW) cloud radiative effects (CRE). While previously it had been thought that the eddy-driven jet was the dominant driver of cloud changes in the mid-latitudes (e.g. Grise et al. 2013), or more recently that the large-scale atmospheric dynamics have no role to play in the changes in Southern Ocean clouds (e.g. Kay et al. 2014), we instead have found a consistent relationship between poleward shifts of the Hadley circulation edge latitude and the central latitude of mid-latitude high clouds. The regression and correlation coefficients are generally larger for regressions on the Hadley circulation latitude rather than on the eddy-driven jet latitude, and those regressions are generally statistically significant in more seasons and in more basins. This suggests that the Hadley circulation, rather than the eddy-driven jet, is the primary dynamical indicator associated with cloud and radiation changes. Trend analysis also suggests that the recent poleward shifts in the edge latitude of the Hadley circulation are more likely to be the driver of recent poleward shifts in the central latitude of the mid-latitude clouds than are poleward shifts in the eddy-driven jet latitude.

While previously it has been hypothesized that poleward shifts in the clouds would produce as positive cloud curtain feedback, our observational analysis instead has found that the consistent relationship between the Hadley circulation and mid-latitude high clouds actually has diverse radiative impacts. As expected, less longwave radiation is trapped when high clouds decrease, and hence the clear correspondence between high cloud shifts and longwave radiative anomalies. However, the shortwave cloud radiative anomalies associ-

ated with high cloud shifts are more varied. In the wintertime North Atlantic, poleward shifts of high clouds are associated with shortwave cloud radiative warming anomalies. The curtain has been pulled back, so to speak, and more sunlight has been allowed to enter the climate systemBender, Ramanathan, and Tselioudis 2012; Grise et al. 2013. This is the first observational evidence for the positive cloud curtain feedback in the wintertime North Atlantic. However, we do not find observational support for the cloud curtain feedback during other seasons or in other ocean basins. For example, high cloud shifts in summertime Southern Hemisphere do not result in any significant shortwave cloud radiative warming anomalies, and, in fact, seem actually to be associated with anomalous shortwave cloud radiative cooling.

We offer two explanations for the different shortwave cloud radiative anomalies associated with circulation shifts, which may not be independent. First, there are differences in the underlying cloud field between wintertime North Atlantic and summertime Southern Hemisphere. The Southern Hemisphere is covered by extensive and persistent low clouds, such that changes in the high cloud field have a negligible impact on the total cloud field and thus negligible shortwave cloud radiative anomalies. This does not appear to be the case over the wintertime North Atlantic. Second, there are different effects of poleward eddy-driven jet and Hadley circulation edge shifts on the lower mid-latitude (30°-45°) subsidence between the wintertime North Atlantic and the summertime Southern Hemisphere. There appears to be a regime transition (as discussed with respect to the +HC-SWCRE and −HC-SWCRE models in Chapter 3), from a regime of weak subsidence or ascent to one of moderately strong subsidence, which occurs in the wintertime North Atlantic when the circulation shifts anomalously poleward. This does not appear to be the case over the Southern Hemisphere, which remains in a regime of strong subsidence.

CMIP5 Models

Our observational results from Chapter 2 have revealed that poleward shifts of the Hadley circulation in the Southern Hemisphere are associated with anomalous shortwave cloud radiative cooling. In light of this finding, which contrasts with the previous work that has focused on future poleward shifts in the storm tracks, we have used the observed linkages between clouds, their radiative effects, and the Hadley circulation in the present climate to help predict how clouds and their radiative properties will change in response to increasing concentrations of CO_2 in the future. We have done this in Chapter 3, in which we have performed the first analysis of the co-variability between the Hadley circulation edge and mid-latitude clouds in global climate models. We have analyzed the output of the CMIP5 ensemble where we have used the observed linkages 1) to evaluate model simulations of the present climate, and 2) to help constrain model estimates of future climate changes.

First, we have evaluated whether global climate models capture the newly observed linkage between the inter-annual shifts of the Hadley circulation and shortwave cloud radiative anomalies which we term the HC-SWCRE, in the current climate. In the observations, we have found that the HC-SWCRE relationship in the lower mid-latitudes of the Southern Hemisphere is dominated by anomalous shortwave cloud radiative radiative cooling. In contrast, the CMIP5 multi-model mean HC-SWCRE pattern shows pronounced and zonally-symmetric shortwave cloud radiative warming anomalies in the lower mid-latitudes, except for small regions of shortwave cloud radiative cooling anomalies that intrude from the sub-tropics and that extend approximately to the climatological edge latitude of the Hadley circulation. Models exhibit unrealistically strong shortwave cloud radiative warming anomalies with poleward shifts of the Hadley circulation edge compared to the observations. Models also poorly represent the climatological position of the Hadley circulation – models place the climatological edge latitude of the Hadley circulation unrealistically equatorward compared to the observations. We have found that the model bias in

the position of the climatological circulation contributes to the model bias in the linkage between clouds and the circulation.

We have correlated the inter-model spread in the climatological Hadley circulation edge latitude with the inter-model spread in HC-SWCRE averaged across the lower mid-latitudes, and have found that models with unrealistically narrow Hadley circulations exhibit unrealistically strong shortwave cloud radiative warming anomalies with poleward shifts in the Hadley circulation edge latitude. We have justified this correlation with a physical basis and have regressed on the inter-model spread in climatological Hadley circulation edge latitude the climatological subsidence in the lower mid-latitudes and the sensitivity of that subsidence to poleward shifts in the Hadley circulation edge. Models with unrealistically narrow Hadley circulations have weaker climatological subsidence in the lower mid-latitudes and tend to have a greater sensitivity of subsidence to shifts in the Hadley circulation edge latitude. The lower mid-latitudes of these models with narrow Hadley circulations transition from a regime of weak subsidence to one of strong subsidence, clearing out low cloud and thus letting in more sunlight.

The model bias in the climatological position of the Hadley circulation as well as the model bias in the linkage between the circulation and clouds both translate into model spread in the uncertainty of the cloud radiative response to increasing CO_2. The co-location of the CMIP5 multi-model mean region of the shortwave cloud radiative warming anomalies related to unforced poleward shifts in the Hadley circulation with the region of shortwave cloud radiative warming response to forcing by $4\times CO_2$ suggests a direct dynamical contribution, which departs from the previous literature that has disputed the impact of dynamical climate changes onto mid-latitude cloud changes (e.g. Ceppi, Zelinka, and Hartmann 2014). We have quantified this dynamical contribution by correlating the unforced HC-SWCRE co-variability in the lower mid-latitudes with the forced shortwave cloud radiative response there. Models which exhibit stronger shortwave cloud radiative warming

anomalies in the lower mid-latitudes with unforced poleward shifts in the Hadley circulation edge also exhibit a stronger shortwave cloud radiative warming response in the same region when the Hadley circulation is forced poleward in response to $4\times CO_2$.

We have linked the model uncertainty in the shortwave cloud radiative warming response in the lower mid-latitudes to the inter-model spread in the climatological HC extent. Models with narrow Hadley circulations in the pre-industrial control runs exhibit a stronger shortwave cloud radiative warming response to $4\times CO_2$ forcing and therefore a larger surface warming response as measured by the equilibrium climate sensitivity. This suggests that the models with HC edge latitudes closer to the observations in the present-day climatology may better predict the future shortwave cloud radiative response and surface air temperature response to increasing CO_2. Thus, we find that the climatological position of the Hadley circulation constitutes a new emergent constraint on the shortwave cloud radiative response and the equilibrium climate sensitivity.

Aquaplanet Experiments

The results from Chapter 3 that have linked the model biases in the climatological position of the Hadley circulation to the model biases in representation of the coupling between mid-latitude clouds and the general circulation as well as to the model uncertainty in the cloud radiative response to increasing concentrations of CO_2 derive from correlations across fully-coupled global climate models which differ by more than only their representation of the Hadley circulation. In Chapter 4, we have verified the results from the correlative analysis of the CMIP5 models by using an idealized aquaplanet model of the global climate to simulate different climate states whose only difference is that each simulation has a different climatological position of the Hadley circulation. We have demonstrated that the closer we push the climatological edge latitude of the Hadley circulation towards the observed value, the more realistic the coupling between the mid-latitude clouds and the circulation become.

That is, we are able to reduce the cloud-circulation coupling bias in a model which exhibits unrealistic "warming" or Type I model behavior (Grise and Polvani 2014b) such that the model behaves like a more realistic "cooling" or Type II model solely by "correcting" the climatological position of the Hadley circulation.

The effect of varying the climatological position of the atmospheric circulation in our aquaplanet simulations resembles the spread across the fully-coupled CMIP5 models. This resemblance suggests that we can learn about the mechanisms of the linkage between clouds and the circulation that the fully-coupled models represent by examining more closely the results from our idealized aquaplanet model. We have found that the anomalous shortwave cloud radiative warming that accompanies poleward shifts in the edge latitude of the Hadley circulation is strongly linked to strengthened subsidence in the lower mid-latitudes. This strengthened subsidence is accompanied by a subsidence warming, which, in turn, reduces the large-scale relative humidity and "burns away" cloud cover via the Clausius-Clapeyron relation. For each of these processes, we find a stronger sensitivity in the simulations with narrow Hadley circulations than in the simulations with wide Hadley circulations.

Further, we show that models with narrower Hadley circulations tend also to have tighter Hadley circulations; that is, with a stronger meridional gradient across the lower mid-latitudes in the mid-tropospheric vertical velocity, compared to models with wider Hadley circulations. The meridional gradient in mid-tropospheric vertical velocity strongly constrains the model uncertainty in the shortwave cloud radiative response. We note that the reduction in the model uncertainty through use of this observational constraint is not uniform across models, but rather acts preferentially to reduce the model uncertainty in models which exhibit the "warming" or Type I behavior. Nevertheless, the differences across our aquaplanet simulations and its similarity to that across CMIP5 models suggests that about half of the model bias in the mid-latitude cloud-circulation coupling and about half of the model uncertainty in the mid-latitude cloud radiative response to increasing CO_2 concen-

trations stems from the model biases in the representation of the Hadley circulation, and thus could be removed by improving the representation of the climatological circulation in models. Therefore, while the previous literature has focused on improving the model representation of cloud microphysics as a path forward to reducing the model uncertainty in the cloud radiative response to increasing CO_2 concentrations, we instead have offered that improving the model representation of large-scale atmospheric dynamics as a promising and perhaps more straightforward way to increase confidence in projections of future climate.

5.3 Future Work

While we have been successful in demonstrating that removing the biases in the model representation of the climatological circulation reduces the model biases in linkage between mid-latitude clouds and the circulation in the current climate, and in showing that these biases in the models' climatological circulation are strongly correlated with the model uncertainty in the shortwave cloud radiative response and and equilibrium climate sensitivity to increasing concentrations of CO_2, we have not gone so far as to demonstrate explicitly that removing the biases in the climatological circulation imprints onto the CO_2-forced response. To do this, future work will employ the methodology described in Chapter 4 to generate climate states whose only difference is the location of the climatological circulation, but instead of using an idealized aquaplanet model with a thermodynamic slab ocean and perpetual January 1 insolation, we will use a general circulation model coupled to a fully-dynamic ocean and with seasonally-varying insolation. We note here that we have performed abrupt $4\times CO_2$ runs in our idealized aquaplanet model, but the global-mean surface air temperature response was much lower than expected ($<2K$), indicating that our simplified set-up may be ill-equipped to answer the climate change question. The lower

than expected surface temperature response is due likely to the strong and persistent shortwave cloud radiative cooling feedback in the high latitudes that is over-represented. Further, it has also been demonstrated that the cloud radiative feedbacks derived from aquaplanets and models with slab oceans do not necessarily represent the cloud radiative feedback in more realistic climate simulations (e.g. Boer and Yu 2003; Frey and Kay 2018).

Regarding the observational analysis of Chapter 2, we have found diverse radiative effects associated with shifts in the atmospheric circulation that seem to depend on the ocean basin, e.g. poleward shifts in the circulation over the Southern Hemisphere are associated with shortwave cloud radiative cooling whereas poleward shifts in the circulation over the North Atlantic are associated with shortwave cloud radiative warming. One hypothesis for the inter-hemispheric differences in the linkage between clouds and the circulation is the presence of land, because we see the shortwave cloud radiative anomalies with poleward shifts in the circulation over the North Atlantic as well as over the South Atlantic in the region east of South America. An idealized model set-up such as the TRACMIP (Voigt et al. 2016) may help to elucidate the effects of the presence of land on the linkage between cloud and the circulation in both the present climate as well as in future climate.

Further, the observational analysis is strictly correlative and, as such, one cannot make any statements about the direction of causality; that is, is it truly the changes in the atmospheric dynamics that cause the changes in the clouds that we have seen? One might argue that the qualitative structure of the atmospheric circulation remains largely the same with and without the atmospheric radiative effects of clouds (see, e.g. Li, Thompson, and Bony 2015; Li, Thompson, and Huang 2017), so that the cloud radiative effects are not of primary importance to setting the structure and magnitude of the atmospheric circulation. In Chapter 4, we apply only a momentum perturbation, and so we can be led to believe that, at least in the particular model set-up we use, it is the change we impose in the dynamics that cause the changes in clouds we see. There could, however, be some change in the clouds

that feeds back onto the change in the atmospheric circulation which ultimately helps to set the equilibrium response that we see.

Conversely, could it be the case that it is actually the changes in the cloud and their radiative properties that cause the dynamical changes? This has been argued by, for example, Ceppi, Zelinka, and Hartmann 2014, who claim that the shortwave cloud radiative response to increasing CO_2 concentrations generates a dipole of surface temperature response with a strong warming in the lower mid-latitudes and a cooling in the higher latitudes which projects onto the low-level baroclinicity that, in turn, shifts poleward the eddy-driven jet. Similarly, Ceppi and Hartmann 2016 and Voigt and Shaw 2015, both using cloud-locking techniques in which the radiative effects of clouds are prescribed to either the control or to the CO_2-forced conditions, as well as Ceppi and Shepherd 2017 all argue that it is the model uncertainty in the cloud radiative response to increasing CO_2 concentrations that is a primary contributor to the model uncertainty in the dynamical climate changes.

Or, is it the case that some third confounding factor mediates the relationship between clouds and the circulation? In Chapter 4 we argue that by applying a momentum perturbation we can change the cloud-circulation coupling in the mid-latitudes. However, by the thermal wind balance, any momentum perturbation must necessarily be accompanied by an atmospheric temperature perturbation. How can we tease out in a physically meaningful way the individual mechanisms and processes that comprise the cloud-thermodynamics-dynamics feedback? An approach complementary to the cloud-locking experiments of Ceppi and Hartmann 2016 and Voigt and Shaw 2015 may be a matrix of dynamics-locking experiments in which the dynamical state is prescribed to either control or to CO_2-forced conditions, and the behavior of clouds subsequently examined in unforced and CO_2 simulations.

With respect to confounding factors, the emergent constraint that we have developed in Chapter 3 is inherently conditioned on a confounding thermodynamic factor, i.e. the

particular spatial pattern of SST which has been observed in the recent past but is likely not a good predictor of the future spatial pattern of SST (e.g. Marvel et al. 2018). For example, it has been shown that the recent spatial patterns of SST have been associated with anomalously strong values of the tropical and sub-tropical boundary layer inversion that yield anomalous shortwave cloud radiative cooling, but that this is not likely to persist into the future (Zhou, Zelinka, and Klein 2016). This limitation of the observations to a sample space that is unrepresentative of future conditions seems to bias low any observationally constrained estimates of ECS (Armour 2017), implying higher true values of ECS.

In addition, Caldwell, Zelinka, and Klein 2018 have independently assessed our emergent constraint – the climatological Hadley circulation edge latitude – and have found that is meets almost all of their criteria to be a credible emergent constraint. However, Caldwell, Zelinka, and Klein 2018 have also identified that the tropical intrusion of anomalous shortwave cloud radiative cooling with poleward Hadley circulation edge shifts contribute to the correlation between the inter-model spread in the climatological Hadley circulation edge and the inter-model spread in ECS. Future work must identify the mechanisms through which poleward expansion of the Hadley circulation affect the cloud radiative response in, not just the mid-latitudes, but also the tropics and sub-tropics.

Throughout this thesis, we have been using the cloud radiative response rather than the cloud radiative feedback as the metric for the future cloud changes. This has not been an oversight, but rather a conscious decision. To define a feedback one must normalize by a temperature response. However, which temperature response should we use? Since we analyze a regional climate feedback processes, it seems physically unmotivated that we should use the global-mean surface air temperature response which defines the traditionally used forcing-feedback framework (Chapter 1, c.f. Dessler, Mauritsen, and Stevens 2018). However, normalizing by the regional surface air temperature response raises a philosophical question over whether the feedback we examine is a local feedback or localized feedback.

By way of example, the sea ice feedback is very likely a local feedback, with a change in sea ice that results from a change in the local surface temperature changes. However, the high latitude shortwave cloud phase feedback might be a localized feedback rather than a local feedback, since the high latitude shortwave cloud phase radiative response acts on a time-scale that is faster than the Southern Ocean surface air temperature response. In the case of the high latitude shortwave cloud phase feedback, using the regional surface air temperature response may artificially introduce time-dependence into the feedback where there is none (Armour, Bitz, and Roe 2013).

Further complicating the picture, the regional surface air temperature response may be communicated remotely through, or even be the result of, the horizontal energy transports that emerge from atmospheric and oceanic dynamical changes (Feldl and Roe 2013; Feldl, Anderson, and Bordoni 2017; Singh, Rasch, and Rose 2017). Similarly, although we believe that we have shown that models' climatological Hadley circulation edge latitude constitutes an emergent constraint on the global-mean surface air temperature, which in itself is of great scientific and societal value, we note that the Hadley circulation edge latitude constitutes a much stronger observational constraint on the shortwave cloud radiative response in the lower mid-latitude region. That is, the results presented herein might have even greater relevance for constraining regional climate changes. For example, Grise and Polvani 2014b show that the model biases in the coupling between the eddy-driven jet and the mid-latitude clouds in the Southern Hemisphere offer a way to constrain the transient climate response there. Given that the Hadley circulation more consistently correlates with the mid-latitude clouds, one might expect that the model biases in the coupling between the Hadley circulation and the mid-latitude clouds to serve as a more robust constraint on the surface air temperature response of the mid-latitude region.

However, the extension to a regional energy balance of the forcing-feedback framework used for the global-mean energy budget introduced in Chapter 1 is frustrated by the

horizontal transports of energy by atmospheric and oceanic dynamics highlighted above. Recalling the Equation 1.1, but retaining spatial dependence $\vec{x}$:

$$\frac{C\left(\vec{x}\right) dT_s\left(\vec{x}\right)}{dt} = R\left(\vec{x}\right) + F\left(\vec{x}\right) - \nabla \cdot \vec{F}\left(\vec{x}\right) \tag{5.1}$$

where $\nabla \cdot \vec{F}$ is the divergence of the energy flux by the atmospheric and oceanic circulation. In the global-mean this term averages to 0, but the regional temperature response explicitly depend on it. In a statistical steady-state, the local TOA radiative response balances both the local radiative forcing as well as the local energy flux convergence:

$$F\left(\vec{x}\right) - \nabla \cdot \vec{F}\left(\vec{x}\right) = -R\left(\vec{x}\right) \tag{5.2}$$

Future work must take into consideration the dynamical climate changes that are forced by increasing CO_2 and how they drive or mediate the regional thermodynamic climate changes and radiative feedback processes.

Bibliography

Andrews, Timothy et al. (2012). "Forcing, feedbacks and climate sensitivity in CMIP5 coupled atmosphere-ocean climate models." In: *Geophysical Research Letters* 39.9.

Armour, Kyle C (2017). "Energy budget constraints on climate sensitivity in light of inconstant climate feedbacks." In: *Nature Climate Change* 7.5, p. 331.

Armour, Kyle C, Cecilia M Bitz, and Gerard H Roe (2013). "Time-varying climate sensitivity from regional feedbacks." In: *Journal of Climate* 26.13, pp. 4518–4534.

Barnes, Elizabeth A and Lorenzo Polvani (2013). "Response of the midlatitude jets, and of their variability, to increased greenhouse gases in the CMIP5 models." In: *Journal of Climate* 26.18, pp. 7117–7135.

Bauer, Mike, George Tselioudis, and William B Rossow (2016). "A new climatology for investigating storm influences in and on the extratropics." In: *Journal of Applied Meteorology and Climatology* 55.5, pp. 1287–1303.

Bender, Frida AM, V Ramanathan, and George Tselioudis (2012). "Changes in extratropical storm track cloudiness 1983–2008: Observational support for a poleward shift." In: *Climate Dynamics* 38.9-10, pp. 2037–2053.

Boer, George J and Bin Yu (2003). "Dynamical aspects of climate sensitivity." In: *Geophysical research letters* 30.3.

Bony, Sandrine and Jean-Louis Dufresne (2005). "Marine boundary layer clouds at the heart of tropical cloud feedback uncertainties in climate models." In: *Geophysical Research Letters* 32.20.

Bony, Sandrine et al. (2015). "Clouds, circulation and climate sensitivity." In: *Nature Geoscience* 8.4, p. 261.

Booth, James F, Shuguang Wang, and Lorenzo Polvani (2013). "Midlatitude storms in a moister world: Lessons from idealized baroclinic life cycle experiments." In: *Climate dynamics* 41.3-4, pp. 787–802.

Bordoni, Simona and Tapio Schneider (2010). "Regime transitions of steady and time-dependent Hadley circulations: Comparison of axisymmetric and eddy-permitting simulations." In: *Journal of the Atmospheric Sciences* 67.5, pp. 1643–1654.

Boucher, O. et al. (2013). "Clouds and Aerosols." In: *Climate Change 2013: The Physical Science Basis. Contribution of Working Group I to the Fifth Assessment Report of the Intergovernmental Panel on Climate Change*. Ed. by T.F. Stocker et al. Cambridge, United Kingdom and New York, NY, USA: Cambridge University Press. Chap. 7, pp. 571–658. ISBN: ISBN 978-1-107-66182-0. DOI: 10.1017/CBO9781107415324.016. URL: www.climatechange2013.org.

Brest, Christopher L, William B Rossow, and Miriam D Roiter (1997). "Update of radiance calibrations for ISCCP." In: *Journal of Atmospheric and Oceanic Technology* 14.5, pp. 1091–1109.

Bretherton, Christopher S and Sungsu Park (2009). "A new moist turbulence parameterization in the Community Atmosphere Model." In: *Journal of Climate* 22.12, pp. 3422–3448.

Brient, Florent et al. (2016). "Shallowness of tropical low clouds as a predictor of climate models? response to warming." In: *Climate dynamics* 47.1-2, pp. 433–449.

Byrne, Michael P and Tapio Schneider (2016). "Narrowing of the ITCZ in a warming climate: Physical mechanisms." In: *Geophysical Research Letters* 43.21.

Caldwell, Peter M, Mark D Zelinka, and Stephen A Klein (2018). "Evaluating Emergent Constraints on Equilibrium Climate Sensitivity." In: *Journal of Climate* 31.10, pp. 3921–3942.

Caldwell, Peter M et al. (2014). "Statistical significance of climate sensitivity predictors obtained by data mining." In: *Geophysical Research Letters* 41.5, pp. 1803–1808.

Caldwell, Peter M et al. (2016). "Quantifying the sources of intermodel spread in equilibrium climate sensitivity." In: *Journal of Climate* 29.2, pp. 513–524.

Ceppi, Paulo and Dennis L Hartmann (2015). "Connections between clouds, radiation, and midlatitude dynamics: A review." In: *Current Climate Change Reports* 1.2, pp. 94–102.

— (2016). "Clouds and the atmospheric circulation response to warming." In: *Journal of Climate* 29.2, pp. 783–799.

Ceppi, Paulo, Dennis L Hartmann, and Mark J Webb (2016). "Mechanisms of the negative shortwave cloud feedback in middle to high latitudes." In: *Journal of Climate* 29.1, pp. 139–157.

Ceppi, Paulo and Theodore G Shepherd (2017). "Contributions of climate feedbacks to changes in atmospheric circulation." In: *Journal of Climate* 30.22, pp. 9097–9118.

Ceppi, Paulo, Mark D Zelinka, and Dennis L Hartmann (2014). "The response of the Southern Hemispheric eddy-driven jet to future changes in shortwave radiation in CMIP5." In: *Geophysical Research Letters* 41.9, pp. 3244–3250.

Ceppi, Paulo et al. (2012). "Southern Hemisphere jet latitude biases in CMIP5 models linked to shortwave cloud forcing." In: *Geophysical Research Letters* 39.19.

Ceppi, Paulo et al. (2017). "Cloud feedback mechanisms and their representation in global climate models." In: *Wiley Interdisciplinary Reviews: Climate Change* 8.4.

Cesana, G et al. (2015). "Multimodel evaluation of cloud phase transition using satellite and reanalysis data." In: *Journal of Geophysical Research: Atmospheres* 120.15, pp. 7871–7892.

Charney, Jule G et al. (1979). *Carbon dioxide and climate: a scientific assessment*. National Academy of Sciences, Washington, DC.

Chen, Gang, Isaac M Held, and Walter A Robinson (2007). "Sensitivity of the latitude of the surface westerlies to surface friction." In: *Journal of the atmospheric sciences* 64.8, pp. 2899–2915.

Collins, William D et al. (2006). "The formulation and atmospheric simulation of the Community Atmosphere Model version 3 (CAM3)." In: *Journal of Climate* 19.11, pp. 2144–2161.

Colman, Robert (2003). "A comparison of climate feedbacks in general circulation models." In: *Climate Dynamics* 20.7-8, pp. 865–873.

Curry, Judith A et al. (1996). "Overview of Arctic cloud and radiation characteristics." In: *Journal of Climate* 9.8, pp. 1731–1764.

Dee, Dick P et al. (2011). "The ERA-Interim reanalysis: Configuration and performance of the data assimilation system." In: *Quarterly Journal of the royal meteorological society* 137.656, pp. 553–597.

Deser, Clara et al. (2012). "Uncertainty in climate change projections: the role of internal variability." In: *Climate dynamics* 38.3-4, pp. 527–546.

Dessler, Andrew E, Thorsten Mauritsen, and Bjorn Stevens (2018). "The influence of internal variability on Earth's energy balance framework and implications for estimating climate sensitivity." In: *Atmospheric Chemistry and Physics* 18.7, pp. 5147–5155.

Dufresne, Jean-Louis and Sandrine Bony (2008). "An assessment of the primary sources of spread of global warming estimates from coupled atmosphere–ocean models." In: *Journal of Climate* 21.19, pp. 5135–5144.

Eastman, Ryan and Stephen G Warren (2013). "A 39-yr survey of cloud changes from land stations worldwide 1971–2009: Long-term trends, relation to aerosols, and expansion of the tropical belt." In: *Journal of Climate* 26.4, pp. 1286–1303.

Feldl, Nicole, Bruce T Anderson, and Simona Bordoni (2017). "Atmospheric eddies mediate lapse rate feedback and Arctic amplification." In: *Journal of Climate* 30.22, pp. 9213–9224.

Feldl, Nicole and Gerard H Roe (2013). "The nonlinear and nonlocal nature of climate feedbacks." In: *Journal of Climate* 26.21, pp. 8289–8304.

Forster, Piers M et al. (2013). "Evaluating adjusted forcing and model spread for historical and future scenarios in the CMIP5 generation of climate models." In: *Journal of Geophysical Research: Atmospheres* 118.3, pp. 1139–1150.

Frey, William R and Jennifer E Kay (2018). "The influence of extratropical cloud phase and amount feedbacks on climate sensitivity." In: *Climate Dynamics* 50.7-8, pp. 3097–3116.

Frierson, Dargan MW, Jian Lu, and Gang Chen (2007). "Width of the Hadley cell in simple and comprehensive general circulation models." In: *Geophysical Research Letters* 34.18.

Fyfe, John C (2003). "Extratropical Southern Hemisphere cyclones: Harbingers of climate change?" In: *Journal of Climate* 16.17, pp. 2802–2805.

Geng, Quanzhen and Masato Sugi (2003). "Possible change of extratropical cyclone activity due to enhanced greenhouse gases and sulfate aerosols?Study with a high-resolution AGCM." In: *Journal of Climate* 16.13, pp. 2262–2274.

Gettelman, A, JE Kay, and KM Shell (2012). "The evolution of climate sensitivity and climate feedbacks in the Community Atmosphere Model." In: *Journal of Climate* 25.5, pp. 1453–1469.

Giorgetta, Marco A et al. (2013). "Climate and carbon cycle changes from 1850 to 2100 in MPI-ESM simulations for the Coupled Model Intercomparison Project phase 5." In: *Journal of Advances in Modeling Earth Systems* 5.3, pp. 572–597.

Grise, Kevin M and Brian Medeiros (2016). "Understanding the varied influence of mid-latitude jet position on clouds and cloud radiative effects in observations and global climate models." In: *Journal of Climate* 29.24, pp. 9005–9025.

Grise, Kevin M and Lorenzo M Polvani (2014a). "Is climate sensitivity related to dynamical sensitivity? A Southern Hemisphere perspective." In: *Geophysical Research Letters* 41.2, pp. 534–540.

— (2014b). "Southern Hemisphere cloud–dynamics biases in CMIP5 models and their implications for climate projections." In: *Journal of Climate* 27.15, pp. 6074–6092.

— (2016). "Is climate sensitivity related to dynamical sensitivity?" In: *Journal of Geophysical Research: Atmospheres* 121.10, pp. 5159–5176.

Grise, Kevin M, Lorenzo M Polvani, and John T Fasullo (2015). "Reexamining the relationship between climate sensitivity and the Southern Hemisphere radiation budget in CMIP models." In: *Journal of Climate* 28.23, pp. 9298–9312.

Grise, Kevin M et al. (2013). "The ozone hole indirect effect: Cloud-radiative anomalies accompanying the poleward shift of the eddy-driven jet in the Southern Hemisphere." In: *Geophysical Research Letters* 40.14, pp. 3688–3692.

Hansen, J et al. (2002). "Climate forcings in Goddard Institute for space studies SI2000 simulations." In: *Journal of Geophysical Research: Atmospheres* 107.D18.

Hartmann, Dennis L and Kristin Larson (2002). "An important constraint on tropical cloud-climate feedback." In: *Geophysical Research Letters* 29.20.

Hawkins, Ed and Rowan Sutton (2009). "The potential to narrow uncertainty in regional climate predictions." In: *Bulletin of the American Meteorological Society* 90.8, pp. 1095–1107.

Haynes, John M et al. (2011). "Major characteristics of Southern Ocean cloud regimes and their effects on the energy budget." In: *Journal of Climate* 24.19, pp. 5061–5080.

Held, I. M. (2000). “The general circulation of the atmosphere.” In: Woods Hole, MA: Woods Hole Oceanographic Institute.

Held, Isaac M and Brian J Soden (2006). “Robust responses of the hydrological cycle to global warming.” In: *Journal of climate* 19.21, pp. 5686–5699.

Hu, Y and Q Fu (2007). “Observed poleward expansion of the Hadley circulation since 1979.” In: *Atmospheric Chemistry and Physics* 7.19, pp. 5229–5236.

Hurrell, James W et al. (2013). “The community earth system model: a framework for collaborative research.” In: *Bulletin of the American Meteorological Society* 94.9, pp. 1339–1360.

IPCC (2013). *Climate Change 2013: The Physical Science Basis. Contribution of Working Group I to the Fifth Assessment Report of the Intergovernmental Panel on Climate Change*. Cambridge, United Kingdom and New York, NY, USA: Cambridge University Press, p. 1535. ISBN: ISBN 978-1-107-66182-0. DOI: 10.1017/CBO9781107415324. URL: www.climatechange2013.org.

Jin, Yao, William B Rossow, and Don P Wylie (1996). “Comparison of the climatologies of high-level clouds from HIRS and ISCCP.” In: *Journal of climate* 9.11, pp. 2850–2879.

Johanson, Celeste M and Qiang Fu (2009). “Hadley cell widening: Model simulations versus observations.” In: *Journal of Climate* 22.10, pp. 2713–2725.

Kållberg, P (2011). *Forecast drift in ERA-Interim, ERA report series, No 10*.

Kang, Sarah M and Jian Lu (2012). “Expansion of the Hadley cell under global warming: Winter versus summer.” In: *Journal of Climate* 25.24, pp. 8387–8393.

Kang, Sarah M and Lorenzo M Polvani (2011). “The interannual relationship between the latitude of the eddy-driven jet and the edge of the Hadley cell.” In: *Journal of Climate* 24.2, pp. 563–568.

Kay, JE et al. (2014). “Processes controlling Southern Ocean shortwave climate feedbacks in CESM.” In: *Geophysical Research Letters* 41.2, pp. 616–622.

Kay, Jennifer E et al. (2016). “Global climate impacts of fixing the Southern Ocean shortwave radiation bias in the Community Earth System Model (CESM).” In: *Journal of Climate* 29.12, pp. 4617–4636.

Keyser, Daniel, Brian D Schmidt, and Dean G Duffy (1989). "A technique for representing three-dimensional vertical circulations in baroclinic disturbances." In: *Monthly Weather Review* 117.11, pp. 2463–2494.

Klein, Stephen A and Alex Hall (2015). "Emergent constraints for cloud feedbacks." In: *Current Climate Change Reports* 1.4, pp. 276–287.

Kushner, Paul J, Isaac M Held, and Thomas L Delworth (2001). "Southern Hemisphere atmospheric circulation response to global warming." In: *Journal of Climate* 14.10, pp. 2238–2249.

Li, Ying, David WJ Thompson, and Sandrine Bony (2015). "The influence of atmospheric cloud radiative effects on the large-scale atmospheric circulation." In: *Journal of Climate* 28.18, pp. 7263–7278.

Li, Ying, David WJ Thompson, and Yi Huang (2017). "The Influence of Atmospheric Cloud Radiative Effects on the Large-Scale Stratospheric Circulation." In: *Journal of Climate* 30.15, pp. 5621–5635.

Li, Ying et al. (2014). "Observed linkages between the northern annular mode/North Atlantic Oscillation, cloud incidence, and cloud radiative forcing." In: *Geophysical Research Letters* 41.5, pp. 1681–1688.

Liao, Xiaohan, William B Rossow, and David Rind (1995). "Comparison between SAGE II and ISCCP high-level clouds: 1. Global and zonal mean cloud amounts." In: *Journal of Geophysical Research: Atmospheres* 100.D1, pp. 1121–1135.

Loeb, Norman G et al. (2012). "Advances in understanding top-of-atmosphere radiation variability from satellite observations." In: *Surveys in geophysics* 33.3-4, pp. 359–385.

Lu, Jian, Clara Deser, and Thomas Reichler (2009). "Cause of the widening of the tropical belt since 1958." In: *Geophysical Research Letters* 36.3.

Lu, Jian, Gabriel A Vecchi, and Thomas Reichler (2007). "Expansion of the Hadley cell under global warming." In: *Geophysical Research Letters* 34.6.

Marvel, Kate et al. (2018). "Internal variability and disequilibrium confound estimates of climate sensitivity from observations." In: *Geophysical Research Letters* 45.3, pp. 1595–1601.

McCoy, Daniel T et al. (2015). "Mixed-phase cloud physics and Southern Ocean cloud feedback in climate models." In: *Journal of Geophysical Research: Atmospheres* 120.18, pp. 9539–9554.

McCoy, Daniel T et al. (2016). “On the relationships among cloud cover, mixed-phase partitioning, and planetary albedo in GCMs.” In: *Journal of Advances in Modeling Earth Systems* 8.2, pp. 650–668.

Mitchell, John FB, CA Senior, and WJ Ingram (1989). “C02 and climate: a missing feedback?” In: *Nature* 341.6238, p. 132.

Morcrette, Jean-Jacques and Yves Fouquart (1986). “The overlapping of cloud layers in shortwave radiation parameterizations.” In: *Journal of the atmospheric sciences* 43.4, pp. 321–328.

Morrison, Hugh et al. (2012). “Resilience of persistent Arctic mixed-phase clouds.” In: *Nature Geoscience* 5.1, p. 11.

Myers, Timothy A and Joel R Norris (2013). “Observational evidence that enhanced subsidence reduces subtropical marine boundary layer cloudiness.” In: *Journal of Climate* 26.19, pp. 7507–7524.

— (2016). “Reducing the uncertainty in subtropical cloud feedback.” In: *Geophysical Research Letters* 43.5, pp. 2144–2148.

Norris, Joel R and Amato T Evan (2015). “Empirical removal of artifacts from the ISCCP and PATMOS-x satellite cloud records.” In: *Journal of Atmospheric and Oceanic Technology* 32.4, pp. 691–702.

Norris, Joel R and Sam F Iacobellis (2005). “North Pacific cloud feedbacks inferred from synoptic-scale dynamic and thermodynamic relationships.” In: *Journal of Climate* 18.22, pp. 4862–4878.

Norris, Joel R et al. (2016). “Evidence for climate change in the satellite cloud record.” In: *Nature* 536.7614, pp. 72–75.

Oinas, V et al. (2001). “Radiative cooling by stratospheric water vapor: Big differences in GCM results.” In: *Geophysical research letters* 28.14, pp. 2791–2794.

Park, Sungsu and Christopher S Bretherton (2009). “The University of Washington shallow convection and moist turbulence schemes and their impact on climate simulations with the Community Atmosphere Model.” In: *Journal of Climate* 22.12, pp. 3449–3469.

Phillips, Norman A (1951). “A simple three-dimensional model for the study of large-scale extratropical flow patterns.” In: *Journal of Meteorology* 8.6, pp. 381–394.

Pithan, Felix et al. (2016). "Climate model biases in jet streams, blocking and storm tracks resulting from missing orographic drag." In: *Geophysical Research Letters* 43.13, pp. 7231–7240.

Pruppacher, H and J Klett (1997). *Microphysics of Clouds and Precipitation. Atmospheric and Oceanographic Sciences Library, Vol. 18*.

Qu, Xin et al. (2014). "On the spread of changes in marine low cloud cover in climate model simulations of the 21st century." In: *Climate dynamics* 42.9-10, pp. 2603–2626.

Roe, Gerard H et al. (2015). "The remote impacts of climate feedbacks on regional climate predictability." In: *Nature Geoscience* 8.2, p. 135.

Roe, Gerard (2009). "Feedbacks, timescales, and seeing red." In: *Annual Review of Earth and Planetary Sciences* 37, pp. 93–115.

Rossow, William B and Leonid C Garder (1993). "Cloud detection using satellite measurements of infrared and visible radiances for ISCCP." In: *Journal of climate* 6.12, pp. 2341–2369.

Rossow, William B and Robert A Schiffer (1999). "Advances in understanding clouds from ISCCP." In: *Bulletin of the American Meteorological Society* 80.11, pp. 2261–2287.

Rozendaal, Margaret A, Conway B Leovy, and Stephen A Klein (1995). "An observational study of diurnal variations of marine stratiform cloud." In: *Journal of climate* 8.7, pp. 1795–1809.

Schneider, Tapio and Simona Bordoni (2008). "Eddy-mediated regime transitions in the seasonal cycle of a Hadley circulation and implications for monsoon dynamics." In: *Journal of the Atmospheric Sciences* 65.3, pp. 915–934.

Schweiger, Axel J and Jeffrey R Key (1992). "Arctic cloudiness. Comparison of ISCCP-C2 and Nimbus-7 satellite-derived cloud products with a surface-based cloud climatology." In: *Journal of climate* 5.12, pp. 1514–1527.

Schwendike, Juliane et al. (2014). "Local partitioning of the overturning circulation in the tropics and the connection to the Hadley and Walker circulations." In: *Journal of Geophysical Research: Atmospheres* 119.3, pp. 1322–1339.

Schwendike, Juliane et al. (2015). "Trends in the local Hadley and local Walker circulations." In: *Journal of Geophysical Research: Atmospheres* 120.15, pp. 7599–7618.

Seidel, Dian J et al. (2008). "Widening of the tropical belt in a changing climate." In: *Nature geoscience* 1.1, p. 21.

Shepherd, Theodore G (2014). "Atmospheric circulation as a source of uncertainty in climate change projections." In: *Nature Geoscience* 7.10, p. 703.

Sherwood, Steven C, Sandrine Bony, and Jean-Louis Dufresne (2014). "Spread in model climate sensitivity traced to atmospheric convective mixing." In: *Nature* 505.7481, p. 37.

Siler, Nicholas, Stephen Po-Chedley, and Christopher S Bretherton (2018). "Variability in modeled cloud feedback tied to differences in the climatological spatial pattern of clouds." In: *Climate Dynamics* 50.3-4, pp. 1209–1220.

Simpson, Isla R, Tiffany A Shaw, and Richard Seager (2014). "A diagnosis of the seasonally and longitudinally varying midlatitude circulation response to global warming." In: *Journal of the Atmospheric Sciences* 71.7, pp. 2489–2515.

Singh, HA, Philip J Rasch, and BEJ Rose (2017). "Increased Ocean Heat Convergence Into the High Latitudes With CO2 Doubling Enhances Polar-Amplified Warming." In: *Geophysical Research Letters* 44.20.

Stevens, Bjorn et al. (2013). "Atmospheric component of the MPI-M Earth System Model: ECHAM6." In: *Journal of Advances in Modeling Earth Systems* 5.2, pp. 146–172.

Storelvmo, Trude, Ivy Tan, and Alexei V Korolev (2015). "Cloud phase changes induced by CO 2 warming?a powerful yet poorly constrained cloud-climate feedback." In: *Current Climate Change Reports* 1.4, pp. 288–296.

Stubenrauch, CJ et al. (1999). "Clouds as seen by satellite sounders (3I) and imagers (ISCCP). Part I: Evaluation of cloud parameters." In: *Journal of Climate* 12.8, pp. 2189–2213.

Su, Hui et al. (2014). "Weakening and strengthening structures in the Hadley Circulation change under global warming and implications for cloud response and climate sensitivity." In: *Journal of Geophysical Research: Atmospheres* 119.10, pp. 5787–5805.

Su, Hui et al. (2017). "Tightening of tropical ascent and high clouds key to precipitation change in a warmer climate." In: *Nature communications* 8, p. 15771.

Sundqvist, Hilding, Erik Berge, and Jón Egill Kristjánsson (1989). "Condensation and cloud parameterization studies with a mesoscale numerical weather prediction model." In: *Monthly Weather Review* 117.8, pp. 1641–1657.

Tan, Ivy, Trude Storelvmo, and Mark D Zelinka (2016). "Observational constraints on mixed-phase clouds imply higher climate sensitivity." In: *Science* 352.6282, pp. 224–227.

Taylor, KE et al. (2007). "Estimating shortwave radiative forcing and response in climate models." In: *Journal of Climate* 20.11, pp. 2530–2543.

Taylor, Karl E, Ronald J Stouffer, and Gerald A Meehl (2012). "An overview of CMIP5 and the experiment design." In: *Bulletin of the American Meteorological Society* 93.4, pp. 485–498.

Tebaldi, Claudia and Reto Knutti (2007). "The use of the multi-model ensemble in probabilistic climate projections." In: *Philosophical Transactions of the Royal Society of London A: Mathematical, Physical and Engineering Sciences* 365.1857, pp. 2053–2075.

Trenberth, Kevin E and John T Fasullo (2010). "Simulation of present-day and twenty-first-century energy budgets of the southern oceans." In: *Journal of Climate* 23.2, pp. 440–454.

Tselioudis, G and D Konsta (2017). "The ?Storm Curtain?Effect: Poleward Shift of Clouds, Their Radiative Effects, and the Role of Midlatitude Storms." In: *Perspectives on Atmospheric Sciences*. Springer, pp. 725–731.

Tselioudis, George and Christian Jakob (2002). "Evaluation of midlatitude cloud properties in a weather and a climate model: Dependence on dynamic regime and spatial resolution." In: *Journal of Geophysical Research: Atmospheres* 107.D24.

Tselioudis, George and William B Rossow (2006). "Climate feedback implied by observed radiation and precipitation changes with midlatitude storm strength and frequency." In: *Geophysical research letters* 33.2.

Tselioudis, George, Yuanchong Zhang, and William B Rossow (2000). "Cloud and radiation variations associated with northern midlatitude low and high sea level pressure regimes." In: *Journal of climate* 13.2, pp. 312–327.

Vallis, Geoffrey K (2017). *Atmospheric and oceanic fluid dynamics*. Cambridge University Press.

Vial, Jessica, Jean-Louis Dufresne, and Sandrine Bony (2013). "On the interpretation of inter-model spread in CMIP5 climate sensitivity estimates." In: *Climate Dynamics* 41.11-12, pp. 3339–3362.

Voigt, Aiko and Tiffany A Shaw (2015). "Circulation response to warming shaped by radiative changes of clouds and water vapour." In: *Nature Geoscience* 8.2, p. 102.

Voigt, Aiko et al. (2016). "The tropical rain belts with an annual cycle and a continent model intercomparison project: TRACMIP." In: *Journal of Advances in Modeling Earth Systems* 8.4, pp. 1868–1891.

Walker, Christopher C and Tapio Schneider (2006). "Eddy influences on Hadley circulations: Simulations with an idealized GCM." In: *Journal of the atmospheric sciences* 63.12, pp. 3333–3350.

Wall, Casey J and Dennis L Hartmann (2015). "On the influence of poleward jet shift on shortwave cloud feedback in global climate models." In: *Journal of Advances in Modeling Earth Systems* 7.4, pp. 2044–2059.

Wang, Xiaolan L, Val R Swail, and Francis W Zwiers (2006). "Climatology and changes of extratropical cyclone activity: Comparison of ERA-40 with NCEP–NCAR reanalysis for 1958–2001." In: *Journal of Climate* 19.13, pp. 3145–3166.

Warren, G et al. (1986). "Global distribution of total cloud cover and cloud type amounts over land." In:

Warren, Stephen G et al. (1988). *Global distribution of total cloud cover and cloud type amounts over the ocean*. Tech. rep.

Weare, Bryan C (2000). "Insights into the importance of cloud vertical structure in climate." In: *Geophysical research letters* 27.6, pp. 907–910.

Webb, Mark J, F Hugo Lambert, and Jonathan M Gregory (2013). "Origins of differences in climate sensitivity, forcing and feedback in climate models." In: *Climate Dynamics* 40.3-4, pp. 677–707.

Wetherald, Richard T and Syukuro Manabe (1980). "Cloud cover and climate sensitivity." In: *Journal of the Atmospheric Sciences* 37.7, pp. 1485–1510.

Wielicki, Bruce A and Lindsay Parker (1992). "On the determination of cloud cover from satellite sensors: The effect of sensor spatial resolution." In: *Journal of Geophysical Research: Atmospheres* 97.D12, pp. 12799–12823.

Williamson, DL et al. (2012). "The APE atlas." In:

Yin, Jeffrey H (2005). "A consistent poleward shift of the storm tracks in simulations of 21st century climate." In: *Geophysical Research Letters* 32.18.

Zelinka, Mark D and Dennis L Hartmann (2011). “The observed sensitivity of high clouds to mean surface temperature anomalies in the tropics.” In: *Journal of Geophysical Research: Atmospheres* 116.D23.

Zelinka, Mark D, Stephen A Klein, and Dennis L Hartmann (2012a). “Computing and partitioning cloud feedbacks using cloud property histograms. Part I: Cloud radiative kernels.” In: *Journal of Climate* 25.11, pp. 3715–3735.

— (2012b). “Computing and partitioning cloud feedbacks using cloud property histograms. Part II: Attribution to changes in cloud amount, altitude, and optical depth.” In: *Journal of Climate* 25.11, pp. 3736–3754.

Zelinka, Mark D, Chen Zhou, and Stephen A Klein (2016). “Insights from a refined decomposition of cloud feedbacks.” In: *Geophysical Research Letters* 43.17, pp. 9259–9269.

Zelinka, Mark D et al. (2013). “Contributions of different cloud types to feedbacks and rapid adjustments in CMIP5.” In: *Journal of Climate* 26.14, pp. 5007–5027.

Zhang, Yuanchong et al. (2004). “Calculation of radiative fluxes from the surface to top of atmosphere based on ISCCP and other global data sets: Refinements of the radiative transfer model and the input data.” In: *Journal of Geophysical Research: Atmospheres* 109.D19.

Zhou, Chen, Mark D Zelinka, and Stephen A Klein (2016). “Impact of decadal cloud variations on the Earth?s energy budget.” In: *Nature Geoscience* 9.12, p. 871.